Hydrological modelling of a catchment supported by the discharge of treated wastewater - A comparison of two model concepts

Dissertation

zur Erlangung des akademischen Grades
„doctor rerum naturalium“- (Dr. rer. nat.)
im Fach Geographie

eingereicht an der
Mathematisch-Naturwissenschaftlichen Fakultät
der Humboldt-Universität zu Berlin

von
Diplom Geoökologe Sebastian Rudnick

Päsidentin der Humboldt-Universität zu Berlin
Prof. Dr.-Ing. Dr. Sabine Kunst

Dekan der Mathematisch-Naturwissenschaftlichen Fakultät
Prof. Dr. Elmar Kulke

Gutachter
1. Prof. Dr. Gunnar Nützmann,
Humboldt-Universität zu Berlin, Geographisches Institut
2. Prof. Dr. Reinhard Hinkelmann,
Technische Universität Berlin, Institut für Bauingenieurwesen
3. Prof. Dr. Dieter Gerten,
Humboldt-Universität zu Berlin, Geographisches Institut

Tag der Einreichung: 14.05.2018

Tag der mündlichen Prüfung: 04.10.2018

Abstract

The climate of North-East Germany is characterised by low annual precipitation sums and low groundwater recharge. Analysis of climatic scenarios showed that groundwater recharge could further decline. Ecologically valuable habitats and the supply of drinking water are endangered by shrinking groundwater reserves. In order to sustain these important resources, new strategies must be developed. One possible strategy is the irrigation of treated wastewater in order to support the landscape water budget. At the Lietzengraben catchment, located north-east of Berlin, Germany, treated wastewater is discharged into irrigation ponds to sustain wetlands and lakes in the catchment during the summer periods. This management strategy was developed previously by scenario analysis, performed by the iteratively coupled, numerical model ArcEGMO-ASM. Limitations of the model, however, were the two dimensional representation of the aquifer and the separated model layers for different hydrological processes. This hampered the estimation of subsurface flow paths and residence times, which are of interest in order to account for the fate of solutes contained in the discharged water.
In this work, the physically based, integrated model HydroGeoSphere was used to simulate the surface and subsurface water flow in the catchment. Based on the simulation results, flow paths and residence times were estimated. The results of the simulations by both models were investigated and compared in order to evaluate the benefits and limitations of HydroGeoSphere. It was possible to reproduce the catchment dynamics regarding discharge and groundwater heads reasonably well with both models. However, the application of HydroGeoSphere was limited due to the inability of the model to represent features like snowfall and controllable weirs, which are represented in ArcEGMO-ASM. Additionally, the computational effort for simulations using HydroGeoSphere was very high and the model was subject to numerical instabilities, due to the simulation of highly non-linear flow in the unsaturated zone and the coarse spatial discretisation.
The calibration of the model yielded parameter values which enabled the model to reproduce the catchment dynamics reasonably well. However, HydroGeoSphere may be limited in its use since the obtained values are partially unrealistic and may not represent the actual physical processes accurately. On the other hand, HydroGeoSphere allowed the approximation of subsurface flow paths and residence times of water which infiltrated at the irrigation ponds. Furthermore, the exfiltration of groundwater to a stream reach was estimated by field measurements and compared to simulation results in order to assess the ability of the models to reproduce the interaction between groundwater and surface water. The comparison showed that both models were not able to reproduce the spatial patterns on a sub-reach scale and the calculated exfiltration rates did not match the observed rates.
The comparison of ArcEGMO-ASM and HydroGeoSphere showed the advantages and limitations of both models. Comparing the overall additional effort to the benefits, however, the application of HydroGeoSphere to investigations regarding management strategies or scenario analyses may not pay off. Since HydroGeoSphere is under steady development and computational resources improve, the use of HydroGeoSphere may be applicable in the near future.

Zusammenfassung

Das Klima Nordostdeutschlands ist geprägt durch geringe Niederschlagsmengen und Grundwasserneubildung. Die Untersuchung von Klimaszenarien ergab, dass die Grundwasserneubildung weiter abnehmen könnte. Ökologisch wertvolle Lebensräume und die Trinkwassergewinnung sind durch schwindende Grundwasservorräte gefährdet. Um diese Ressource zu erhalten müssen neue Strategien entwickelt werden. Eine Möglichkeit ist die Einleitung von Klarwasser, um den Wasserhaushalt zu stützen. Im Gebiet des Lietzengrabens, nordöstlich von Berlin, wird Klarwasser in Verrieselungsteiche geleitet, um Feuchtgebiete und Seen während der Sommermonate zu erhalten. Diese Strategie wurde durch eine Szenarioanalyse erarbeitet, die sich auf das iterativ gekoppelte Modell ArcEGMO-ASM stützte. Die Möglichkeiten des Modells sind jedoch durch den zweidimensional repräsentierten Grundwasserleiter und verschiedene Modellebenen für die hydrologischen Prozesse begrenzt. Unterirdische Fließpfade und Aufenthaltszeiten können damit nicht bestimmt werden. Diese sind von Interesse, um den Verbleib von im eingeleiteten Wasser gelösten Stoffen zu klären.
In dieser Arbeit wurde das physikalisch basierte, voll integrierte Modell HydroGeoSphere genutzt, um den Fluss von Wasser an der Oberfläche und im Untergrund des Einzugsgebiets zu simulieren. Basierend auf dieser Simulation wurden Fließpfade und Aufenthaltszeiten abgeschätzt. Die Ergebnisse beider Modelle wurden analysiert und verglichen, um den Nutzen von HydroGeoSphere zu evaluieren. Mit beiden Modellen war es möglich, die Abfluss- und Grundwasserdynamiken im Einzugsgebiet angemessen zu reproduzieren. Bei der Anwendung von HydroGeoSphere zeigten sich die Grenzen dieses Modells. Es fehlten Möglichkeiten zur Berücksichtigung von z.B. Schneefall und steuerbaren Wehren, welche in ArcEGMO-ASM vorhanden sind. Darüber hinaus war der rechnerische Aufwand für die Simulation des Einzugsgebiets mit HydroGeoSphere sehr hoch und das Modell war numerisch instabil, bedingt durch die nicht-linearen Prozesse in der ungesättigten Zone und der groben räumlichen Diskretisierung.
Die Kalibrierung des Modells lieferte Parameterwerte, die eine annehmbare Reproduktion der Einzugsgebietsdynamiken erlaubten. Allerdings könnte HydroGeoSphere nur eingeschränkt nutzbar sein, da die Werte teils unrealistisch waren. Andererseits ermöglichte HydroGeoSphere die Abschätzung von unterirdischen Fließpfaden und Aufenthaltszeiten.
Im Weiteren wurde der Austritt von Grundwasser in einen Bachabschnitt durch Messungen bestimmt und mit den Simulationen verglichen. So wurde die Fähigkeit der Modelle, die Interaktion zwischen Grundwasser und Oberflächenwasser abzubilden, bewertet. Der Vergleich zeigte, dass keines der Modelle geeignet war, die räumlichen Muster auf der Skala eines Bachabschnitts zu reproduzieren. Die simulierten Exfiltrationsraten wichen von den beobachteten ab.
Der Vergleich von ArcEGMO-ASM und HydroGeoSphere zeigte die Vorteile und Grenzen der Modelle auf. Der Einsatz von HydroGeoSphere bei Untersuchungen von Bewirtschaftungsstrategien macht sich noch nicht bezahlt, wenn man den zusätzlichen Aufwand mit den Vorteilen vergleicht. Da HydroGeoSphere weiterentwickelt wird und die Rechenkapazitäten zunehmen, könnte das Modell in der nahen Zukunft in der Praxis nutzbar sein.

Acknowledgements

Firstly, I would like to express my sincere gratitude to my supervisor Prof. Dr. Gunnar Nützmann for the continuous support of my studies and the fruitful discussions on the model. His enduring encouragement and patience helped me during my research and the writing of this thesis.

My sincere thanks also goes to PD Dr. Jörg Lewandowski, who contributed greatly to my research with his knowledge and many interesting discussions on results and methods.

I would also like to thank the head of the project "ELaN", Prof. Dr. Gunnar Lischeid for the opportunity to work on this topic.

I wish to thank Dr. Bernd Pfützner and Dr. Silke Mey for the provision of the model ArcEGMO-ASM and the support regarding the application of the model. Dr. Klaus Möller and his staff provided valuable discharge and groundwater data and aided me by providing information on the Lietzengraben catchment and management measures, for which I am greatly thankful.

This work would not have been possible without the wonderful support of the staff at the Leibniz-Institute of Freshwater Ecology and Inland Fisheries. I want to thank in particular Grit Siegert, Christine Sturm and Jörg Friedrich.

Lea, Steffi, Silke, Sandra, Basti, Helga, Vanessa, Flo, Elsa, Lisa, Hannes and Karin made this work possible with their unfailing optimism and backup during every stage of this thesis. Thank you!

Last but not the least, I would like to thank my parents and my brothers for the encouraging words,the understanding, and unconditional support.

Contents

List of Figures

List of Tables

1 Introduction

1.1 Motivation & study framework

Freshwater is a precious resource, from a socio-economic point of view as well as for ecological reasons. At the same time, freshwater ecosystems are threatened by climate change and shifts of land use (Young et al., 2016). One of today's challenges is the preservation and sustainable utilisation of this resource while facing climate change.

Freshwater includes surface waters like lakes and rivers, as well as subsurface waters like soil water and groundwater. Surface water bodies are an important part of terrestrial ecosystems, they are habitats for aquatic organisms, provide resources for terrestrial animals and hatching ground for insects. Thus, they contribute to species richness in their surrounding (Baron et al., 2002). Furthermore, lakes and streams are of high recreational use, especially in the densely populated areas of Central Europe. The ecological state of surface waters is determined by their morphological structure and water quality (Schwoerbel, 1999). These parameters are highly dependent on the catchment of the surface water body, and therefore influenced by its terrestrial parts and their properties like e.g. land use and climate (Baron et al., 2002).
Not only surficial influences are important to the state of surface waters. Surface- and subsurface water bodies are not isolated from each other. They are in most cases linked and interact depending on the hydrological and/or meteorological conditions. For example, during periods with high surface water levels, groundwater is recharged by streams and lakes through infiltration. During dry periods with low amount of rainfall high evapotranspiration rates and low surface water levels, streams and lakes are fed by groundwater via base flow (Winter et al., 1998). In addition to effects on the quantity (discharge, water levels), the close linking between surface and subsurface water bodies can have considerable impacts on the quality of streams and lakes. Over the last years, various authors examined the role of groundwater - surface water interaction and showed its importance.
For example, the ecological condition of lakes is strongly influenced by the groundwater quality, since nutrient input via groundwater can play a major role in the nutrient mass balance of lakes (Nakayama and Watanabe, 2008; Meinikmann et al., 2013). Also, the interaction between streams and groundwater can have a significant effect on the turnover rates of nutrients and pollutants. The exchange of (surface) water in the hyporheic zone, where groundwater and surface water mix is known to be a hot spot for biogeochemical reactions and can alter the concentrations of solutes significantly (Krause et al., 2011; Brunke and Gonser, 1997).
Alongside its contribution to stream discharge, surface water levels, and nutrient concentrations, groundwater can be crucial for the water supply of plants. This is especially true for lowlands with shallow groundwater bodies near the land surface. Many plants have root systems reaching deep enough into the soil to feed from groundwater or the capillary fringe in the unsaturated zone (Winter

et al., 1998). During periods with low or no precipitation, this is an important source of water supply (Canadell et al., 1996).
Furthermore, the extraction of groundwater from sandy aquifers is the main source of drinking water supply in Central Europe. Any degradation in water quality and/or quantity has long term effects due to the low water flow velocities in these aquifers (Winter et al., 1998).
To preserve this ecological and socio-economic resource, a sufficient groundwater recharge and protection from pollutants is essential. The water storage of aquifers is mainly refilled by precipitation. The fraction of precipitation which is neither evaporated by plants and open water evaporation, nor discharged quickly to surface streams by overland flow, reaches the saturated zone via percolation. The amount of groundwater recharge is highly dependent on the seasonal distribution of precipitation and the evapotranspiration by plants, which is closely linked to temperature and water availability within their root zone. The availability of water for plant evapotranspiration, on the other hand, is linked to topography (Lischeid and Nathkin, 2011). In lowlands the availability of groundwater for evapotranspiration by plants is potentially high due to the shallow groundwater table and hence good water availability. This leads to groundwater recharge rates of only about 100 mm to 200 mm per year, depending on the depth to the groundwater table (Lahmer and Pfützner, 2003). Eventually, the yearly budget can be negative for sites with very high evapotranspiration and good availability of water, which results in a reduction of the groundwater volume stored in the aquifer (Lahmer and Pfützner, 2003).
Additionally to the generally low groundwater recharge rates at sites with high evapotranspiration, Gerstengarbe et al. (2003) described decreasing groundwater levels and falling lake levels in Brandenburg during the last decade. This is most likely a consequence of climate change causing shifts in the spatial and temporal distribution of precipitation and elevated evapotranspiration rates due to rising temperatures. A drastic symptom of this rapid change has been observed in some parts of North-East Germany, where lakes were found to suffer major decreases of water levels (Gerstengarbe et al., 2003).
Alongside different land use strategies (Lischeid and Nathkin, 2011) to alter the landscape water budget, the re-use of treated wastewater is another possibility to provide water for the growth of crops, the supply of ecologically valuable wetlands and lakes, and the recharge of groundwater storage. This has successfully been undertaken for many years in different regions worldwide (Asano and Lavine, 1996; Anderson, 2003). In Germany, this strategy is not common, mostly due to legal restrictions concerning the degradation of groundwater in quality (*Verordnung zum Schutz des Grundwassers: GrwV*). Hence, treated waste waters are directly discharged to streams and rivers and leave the catchments without noteworthy contributions to the (subsurface) water budget. Only few attempts were made to make use of these waters. The so called “Braunschweiger Modell” is one example (Abwasserverband Braunschweig, 2017).
With expected further intensification of water scarcity in North-East Germany (Spekat et al., 2007; Jacob et al., 2008; Gerstengarbe et al., 2003) and the resulting demand for practical solutions to arising problems, the re-use of treated waste water has been examined to evaluate possibilities and minimise risks of this strategy.
The project “ELaN” was an interdisciplinary approach to investigate the development of an integrated land management by sustainable use of water and matter in

North-East Germany. The study site has been the former sewage farm Hobrechtsfelde, located north-east of Berlin, Germany. To support lakes and wetlands that are threatened by decreasing groundwater heads and water levels, treated wastewater has been discharged to ponds in the catchment (Ginzel, 1999; Fritz et al., 2004).
Since modern sewage plants eliminate nutrients quite effectively, the major concern with the use of treated waste water is the influence of organic micropollutants on biota, which may restrict the re-use of treated wastewater (Wintgens et al., 2008). These substances exhibit highly variable degradation rates, which depend on the biochemical regime, redox conditions and residence times (Rühmland et al., 2015). One of the goals of "ELaN" was therefore to assess the degradation of organic micropollutants during the passage through the unsaturated and the saturated zone.
Due to the temporal variability of meteorological and hydraulic boundary conditions, the hydraulic flow field in the aquifer is not stationary as flow directions and velocities vary seasonally. Hence, basic groundwater head measurements and a two dimensional interpolation of these are misleading since they only represent the hydraulic conditions at the time of measurement and do not account for temporal patterns. Furthermore, vertical hydraulic head differences are not considered due to the lack of sufficient data and the interpolation procedure. More detailed informations on the groundwater flow field dynamics can be obtained by the use of numerical models on the basis of observed groundwater heads and surface water discharge.

This thesis originates in the request for numerical modelling of highly transient hydraulic flow fields to determine flow paths and residence times of solutes, while accounting for the interaction between surface water and groundwater. Furthermore, as management measures in the catchment have to be considered, an adequate estimation of the landscape water budget is important. The overarching aim of my thesis is to evaluate the possibilities, challenges and limitations of a physically based and fully integrated numerical model mostly used in academia in comparison to a well-established coupled iterative modular model used in practical applications, and to estimate residence times and changes in flow paths in a lowland river catchment affected by water shortage.

1.2 Current state of research

1.2.1 Groundwater - surface water interaction

Groundwater - surface water interaction refers to the exchange of water between subsurface water of the saturated zone and surface water in both directions and covers direction and quantity of exchange fluxes. This section is mainly based on the comprehensive review by Sophocleous (2002), since it is focused on aspects of groundwater - surface water interaction relevant to this work.
Any difference in hydraulic heads between two points within a water body induces flow of water along the hydraulic gradient.
In groundwater the spatial patterns of hydraulic heads and the resulting flow fields in the subsurface are controlled by various factors, which include a wide range of spatial and temporal scales and material properties and terrestrial influences.

The groundwater surface elevation is closely linked to topography and the spatial distribution of groundwater recharge (Sophocleous, 2002). Groundwater recharge is controlled by the spatial distribution of precipitation and actual evapotranspiration, which is controlled by vegetation types and water availability (i.e. the depth to groundwater table, soil moisture and soil type) (Scanlon et al., 2002; Zomlot et al., 2015).
Also physical aquifer properties influence the flow field in the subsurface, hydraulic conductivity controls the flow velocity and hence the flow volumes which result from gradient, while storage coefficient is a measure for the aquifer's ability to store water (groundwater recharge) without proportional changes in the hydraulic heads. The combination of these two parameters is called hydraulic diffusivity.
The interaction with surface water bodies also has significant effects on the hydraulic head distribution in aquifer systems. Streams can serve as drainage and discharge groundwater to the catchment outlet or provide water for groundwater recharge. Lakes, especially lakes without surficial in- and outflow, include zones of groundwater exfiltration and surface water infiltration.
In the following, the main focus is on the interaction between groundwater and streams/rivers since this work accounts for this connection. The interaction between groundwater and lakes is basically driven by the same mechanisms, yet has some differences regarding to e.g. clogging and temporal dynamics.
Streams can be classified regarding their general type of interaction with sub-

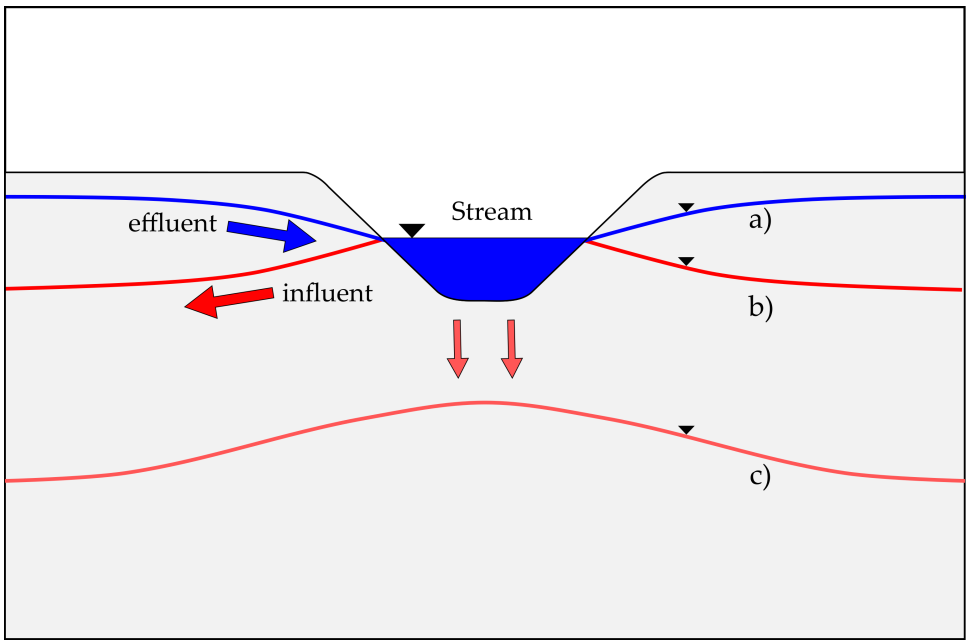

FIGURE 1.1: Hydraulic conditions at a) perennial streams, b) ephemeral streams, and c) ephemeral streams with no hydraulic connection between groundwater and stream; intermittent streams are characterised by shifts between a) and b)

surface water bodies (Figure 1.1). If the stream water levels are generally lower than the hydraulic head in the adjacent aquifer these are described as perennial streams. Perennial streams have gaining or effluent conditions and there is a more or less constant flow of groundwater discharge to the stream. The discharge of groundwater to streams originating in the storage capacity of the aquifer is called base flow.

Intermittent streams underlie gaining or losing conditions, the shift between these two states is often linked to a seasonal cycle. During periods with higher precipitation or e.g. snow melt, the stream water level is higher than the adjacent groundwater heads and water is infiltrating from the stream to the aquifer. These losing conditions end in the warmer season, when evapotranspiration through plants and lower precipitation rates lead to decreased stream discharge and hence water levels. Then, the interaction shifts to gaining conditions, where water exfiltrates from the aquifer to the stream via base flow. This depletion and following recharge of the aquifer via stream water is an important ecological factor since it provides a certain base discharge and hence the sustainability of surface streams. If the groundwater heads are always lower than the stream water values, these streams are called ephemeral streams. They are characterised through losing or influent conditions throughout the year. In cases where the groundwater table is much lower than the stream level, it is possible, that the hydraulic connection between stream and subsurface water body is cut and an unsaturated zone between these two water bodies develops (Wittenberg et al., 2013)
The direction of groundwater surface water interaction/exchange can be described due to hydraulic head differences and is relatively easy to determine. The quantity of this exchange, however, is controlled by physical properties of the aquifer and the streambed sediments. The hydraulic conductivity of the streambed in combination with the thickness of the sediment layers is the dominant factor for the exfiltration of groundwater respectively the infiltration of stream water. Both parameters are hard to quantify and are therefore often combined as a leakage coefficient to describe the physical parameter of the streambed (Wiese and Nützmann, 2009), especially when the information is needed for calculation/numerical modelling of the interaction. An important factor for the effective hydraulic conductivity of streambed sediments is clogging. Clogging describes the reduction of the hydraulic conductivity and porosity of streambed sediments. There are different forms of clogging, depending on the mechanism. External clogging describes layers of fine sediments settling on top of the streambed, as shown in Figure 1.2 on the left. Internal clogging describes the intrusion of fine particles into the pores of the streambed and decreasing pore space and thus hydraulic conductivity as shown in Figure 1.2 on the right. Internal clogging includes physical mechanisms as well as hydrogeochemical reactions which precipitate e.g. solid ferric iron or biological mechanisms, where biofilms can reduce hydraulic conductivity significantly (Hoffmann and Gunkel, 2011). Clogging is reversible, in natural systems discharge events clear the streambed of fine sediments and are even able to remove the upper layers of sediments. This can then reduce the effect of internal clogging.
The amount of clogging is linked to factors like the discharge volume and stream velocity. Furthermore, terrestrial factors like land use, soil type, and land slope, can alter sediment load and nutrient content and therefore influence clogging processes. Management measures like weirs can also have significant impacts since they potentially reduce flow velocities (Schälchli, 1992; Brunke, 1999; Wharton et al., 2017).
Physical attributes of stream beds are not distributed equally and underlie high heterogeneity. This affects hydraulic conductivity and thickness of the sediments. Rocks, for example, can provide preferential flow paths alongside their surface and alter the patterns and exchange volumes significantly. Different zones of streams, depending on the prevailing flow velocities can have different grain size distribution of the sediments due to different settling velocities. This leads to a

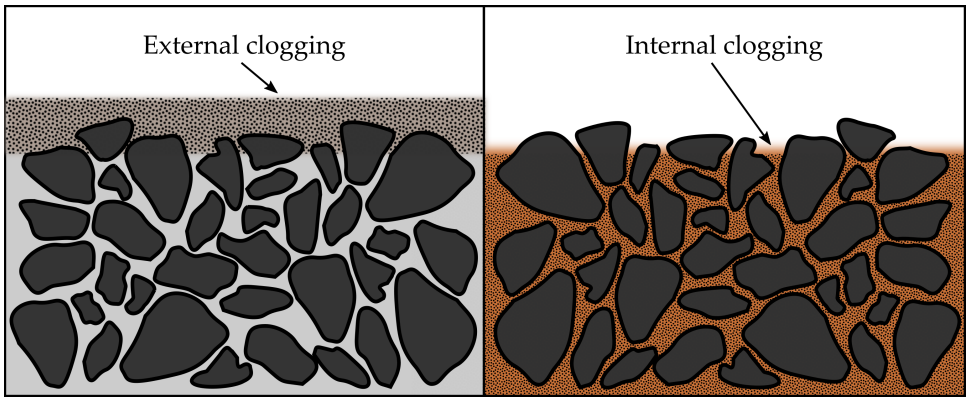

FIGURE 1.2: Conceptual drawing of external clogging (left) and internal clogging (right)

high amount of heterogeneity within the streambed.
There are also different factors which influence the groundwater - surface water interaction on a larger scale, aside of the streambed and its proximity. As mentioned above, land use in the upstream areas can control sediment load and content of nutrients and organic matter, which affects clogging processes. The topography and morphology of the catchment can have also an effect on interaction behaviour. This includes the slope of the streambed in comparison to the general slope within the valley, the shape of slopes adjacent to the streams, the geometry of the stream in terms of width and depth, the abundance or absence of meanders. The soil types present in the catchment and their spatial distribution have also an effect on the groundwater - surface water interaction, since they alter actual evapotranspiration and hence groundwater recharge as well as the hydraulic conductivity has influence on surface runoff and lateral flow of subsurface water.
Furthermore, the underlying aquifer can show very different hydraulic conductivities and alter flow fields significantly. Also, different storage coefficients can lead to different discharge behaviour after precipitation events and increased groundwater exfiltration to the stream. The aquifer distribution, i.e. the thickness of the uppermost aquifer as well as hydrogeological units and structures influence the flow pattern in the aquifer and hence the differences between groundwater head and stream water level.
As described above, there are various influences on the spatial patterns of groundwater - surface water interaction. Groundwater - surface water interaction is also variable on a temporal scale. Different hydrological boundary conditions caused by seasonal dynamics of precipitation and evapotranspiration rates lead to a distinct seasonal fluctuation of exchange behaviour between subsurface and surface water bodies. Especially intermittent streams (or stream reaches) feed from base flow of groundwater to the stream during the vegetation period. During periods with higher stream water levels, i.e. during snow melt, groundwater is recharged by stream water due to surface water infiltration. On a smaller time scale, single precipitation events can alter interaction patterns due to changed surface flow characteristics, fast response of the groundwater body, or interflow (Sophocleous, 2002).
The material properties, spatial attributes, and hydrological conditions affect the interaction of groundwater and surface water on different spatial scales at a different extent.

On the regional scale catchment topography, land use, soil types and hydrogeologic stratigraphy influences the interaction. The type of streams (ephemeral, intermittent, perennial) is determined by topography and hydrogeological boundary conditions. Land use is an important driver of evapotranspiration and hence seasonal fluctuations as well as the stream water quality and clogging potential of the streambed.
On the other hand, surface-subsurface interaction on the micro scale is mostly driven by small scale structures in the streambed like riffle-pool sequences, surface flow velocities, heterogeneity on the hydraulic conductivity or preferential flow paths. Most of these interactions can be described as hyporheic flow, which means that water, which infiltrates from the stream to the streambed exfiltrates back to the stream. This occurs, for example, at riffle-pool sequences, where the exchange is driven by differences in hydraulic pressure.
On the stream reach scale exchange patterns are driven by the groundwater flow field in the adjacent aquifer and the differences to the stream water table. While the hydraulic gradients determine the stream reach as gaining or losing, actual spatial exchange flow patterns can be quite patchy. First of all, streambed geometry has an influence on the quantity and spatial distribution of interaction. Width and depth of the stream as well as the channel cross section geometry influence flow fields and hence distribution of potential exfiltration or infiltration zones. Actual exchange fluxes between surface and subsurface then also depend on streambed characteristics. This includes clogging layers, which can vary due to different surface stream velocities and hydraulic conductivity and thickness of streambed sediments. Spatial heterogeneities in the subsurface influence spatial distribution of groundwater exfiltration or surface water infiltration also significantly.
The wide range of relevant parameters for groundwater - surface water interaction and their entanglement to different spatial and temporal scales raises challenges. In dependency on the problem different parameters have to be taken into account. To determine exchange fluxes relevant to the examined scale, appropriate methods have to be chosen. The stream network in the Lietzengraben catchment is complex and formed by human activities. It was not possible to take the whole stream network into account within this work. We focused on a single stream reach adjacent to an irrigation pond, to test assumptions and investigate the differences and consistencies between measurements and simulations on this scale. Hence, the methods described in the following paragraph aim to estimate groundwater - surface water interaction patterns and exchange fluxes on a reach scale.

1.2.2 Estimation of groundwater - surface water interaction

The temporal and spatial patterns of exchange fluxes between surface water and groundwater can vary significantly. The scale of spatial patterns range from centimetres due to small scale ripple structures in the riverbed up to hundreds of metres, when the hydraulic regime shifts from groundwater discharge to the river (gaining stream reach) to groundwater recharge by surface water (loosing stream reach) or vice versa, and their underlying mechanisms are highly dependent on the scale. Small pressure differences due to the structure of the riverbed, changing hydraulic gradients due to topography, or the heterogeneity of the subsurface can cause different spatial patterns of interaction between surface- and subsurface water (Sophocleous, 2002; Gomez-Velez et al., 2014). Also, the interaction

between surface waters and subsurface water are controlled by the hydrologic regime which causes alterations in stream velocity and water levels (surface and groundwater) and show seasonal oscillations (Anibas et al., 2016). Since the ecologic importance of the interaction between groundwater and surface water has come more in the focus of science within the last two decades (for instance Brunke and Gonser (1997) and Hayashi and Rosenberry (2002)), the development of new methods and the improvement of existing methods is a major topic in environmental sciences. In the following I will discuss some of the established and new techniques to investigate groundwater surface water interactions with their capabilities and limitations.

As shown above, the temporal and spatial scales of patterns span over a wide range. Therefore, the methods to determine patterns and/or flux rates differ in their spatial and temporal resolution.

Discharge of groundwater to streams and lakes or infiltration of surface water can be measured directly using seepage meters (Rosenberry and LaBaugh, 2008). To derive flux rates, the volume of water exchanged over a period of time is measured and thus exchange rates are calculated. While originally plastic bags where used to measure volumes (Rosenberry, 2008; Rosenberry, 2005), newer studies make use of electromagnetic flow measurements (Rosenberry and Morin, 2004) or use heat as a tracer (Mwashote et al., 2010). While the principle of this method is simple, there are some limitations. The installation of seepage meters causes distortion in the sediments and can lead to preferential flow paths (Rosenberry et al., 2010). Also, external forces like waves can have an effect on the results (Rosenberry, 2008). Furthermore, caution is advised when flow rates lie below a certain treshold (Cable et al., 2006). Seepage meter measurements are point measurements, which need time and quite some effort for installation, the methods ability to collect data over many points is limited by practical considerations.

Like in other parts of hydrology, the use of natural tracers is also common. Depending on the questions to be investigated and boundary conditions at the study site different approaches are used in research. In the last decade, the use of heat as a natural tracer has become more and more popular. Based on an analytical solution of the equation describing convective heat transport in a porous medium for 1D vertical flow under steady state conditions, exchange rates can be calculated (Bredehoeft and Papaopulos, 1965). Schmidt et al. (2006) developed a lance with thermistors included to measure depth profiles of temperatures in the sediments and then derived flux rates from fitting parameters of the heat-transport equation to measured data.

However, the solution by Bredehoeft and Papaopulos involves the assumptions of steady state conditions, homogenous material, and vertical flow and therefore has its limitations in practice, when it is unclear if these assumptions are valid. Violation of these assumptions cause errors in the estimation of flux values (Schornberg et al., 2010; Anibas et al., 2009). Despite these limitations, the method was used to investigate groundwater flow to lakes (Meinikmann et al., 2013; Rudnick et al., 2014) and streams (Schmidt et al., 2006; Schmidt et al., 2007; Anibas et al., 2011; Suck, 2008) and yielded reasonable results. Using techniques from time series analysis, Anibas et al. developed a method to estimate exfiltration and infiltration fluxes over time from recorded temperature profiles (Anibas et al., 2016).

Selker et al. established a method to estimate exchange patterns based on sediment temperatures measured by fibre optical temperature sensing (FO-DTS) (Selker et al., 2006a; Selker et al., 2006b). The FO-DTS technique, which originates

in engineering, allows to identify stream reaches with influent or effluent conditions (Lowry et al., 2007; Krause et al., 2012). Vogt et al. (2010) used a different setup of the fibre optical cable to measure vertical temperature profiles at a high spatial resolution. Despite the advantages of this FO-DTS, namely continuous measurements over long distances at a spatial resolution of metres, there are some limitations.
Rose et al. (2013) investigated the limitations of FO-DTS due to signal amplitudes needed to get reliable results. The influence of seasonal variations on the results of fibre-optical temperature measurements was also investigated (Krause and Blume, 2013). They found that measurement campaigns are best done during winter with lower daily oscillations of air temperature and using a specific mode for temperature measurements using FO-DTS.
Numerous studies used FO-DTS to investigate groundwater exfiltration to lakes and streams and showed the general reliability of this method despite its general limitations (Hare et al., 2015; Vogt et al., 2012; Anderson et al., 2014).
To extend the possibilities of the FO-DTS technique, Kurth et al. (2013) suggested to heat the metal coating of a fibre-optical cable to derive thermal properties of the surrounding material and estimate flow rates and interaction patterns by measuring the rate of cooling of the cable afterwards.
While the use of fibre-optic cable accounts for scales of metres to kilometres, very small scale flow patterns of water in streambed sediments can be investigated using the heat-pulse technique developed by Lewandowski et al. (2011) and further improved by Angermann et al. (2012). The device measures breakthrough curves of sediment temperatures at various thermistors arranged around a heat source. An algorithm then calculates three dimensional flow direction and flow velocity based on time lags and amplitude dampening in the measurements. However, this method only applies on small scale flow in the order of centimetres and is work intensive (Lewandowski et al., 2011).
To asses spatial patterns of groundwater - surface water exchange along a stream reach and estimate exfiltration rates a combination of two methods seemed promising. FO-DTS measurements provide temperature values with a spatial resolution of 1 metre and thus allow the estimation of spatial patterns along the stream reach. Measurements of sediment temperature profiles and processing them on the method described by Schmidt et al. (2006) provide discharge rates of groundwater at various points along the stream. To determine the seasonal variation of the spatial distribution of groundwater discharge, multiple measurements can be conducted. Since both methods rely on heat as a natural tracer, the results can be compared well with each other and provide a good basis for the overall estimation of groundwater - surface water exchange patterns along the stream reach. Due to the morphological and hydraulic boundary conditions, mostly effluent conditions are expected. Therefore, the limitation of the examination of sediment temperature profiles to only quantify groundwater exfiltration is not disadvantageous.

1.2.3 Modelling approaches

As shown in the previous sections, mechanisms of the exchange between subsurface water and surface water have been understood in theory and concepts, which explain a wide range of observed spatial and temporal patterns, have been developed. Furthermore, various methods to determine these fluxes have been developed and validated. To investigate processes and improve the understanding

of the complex interaction patterns between subsurface and surface, it is necessary to combine hypothesis and measurements with numerical experiments. This not only gives the opportunity to test conceptual models, but also allows applying the gained knowledge to practical problems concerning management strategies, the impact of climate change and general environmental consequences caused by changes of the meteorological and/or hydrological boundary conditions.
Over the last decades, numerical models have been increasingly used. This development is closely linked to the progress in computation and the improvement in the implementation of numerical methods as well as underlying concepts of numerical models describing surface water-groundwater interaction.
This section summarises concepts and their challenges, limitations and advantages. Previous studies based on the two models used in this work will be briefly summarised. A further overview of code used for the simulation of groundwater - surface water interaction can be found for example in Wittenberg et al. (2013), together with more details and references to relevant articles. Therefore, this work just mentions the main concepts and some advantages and challenges of the different concepts.
Afterwards the reasons for the choice of the models we used will be summed up.

Concepts

To simulate the exchange between surface and subsurface water, models describing groundwater flow are linked to models simulating surface water movement. The exchange between the models can be controlled by a leakage coefficient, which reflects sediment thickness and its hydraulic conductivity (Wiese and Nützmann, 2009).
The concepts underlying the simulation of groundwater - surface water interaction can be divided in three different types: (fully) integrated models, alternating iterative models, and external (sequential) models (Morita and Yen, 2002). No model or type of model can be considered superior in general since all of have strengths and weaknesses. This is the reason why the number of different codes used for the simulation of groundwater, surface water and their combination is large.
External (sequential) models rely on the exchange of simulation results of separate models. Mostly, surface models are used as a first step, since surface runoff reacts much faster than groundwater flow to external forces (e.g. precipitation) (Wittenberg et al., 2013). Big advantages of these modelling systems are the shorter computational times since no iteration between the involved models is needed and the possibility to use existing models for one domain and expand it to the other domain and the interaction between these. Despite being not as accurate as iterative or integrated models, the use of existing models without a new parametrisation is very time-saving. Also, both models can use different spatial and temporal discretisation.
Alternating iterative coupling of surface and subsurface flow models is very common and a lot of different modelling systems are available. Wittenberg et al. (2013) describes some of the most well-known codes currently used. This type of coupling allows the use of different, already available models to form a new coupled modelling system. The exchange of internal boundary conditions is controlled by a model framework and makes use of internal (software) interfaces (Becker, 2010). The internal boundary conditions between groundwater and surface water

model are exchanged and considered until a certain error criteria is reached (Wittenberg et al., 2013). This type of model is very suitable to deal with questions on catchment or regional scale since it is not necessary that spatial discretisation of the two models concur. Only the points of time, at which solutions are exchanged between the models, have to be the same. This allows using different, appropriate, temporal and spatial resolution for the two models, which saves computational resources.
Integrated models have been already conceptualised by Freeze and Harlan (1969). Due to the lack of sufficient computational resources, the application on a reach or catchment scale has not been possible until a decade ago. This type of model is based on the principle of conservation of mass and momentum between surface and subsurface water. This allows investigating, for example, processes in the hyporheic zone or transport of solutes across the groundwater - surface water interface. Unfortunately, these models have a high demand in computational power, parameter datasets and are therefore predominantly used within academia.

Challenges

The numerical modelling of the exchange between surface water and subsurface water faces some challenges.
Scale: Surface water-groundwater interaction stretches over various scales. Numerical models are limited in terms of computational resources e.g. computational time. As a consequence, the simulation of, for example, micro flow paths due to small streambed structures on a catchment scale is not possible. Topography, which is a very important driver for exchange fluxes, makes it necessary to represent governing structures accurately. This is of high importance when it comes to small scale hyporheic flow. This requirement influences the grid, i.e. the spatial discretisation of the model. Hence, the modelling of surface water-groundwater interaction is always a trade-off and it is essential to adapt to the question to be worked on.
Parameter availability: Most models, especially physically based models, need a large amount of parameter data describing the physical properties of the aquifer, streams and other important factors like land use (vegetation, sealing, urbanisation, agriculture), and so on. The possibility to work with physically based equations is a huge advantage when it comes to process understanding and testing of hypothesis. On the other hand, parameters have to be chosen carefully; ideally one has measurements of parameters at the scale of spatial discretisation of the model. Since this is not possible due to measurement limitations (suitable methods, time, funds), it is common to use values from literature and to calibrate the model by changing unknown parameters (Hill and Tiedeman, 2007). This leads to a degree of uncertainty due to the over-parametrisation and the resulting ambiguousness, since different sets of parameters can lead to the same (reasonable) result yet describing mechanisms and processes incorrectly (Beven, 1989). Therefore, it is important to choose parameters carefully and test the model for sensitivity to the parameters.
Numerical stability: Despite most models use numerically robust techniques, numerical instabilities can cause major problems, especially in integrated models. The velocities of groundwater flow and surface water movement differ by orders of magnitude, processes of drying and re-wetting of unsaturated zones can cause situations, where the solution of the time step does not converge, causing the model to stop. Mostly, these problems can be avoided using appropriate spatial

and temporal discretisation. This can lead to very long computational times and complicate the application of these models for practical problems (Huyakorn and Pinder, 1988; Brunner and Simmons, 2012).

Applied models

The models used in this work to simulate the groundwater - surface water interaction represent two different concepts. ArcEGMO-ASM is a hydrological iterative model which is mostly used for practical applications, while HydroGeoSphere is an integrated model and has been used for research purposes. This section gives an excerpt of studies which have been conducted using these models in the past. At the end of the section, the reasons for the choice of these models within this study are summed up.

ArcEGMO-ASM (Iterative model) ArcEGMO (Becker et al., 2002) is a hydrological iterative model of modular structure. Like the name suggests, it is equipped with an interface to GIS-applications. Different parts of the hydrological cycle are accounted for in a modular manner. Depending on the particular questions to be answered, different modules are available within the software and coupling with different models accounting for soil water or groundwater is possible.
In the original form, groundwater is simulated as a transient storage. Within this work, the two-dimensional finite difference model ASM (Kinzelbach and Rausch, 1995) was used to account for groundwater flow and coupled to ArcEGMO using internal interfaces. In section 1.2.3 this is described in more detail. The structure of the model and the joining of areas of similar hydrological properties to so-called “hydrotopes” allow a fast simulation of relatively large catchments to investigate the influence of changes in land use, climate or different management strategies on the landscape water budget, discharge volume and groundwater levels. The structure of the model and the possibility to choose from different software libraries to adapt the model to the application made it an interesting tool to work on different kinds of problems.
Lahmer et al. (2001) tested the effects of land use and climate change scenarios on the discharge behaviour in two separate sub-catchments of the Elbe River. The catchments were 575 km^2 respectively 1.158 km^2 large. Pfützner et al. (2006) used ArcEGMO in combination with the soilwater model PSCN (Klöcking et al., 2012) and the groundwater model ASM (Kinzelbach and Rausch, 1995) to investigate the consequences of the termination of the irrigation of wastewater to the Lietzengraben catchment. They furthermore evaluated different strategies to overcome the resulting water-shortage and dry fall of lakes and streams. This model was used within this thesis with some minor changes and updated input parameters. Mey (2011) used the same model combination to work on the water shortage in the Luchsee area which leads to ongoing peat degradation. Possible drivers for this development such as drainage channels, groundwater extraction and land use (mainly forests) were evaluated to find the main factor for the decreasing groundwater levels. Nützmann and Mey (2007) investigated possible reasons for the observed decrease in stream discharge in a small lowland stream without any remarkable changes in precipitation.
The list of examples for the use of the model in catchments located in the lowlands of North Germany is much longer. The model is widely used to evaluate land use changes, changes in climate, management strategies, soil moisture budget and has demonstrated that it is a reliable tool to answer questions concerning water

budget and discharge behaviour in catchments of various sizes.
The modelling system ArcEGMO-ASM was used in this work for several reasons. The model represents a common and widely used type of model and has often been applied successfully to lowland catchments in North Germany. The model has already been built for the Lietzengraben catchment and has been carefully validated and has successfully been used to develop management strategies in the catchment (Pfützner, 2004; Pfützner, 2005; Pfützner, 2007). Hence, it provided a good basis and only minor updates have been necessary to obtain a model which could be used as a reference model from practice.

HydroGeoSphere (Integrated model) HydroGeoSphere (Therrien et al., 2012) is a physically based integrated model which includes two dimensional surface flow and variable saturated subsurface flow in three dimensions. The wide variety of possibilities provided by HydroGeoSphere makes it an excellent and increasingly popular model to investigate processes and mechanisms in hydrology. Especially the conservation of mass across the groundwater - surface water interface makes it an interesting tool when it comes to the transport of solutes.
The capability of HydroGeoSphere to simulate groundwater flow and discharge behaviour on a catchment scale has been shown by various authors after the release of HydroGeoSphere.
The HydroGeoSphere code was proven applicable on a catchment scale first by Sudicky et al. (2008), when a sub-catchment of approx. 17 km^2 was modelled. They showed that the model was able to reproduce discharge responses to rainfall events and hydraulic head distribution moderately well. They emphasized the need for better parametrisation and incorporation of evapotranspiration processes to improve model results (Sudicky et al., 2008). In a following study, which included the whole catchment, Jones et al. (2008) then showed that also on this scale HydroGeoSphere is able to reproduce the discharge and hydraulic heads and concluded its suitability to address large scale watershed problems.
Li et al. (2008) managed to calibrate a model of a 287 km^2 catchment to measured discharge records, but also pointed out, that the evapotranspiration processes have a critical role in order to represent discharge behaviour well. Also, they underlined the importance of the choice of appropriate initial conditions for calibration.
Since the general validity of the model had been shown and the fully coupled approach opened new possibilities in numerical modelling, scientists used the code to address different scientific questions and problems.
Frei et al. (2012) investigated the effects of small topographic structures of wetlands on the exchange between surface and subsurface water and the runoff generation using a synthetic topographic dataset and HydroGeoSphere. They showed, that biogeochemical hotspots can also relate to subsurface flow patterns triggered by topography and not only by subsurface heterogeneity.
To look at the whole catchment, Frei and Fleckenstein (2014) managed to represent the micro topography within HydroGeoSphere using a set of superficial surface property parameters.
Using the hydraulic mixing cell method, which allows to account for the amount of groundwater in the surface water at any point of a stream (Partington et al., 2011) and improving it, Partington et al. (2013) interpreted the mechanisms of streamflow generation.
Liggett et al. (2015) used the model to investigate the transport of dissolved organic carbon in the catchment. They were able to reproduce some aspects of

the transport mechanisms in the catchment while they missed others. They concluded, that the use of fully integrated surface-subsurface models can be helpful, but needs data from field measurements since there are still some problems regarding dispersion across the interface surface-subsurface and ambiguousness of the transport equation.
In summary, this series of studies shows impressively, how to make use of HydroGeoSphere model which incorporates surface-subsurface flow in a fully coupled manner to investigate the influence of topographic features on a small scale on discharge behaviour and subsurface flow patterns, the significance of these flow patterns on biogeochemistry, transfer the yielded information on the whole catchment and investigate the distribution of solutes using the information which was collected.
HydroGeoSphere was also used to assess the impact of climate change scenarios on the groundwater reserves in a 465 km^2 catchment (Goderniaux et al., 2009), to evaluate the uncertainty connected to the simulations (Goderniaux et al., 2011), and to address the issue of the influence of spatial discretisation on the performance of this large-scale model (Wildemeersch et al., 2014).
Others investigated the influence of spatial discretisation on the ability of models to describe the soil moisture distribution with HydroGeoSphere (Sciuto and Diekkrüger, 2010; Cornelissen et al., 2013; Cornelissen et al., 2014) and compared the results of HydroGeoSphere with other hydrological models, namely MIKE SHE and ParFlow-CLM (Koch et al., 2016).
The ability of HydroGeoSphere to simulate heat transport was used by Brookfield et al. (2009) and Munz et al. (2016).
The decision to use HydroGeoSphere in this work was made due to its ability to simulate flow paths of particles from the surface to the subsurface via infiltration and back to surface water bodies through exfiltration. Postprocessing of the simulation results allows the estimation of residence times. Since HydroGeoSphere has not been applied to a heavily anthropogenic influenced catchment on this scale yet, to the knowledge of the author, it was a good choice to evaluate the possibilities of this physically based modelling system in a case, where in practice more simple models like ArcEGMO-ASM are used. The trade-off between spatial details, important for stream networks, irrigation ponds, and management measures like weirs, and the computational resources needed to apply the model on a catchment scale was challenging and a benchmark for the usefulness of scientific models to practical application. It was the highly sophisticated, elaborate counterpart to the established but simpler model system ArcEGMO-ASM.

1.3 Research questions

The previous sections describe the motivation and goals of this study in general and available tools to estimate groundwater - surface water interaction and different concepts and software to simulate this interaction numerically. In the following section research questions are derived from the general study goals. These questions provide a “road map” for the preparation of sub-questions and the approach to answer these.
HydroGeoSphere was used in previous studies at various scales. Since it is not necessary to designate surface water bodies while building the model, handling of stream networks differs from iterative models, where surface water bodies have to be defined in advance.

Depending on the scale and study goal, surface elevation has been smoothed along nodes with surface streams (Li et al., 2008) to ensure gravitational flow, the riverbed has been represented quite accurately (Brookfield et al., 2009) along a short reach, or digital elevation models were used without any modification (Goderniaux et al., 2009). The representation of a network consisting of mostly drainage channels of anthropogenic origin on a catchment scale has not been done, to the knowledge of the author. The bottom of these streams is much lower than the adjacent terrain and therefore effective for the drainage of groundwater. On the other hand, the size of these streams is very small, compared to the catchment. This big difference in scale is significant and challenging. Additionally, the discharge of big volumes of treated wastewater to the system is also quite unusual and has not been simulated using HydroGeoSphere. Other management measures like weirs have also not been included in studies using HydroGeoSphere. The combination of the numerical modelling of a catchment characterised by artificial drainage channels, discharge of large amounts of additional water to some areas and the presence of weirs is clearly challenging and brings the question if a physically based fully integrated model can be used with appropriate effort to yield equal or better model performance by means of system behaviour in comparison to established iterative models.
The basis for this work is the hypothesis that, given reasonable simplification and careful parameter handling, the catchment modelling using a highly sophisticated model is possible and gives additional insights into system behaviour and mechanisms, which is not possible using iterative modular models.
Since the previous modelling of the Lietzengraben catchment included 2D modelling of groundwater heads coupled iteratively to surface modelling, the results gained by using a fully integrated approach with three dimensional representation of the subsurface flow will differ and allow more accurate estimation of residence times. This is also valid for the calculation of residence times using gradients derived from measured groundwater heads.
The performance of different models in simulating for example soil moisture (Koch et al., 2016) and connectivity between surface streams and subsurface (Brunner et al., 2010) has been investigated in the past. However, these studies were conducted with a scientific background and assessed different parameter sets or equations. Since computational resources and therefore the possibilities to use more complex models have grown in the last decade and will most likely improve in the future, it is worth looking at the possibilities of highly sophisticated models like HydroGeoSphere within questions arising from practise. As it was mentioned in Section 1.2.3, HydroGeoSphere was used to evaluate the consequences of climate change for groundwater reserves, for example by Goderniaux et al. (2009). This study, however, did not include smaller streams and was focused on one larger river, which was sufficient for the scope of the study. Like mentioned in the previous section, a fully integrated model should give more insight into transport paths and residence times than it is possible for an iterative model. On the other hand, it is unclear to what extent the simulation of a catchment using two different model concepts come up with different results regarding water balance, groundwater heads, and discharge behaviour. Since the more complex model includes mechanisms and processes on a physically driven basis, it is to be expected, that the representation of discharge behaviour and groundwater heads is more accurate than using an iterative model, and that elements of the water balance are reproduced correct as well.

1.4 Approach

In order to investigate the research questions formulated in the previous section and survey the hypothesis stated, the main questions were split into different tasks.
HydroGeoSphere was the model of choice to investigate the possibility of simulating a heavily anthropogenic influenced catchment using a fully integrated model. To allow for comparison, data already used in an existing iterative model (ArcEGMO-ASM) was used for parametrisation whenever possible. We started using high spatial resolution of the grid for the simulation, and then coarsened the grid and hence parameter distribution until it was possible to actually run the model on our hardware. Calibration was conducted using the automated calibration algorithm PEST (Doherty, 2010). The results from the calibration were used to assess parameter sensitivity.
The resulting HydroGeoSphere (HGS) model of the catchment was used to estimate flow paths and residence times of solutes which infiltrate beneath the irrigation ponds. To obtain these, the particle tracking capability of the post-processing software TECPLOT was used.
To compare the results gained by using HGS, the existing ArcEGMO-ASM model had to be updated in terms of input time series and complemented with an irrigation pond, which has not been included in the original model.
After validation of this updated model a comparison of the results gained from HydroGeoSphere, ArcEGMO-ASM, and field measurements had to be undertaken to compare quality of the models and to test hypothesis stated earlier. The focus of these comparisons were the general representation of the catchment dynamics (groundwater heads and stream discharge), the representation of groundwater - surface water interaction in comparison to field measurements undertaken downstream of pond “Teich 11”, resulting water budgets of the simulations, the estimation of flow paths and residence times from particle tracking based on HydroGeoSphere, 2D groundwater data from ArcEGMO-ASM and interpolated field measurements of groundwater heads.
In order to evaluate handling and feasibility of the different models, experiences and notable differences in the process of this work have been compared and their advantages and limitations have been highlighted.

2 Study site

2.1 Lietzengraben catchment

The Lietzengraben catchment (Figure 2.1) is located north-east of Berlin, Germany. It is a lowland catchment and about 54 km^2 in size with elevations ranging from 91 m.a.s.l. in the north-east to 48 m.a.s.l. in the south. The main stream is the Lietzengraben, which originates in the northern part of the catchment south-east of Lake Gorin, and discharges into the river Panke at the southern boundary of the catchment. The Lietzengraben stream and the stream "Graben 2" are the only streams in the catchment which are of natural origin. In course of the wastewater irrigation at sites within the catchment from 1905 to 1985 (Ginzel, 1999), a multitude of drainage channels were installed and a network of these still exists today. The majority of the streams in the catchment exhibits a streambed substantially lower than the surrounding terrain to ensure an effective drainage of the adjacent area. The network of streams and drainage channels influences the discharge dynamics of the stream as it contributes and diverts discharge. In the central part of the catchment, upstream of gauge OW2, streams from the irrigation ponds discharge into the Lietzengraben. Further downstream, the Seegraben diverges from the Lietzengraben and flows into the lake Bogenseekette (labeled as (2) in Figure 2.1). The outlet of the lake confluences with the Lietzengraben at the southern end of the lake.
Downstream of stream gauge OW6, some of the water from the Lietzengraben is sidelined to the Karower Teiche (labeled as (3) in Figure 2.1), which are not part of the surficial catchment of the Lietzengraben, but are included into this study since they are connected to the Lietzengraben and hence are part of the hydrological system. They have been under investigation in previous studies (Pfützner, 2007; Mey, 2011). Downstream of the sideline to the Karower Teiche, the Lietzengraben discharges into the River Panke. Water from the Karower Teiche also discharges into the River Panke, in some distance downstream to the confluence of the Lietzengraben to the Panke. Three lakes are located within the catchment. Lake Gorin in the north-western part of the catchment is a groundwater fed, shallow lake with no direct connection the Lietzengraben stream. Lake Bogenseekette is a group of four connected, lined up, shallow lakes in the lower part of the catchment. The lake is fed by the streams "Seegraben", which is a branch of the Lietzengraben, and "Waldgraben". Both streams discharge into the northern lake of the chain of connected lakes. The lakes are connected to Lietzengraben at the southern end of the chain of lakes. The Karower Teiche and the lake Bogenseekette and the surrounding wetlands and meadows are ecologically important habitats for birds and are a nature conservation area (Kempe, 1991; Klemm and Lindner, 1995). The Karower Teiche are a group of four ponds south of the Lietzengraben near its outlet into the river Panke. Like the Bogenseekette, these ponds are shallow, connected to and fed by the Lietzengraben, and they discharge to the river Panke via a stream outlet at the western side of the lakes.
The previous description of the water bodies and streams only includes the most important features of surface water in the catchment. As it is shown in Figure 2.1,

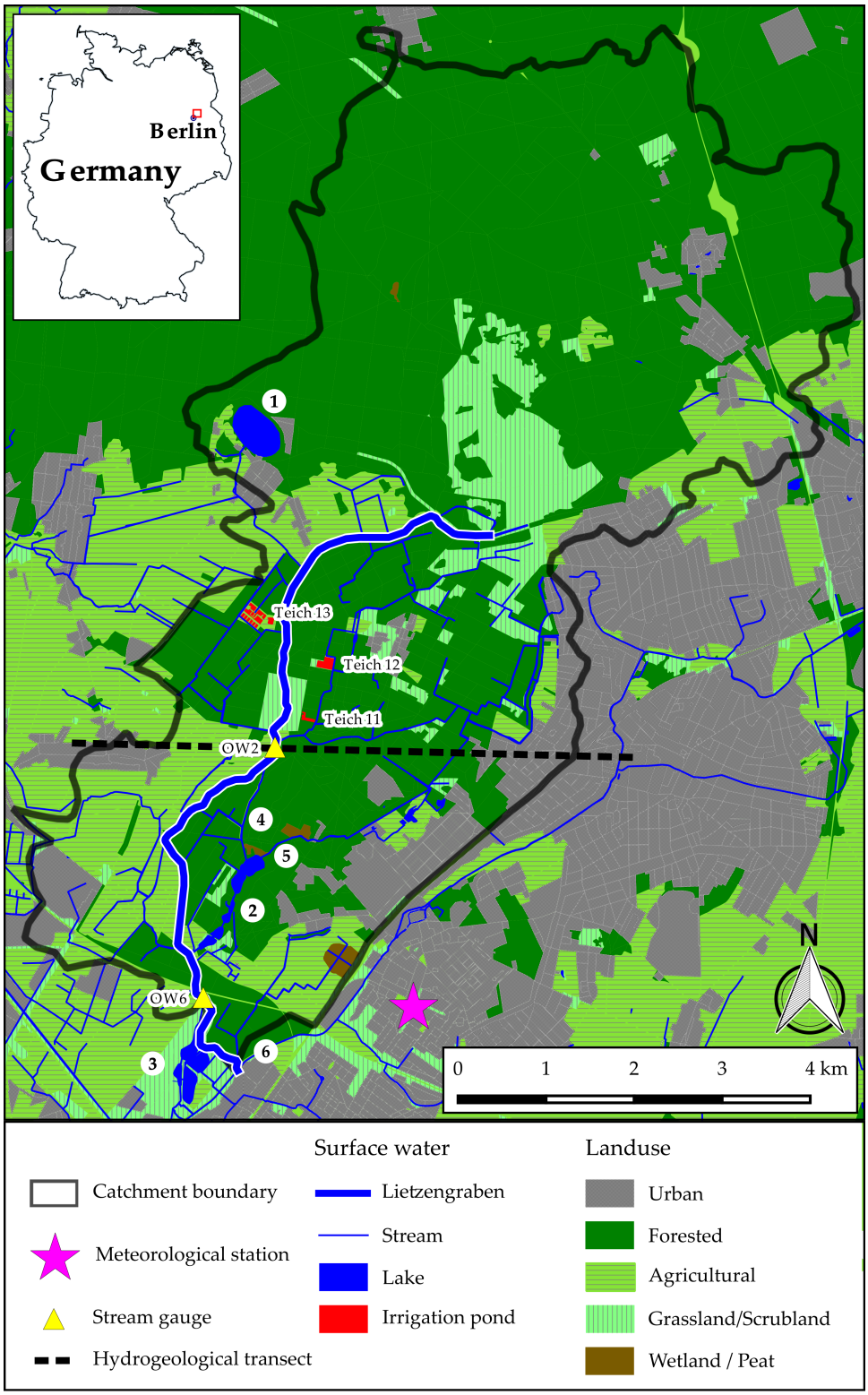

FIGURE 2.1: Map of the land use in the Lietzengraben catchment; (1) Lake Gorinsee, (2) Lake Bogenseekette, (3) Karower Teiche, (4) Seegraben, (5) Waldgraben, (6) River Panke, the hydrogeological transect is shown in section 2.5; source: GeoBasis-DE 2013

the catchment incorporates a multitude of streams and drainage ditches.

2.2 Land use

The Lietzengraben catchment is dominated by forested areas, scrublands, meadows, and agricultural areas. Some small wetlands are present along the Lietzengraben stream. Some areas along the south-eastern boundary of the catchment are urban, only few villages are located within the catchment.
The consideration of the historical development of the land use in the Lietzengraben catchment over the last century is of importance to understand the present day conditions and the questions linked to this development. Beginning in 1905, parts of the untreated wastewater from Berlin was irrigated to irrigation fields located in the Lietzengraben catchment. The infiltration into the sandy soils and the subsurface passage to drainage channels removed nutrients and contaminants. While the discharge volumes in relation to the irrigation area were moderate with 1,500 mm in the beginning, they increased drastically over time and reached up to 10,000 mm after the 1970s (Ginzel and Nützmann, 1998). These volumes exceeded the infiltration capacities of the soils and discharged directly into surface streams. Furthermore, due to the increase of industrial activities, the load of nutrients and pollutants increased, beginning in the 1960s. In 1985 operations were suspended after a sewage treatment plant became operational. The shutdown of the discharge of wastewater became noticeable in 1989/1990. The groundwater table was declining, affecting wetlands and forested areas. Furthermore, a mobilisation of the nutrients and heavy metals, which had been accumulated in the soil as a consequence of the discharge of contaminated wastewater, was expected (Nützmann et al., 1992). Hence, studies were conducted to assess the risks of the contaminants and suggest measures and strategies to handle these. Ginzel and Nützmann (1998) found very high concentrations of heavy metals like, for example, lead, cadmium, and nickel in the uppermost soil layers in areas of former irrigation fields. Due to oxidation processes and the resulting acidification of the soil, heavy metals were mobilized and found in groundwater samples. Partially, the concentrations exceeded critical values by an order of magnitude (Ginzel and Nützmann, 1998). The contaminants reached surface streams via groundwater exfiltration. Ginzel (1999) suggested measures to immobilize contaminants in the soil in order to prevent ongoing leeching of heavy metals into the groundwater, and to stabilize the water balance. Key measures were the reduction of groundwater recharge in the contaminated areas to reduce leeching of contaminants by the introduction of marl in the upper soil and reforestation of affected areas. To stabilize the water balance, the discharge of additional water in the catchment and the installation of weirs to obtain higher groundwater levels were suggested. The deficit in the water balance became apparent in 2003, when the Karower Teiche fell dry. The increased evapotranspiration due to reforestation and climatic changes decreased the baseflow to streams and lead to a substantial lack of water.
Various management measures have been implemented. The water levels have been elevated by installing groundsills at different streams in the lower catchment. The installation of weirs allowed a controlled elevation of water levels in the streams to recharge the adjacent aquifer during wet periods. However, most of the weirs are not controlled actively, except to prevent damage to the structures

during exceptional discharge events.
Possible management strategies to improve the situation by discharge of treated wastewater and the use of weirs were evaluated by the the consultants of "Büro für Angewandte Hydrologie" in Berlin (Pfützner, 2004; Pfützner, 2005; Pfützner, 2007; Mey, 2011). The discharge of treated wastewater into ponds started in 2005 and the discharge conditions during the vegetation period were improved.
As a result of the history and today's management strategies, the area is dominated by a network of streams, forested areas, and the agricultural use is limited to grassland.

2.3 Climate

The climate of the Lietzengraben catchment was characterised as a transition climate between maritime and continental with an urban influence (Hupfer and Chmielewski, 1990). Figure 2.2 shows the monthly mean temperature and the monthly mean precipitation sums during the period from January 1969 to December 2013 at the meteorological station Berlin-Buch (52.6336° N, 13.5042° E, 63 m.a.s.l.). The climatic conditions are humid with an average annual precipitation of around 590 mm and an average temperature of approx. 9.1 °C. For the north-east of Germany Gerstengarbe et al. (2003) determined an average evapotranspiration of 510 mm and a precipitation of 610 mm per year. This results in 100 mm runoff per year, of which 80 mm are groundwater recharge (Gerstengarbe et al., 2003; Lahmer and Pfützner, 2003). The amount of groundwater recharge is highly dependent on the topography of the respective area. While in lowlands the groundwater recharge can be negative, it can be up to 200 mm per year on hilly grounds, as a consequence of the distance between the saturated zone and land surface, limiting the availability of water for evapotranspiration (Lahmer and Pfützner, 2003). Pfützner (2005) determined an annual actual evapotranspiration

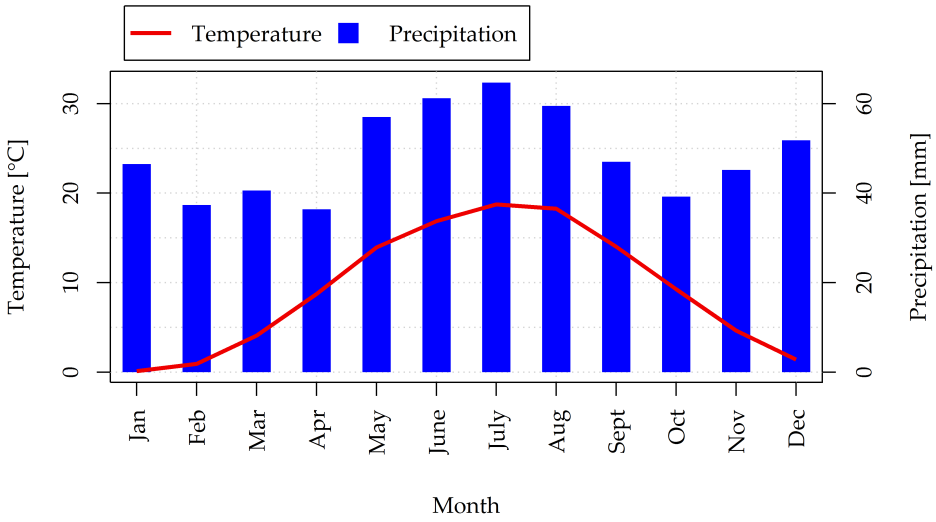

FIGURE 2.2: Monthly mean temperature and montly mean precipitation sum during the period 1969 - 2013 at the meteorological station Berlin-Buch

of roughly 505 mm for the Lietzengraben catchment and a groundwater recharge of 107 mm per year. However, the climatic conditions in North-East Germany have been subject to changes over the past decades. Gerstengarbe et al. (2003)

determined decreasing annual precipitation sums, increasing temperatures and, as a consequence, increasing evapotranspiration rates. Furthermore, precipitation will most likely decrease during the summer months and increase during the winter months (Lischeid and Nathkin, 2011). Hence, droughts and decreasing groundwater levels are a major concern in the region, which will intensify in the future. The water shortage affects economical goods such as agricultural and silvicultural production, as well as important contributors to biodiversity like wetlands, small lakes, and streams.

2.4 Hydrology

The system of streams and lakes in the catchment is highly influenced by the past operation of wastewater irrigation, as described in the previous sections. Figure 2.1 shows an overview of streams and lakes, with the Lietzengraben being highlighted. The stream gauges OW2 and OW6 monitor the discharge downstream of the outlets of the irrigation ponds and OW6 monitores the discharge at the catchment outlet, respectively.

Lowland streams are generally dominated by groundwater baseflow, which contributes major parts of the discharge, especially during dry periods (Nützmann and Mey, 2007). Most of the streams in the catchment, with exception of Lietzengraben and "Graben 2" (south of pond "Teich 11"), are artificial and constructed to drain the adjacent areas. Hence, the exfiltration of groundwater is enhanced due to elevation differences.

The suspension of the wastewater irrigation in 1985 lead to a decrease of the stream discharge from $1.2\,m^3\,s^{-1}$ to less than $50\,l\,s^{-1}$ (Pfützner, 2003; Mey, 2011). With dropping groundwater tables, some of the streams fell dry during dry periods due to insufficient baseflow. The gravity of water deficit became apparent in 2003, when parts of the lakes and wetlands fell dry (Pfützner, 2004). Mey (2011) showed that a minimum discharge of $50\,l\,s^{-1}$ at OW2 is needed to sustain wetlands and lakes during summer.

Since the year 2005, treated wastewater is discharged into ponds. The annual sum of the discharge is about 1.8 million $m^3\,a^{-1}$. The temporal distribution of discharge volumes have been constantly $5{,}000\,m^3\,d^{-1}$, and were changed in 2010 to higher volumes in summer and lower volumes in winter with a unchanged annual sum of discharged water. The total discharge of water into the irrigation ponds is shown in Figure 2.3 on a daily basis. The water is discharged to three ponds or group of ponds, respectively. Pond "Teich 13" is located west of the Litzengraben and consists of multiple ponds. One group of these discharges into a stream north of the ponds while the other discharges into a stream south of the ponds. Both streams confluence and discharge into the Lietzengraben in the central part of the catchment, south of pond "Teich 13". Pond "Teich 12" is located east of the Lietzengraben and discharges into a stream to the North. The stream changes direction to the south were water from pond "Teich 11" discharges into it. The water then discharges into the Lietzengraben south of the discharge of water from pond "Teich 13" to the Lietzengraben. Contrary to the other ponds, pond "Teich 11" became operational in the beginning of 2007, two years after the start of discharge of treated wastewater to the catchment.

The mean discharge observed at the stream gauge OW2 (Figure 2.3), located

between the confluence of the lake Bogenseekette outlet and the branch-off to the Karower Teiche (Figure 2.1) during the period 2005 to 2012 was 78 l s^{-1}. The minimum discharge volumes occurred in most years during the growing season. The mean annual minimum discharge in the period 2005 to 2012 was 33 l s^{-1}. The maximum discharge was reached in the beginning of the year, with an mean annual maximum of 180 l s^{-1}. The mean discharge observed at the stream gauge OW6 (Figure 2.3), located downstream of the discharge of the pond outlets to the Lietzengraben (Figure 2.1), during the period 2005 to 2012 was 138 l s^{-1}. The minimum discharge volumes occurred in most years during the growing season. The mean annual minimum discharge in the period 2005 to 2012 was 36 l s^{-1}. The maximum discharge was reached in the beginning of the year, with an mean annual maximum of 392 l s^{-1}. The meteorological conditions in 2011 were exceptional, since low temperatures and higher precipitation than normally limited the baseflow conditions to short period in July and August which was followed by precipitation and high discharge volumes (Scheffler and Werkethin, 2012).

The effect of the discharge of treated wastewater is substantial. The compari-

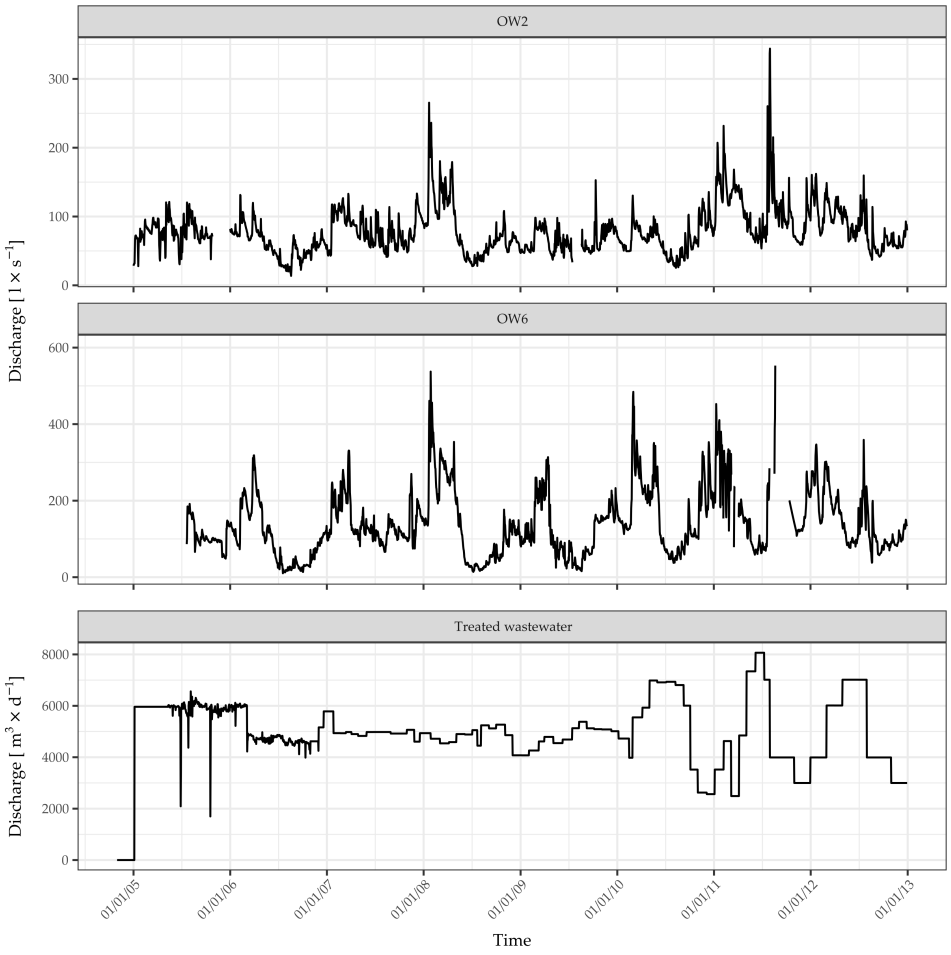

FIGURE 2.3: Stream discharge at the gauges OW2 and OW6 (top) and daily values of the discharge of treated wastewater, summarized for all ponds (bottom)

son of the period with a constant discharge rate with the period with dynamic discharge rates showed the importance of this additional water. During the years 2006, 2008, and 2009, the discharge at OW2 dropped to a annual minimum discharge between 14 and 33 l s^{-1}, hence below the discharge volume which is

required to sustain lakes and wetlands (Mey, 2011). At the gauge OW6 this was more distinct, with values between 10 and 15 l s^{-1}. This showed the great evapotranspiration potential of the area between the gauges, which includes wetlands and lake Bogenseekette . The year 2007 was richer in precipitation and hence did not exhibit a water shortage. After the discharge to the ponds had been altered during the year, beginning in 2010, the minimum discharge during the summer months was higher and the duration of these low flow conditions was shorter. At OW2 the discharge ranged from 25 to 53 l s^{-1}, at OW6 from 37 to 58 l s^{-1}. Therefore, the temporal distribution of the discharge of treated wasterwater is important in order to sustain wetlands and lakes.

2.5 Hydrogeology

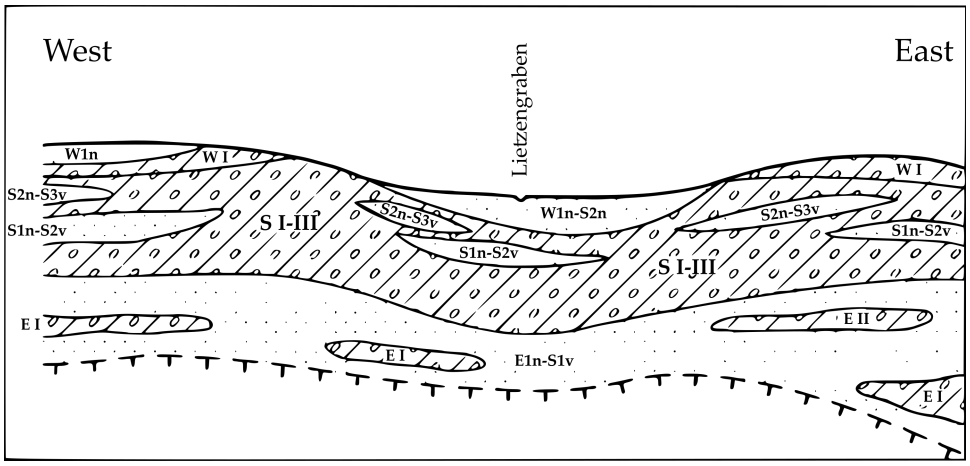

FIGURE 2.4: Conceptual illustration of a cross-section through the catchment from West to East, after Ginzel (1999); the location of the transect is shown in Figure 2.1

The hydrogeological relevant units for this study were formed in the late Pleistocene, during glacial periods. A conceptual illustration of a cross-section through the catchment is shown in Figure 2.4. The main aquifer was formed during Elsterian stadial (E1n-S1v). It consists of fine to medium sands with an average hydraulic conductivity of 5×10^{-4} to 9×10^{-4} m s^{-1} (Nützmann et al., 1992). The thickness of the main aquifer reaches up to 50 m, which is, in combination with the high hydraulic conductivity, the reason why this aquifer is used for drinking water abstraction (Nützmann et al., 1992). The overlying stratum, the Saale I-III aquitard, separates the main aquifer from the upper, unconfined aquifer (W1n-S2n). It reaches a thickness up to 50 m and is considered to separate the main aquifer and the unconfined aquifer effectively (Nützmann et al., 1992). The aquitard also contains inclusions of sand deposits from the melt water of the Saalian glacial periods (S1n-S2v / S2n-S3v). These inclusions partly divide the Saale I-III aquitard in separate horizons. The uppermost aquifer includes fine to medium sand deposits originating in the Warthe stage of the Saalian glaciation (S2n) as well as sand deposits of the Brandenburg stage of the Weichselian glaciation (W2n). Since the melt waters from the glaciers during the Brandenburg stage eroded most of the ground moraine of the Saale I glacial period, the deposits of S2n and W2n establish a continuous aquifer. Due to the location of the catchment in a depression, this aquifer is confined in its lateral extent.

3 Methods and material

3.1 Estimation of groundwater - surface water interaction

The estimation of groundwater - surface water interaction was conducted by the use of heat as a natural tracer. The temperature of a surface water body depends on the air temperature. Hence, the water temperature is subject to seasonal changes and exhibits an annual cycle. On the contrary, groundwater temperatures are very stable and are linked to the mean annual temperature. In Germany, typical groundwater temperatures range from 8 to 12°C. The maxima of the temperature difference between surface water and groundwater occur during winter and summer. During winter, the groundwater is warmer than the surface water and it is colder than the surface water in summer. This difference offers the possibility to estimate the interaction between surface and subsurface water bodies by the measurement of streambed temperatures.

3.1.1 Fibre-optical temperature sensing

Theory

The spatial patterns of groundwater exfiltration in lakes and streams can be determined by the spatial analysis of sediment temperatures. At locations with groundwater exfiltration the sediment temperatures deviate from temperatures at locations with no exchange or surface water infiltration. Fibre-optical distributed temperature sensing (FO-DTS) provides a technique to determine the spatial patterns of sediment temperatures. With a spatial resolution of down to 1 m and maximum cable lengths of several kilometres (Selker et al., 2006a), this method allows to investigate groundwater - surface water interaction at the reach or lake scale. For example, Lowry et al. (2007) and Krause et al. (2012) determined spatial patterns of groundwater exfiltration along a stream reach using FO-DTS while Blume et al. (2013) determined spatial patterns of lacustrine groundwater discharge.

Fibre-optical cables used for FO-DTS systems consist of optical fibres on the inside, coated with material to protect the cable from mechanical stress. Cables which are used for hydrological applications often include a copper core, to increase the weight of the cable and improve the ability to submerge quickly in water.
During the measurement procedure, a short pulse of light with a known wavelength is emitted into the fibre. Parts of the incident pulse are scattered in the fibre material. A detector senses the intensity and wavenlength of the backscattered light returning through the fibre. The backscattered light differs in its composition of wavelengths from the incident light. An illustration of a spectrum of back- light is shown in Figure 3.1. The maximum intensity of the backscattered light occurs at the wavelength of the incident light pulse and is caused by Rayleigh scattering. The other parts of the return signal shown in Figure 3.1 can be split into two types

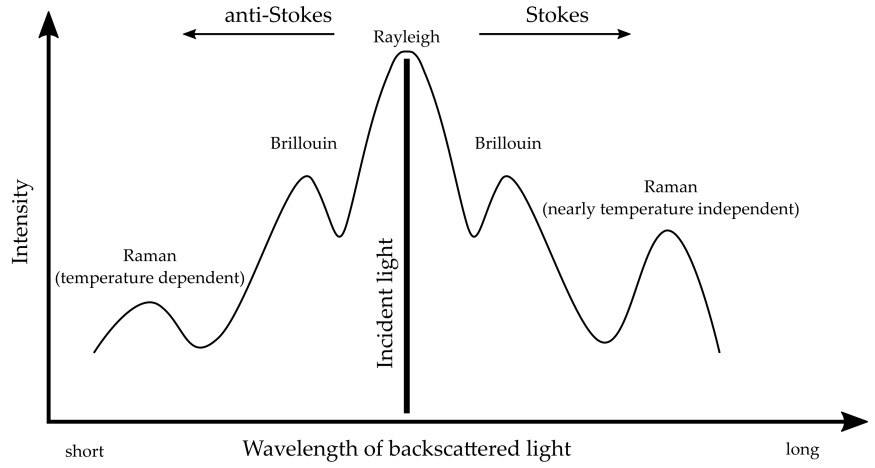

FIGURE 3.1: Conceptual drawing of wavelengths and amplitudes of the backscattered light

of backscattering, Brillouin scattering and Raman scattering. Both types of scattering lead to a shift of the wavelength of the backscattered light in comparison to the incident light, to shorter and longer wavelengths. Shifts to shorter wavelengths (higher frequencies) are referred to as anti-Stokes scattering, while shifts to longer wavelengths (lower frequencies) are referred to as Stokes scattering. The amplitues of the Brillouin scattering are independent from the temperature of the material. However, the amplitudes of the Raman scattering are linked to the temperature of the fibre. While the amplitude of the Stokes Raman scattering is very little dependent on the temperature, the amplitude of the anti-Stokes Raman scattering is highly dependent on the temperature (Suárez et al., 2011b). These different dependencies are the basis of the FO-DTS method which uses the ratio of the amplitude of anti-Stokes to the amplitude of Stokes Raman scattering to calculate the temperature of the cable. To tie the temperatures to locations along the cable, the timelag between the emmision of the light pulse and the detection of the backscattered light is measured. Accounting for the speed of light in the fibre, the measured time allows the calculation of the distance between the detector and the point of origin of the detected backscattered light. Today's FO-DTS instruments emit pulses of 10 to 20ns, which allows a spatial resolution of 1 m (Suárez et al., 2011b). The resolution of the calculated temperatures is limited by the precision of the determined ratio between anti-Stokes and Stokes Raman scattering and ranges down to about 0.01 °C (Selker et al., 2006a). The accuracy of temperature measurements depends on the resolution and the calibration procedure. The length of the FO-DTS cable can range up to 10 km (Selker et al., 2006a) and is limited by the attenuation of the signal within the optical fibre.

In order to determine absolute temperatures, a calibration of the FO-DTS system is necessary. Two different calibration methods are available. The internal calibration method relies on the assumption that the estimation of the attenuation of the signal in the optical fibre and the calibration parameter before the measurements is sufficient. Hence, one accurate calibration is the basis for all following measurements. For the extended calibration method the attenuation and the calibration parameter are determined after the measurement and hence a calibration in advance is not necessary. Suárez et al. (2011a) described a method

to calibrate the FO-DTS device after the latter method by applying known temperatures to sections or points along the cable. In the post-processing of the data, the temperatures are calculated incorporating the measured ratio between anti-Stokes and Stokes Raman scattering and the known temperatures at the calibration sections. The method described by Suárez et al. (2011a) was used in this work and is presented in the following paragraph in detail.

Equation 3.1 describes the calculation of the temperature at a location z for a known ratio $R(z)$ of anti-Stokes to Stokes scattering (see Equation 3.2) and the parameters γ, $\Delta\alpha$, and C:

$$T(z) = \frac{\gamma}{\ln C - \ln R(z) + \Delta\alpha z} \tag{3.1}$$

where:

$T(z)$ = Temperature [K] at distance z [m]
γ $= \Delta E k^{-1}$ [K]
ΔE = Difference in molecular energy responsible for Raman scattering [J]
k = Boltzman constant [J K^{-1}]
C = Calibration parameter [-]
$R(z)$ = Ratio of anti-Stokes to Stokes Raman scattering intensities [-]
$\Delta\alpha$ = Differential attenuation of backscattered Raman intensities [m^{-1}]

The ratio of anti-Stokes to Stokes Raman scattering can be described as:

$$R(z) = I_{aS}(z) / I_S(z) \tag{3.2}$$

where:

$I_{aS}(z)$ = Anti-Stokes Raman intensity [arbitrary unit]
$I_S(z)$ = Stokes Raman intensity [arbitrary unit]

While $R(z)$ is derived by the measurements, the parameters have to be calculated based on the known temperatures.
The differential attenuation of the signal during the passage through the optical fibre is estimated by the comparison of $R(z)$ at two known locations with the same temperature, as described in Equation 3.3:

$$\Delta\alpha = \frac{[\ln R(z_1) - \ln R(z_2)]}{(z_1 - z_2)} \tag{3.3}$$

The calibration parameter C accounts for the specifications of the light pulse emitter, the detector, the optical fibre, and the environmental conditions, under which the FO-DTS device is operated during the measurement. With a known $\Delta\alpha$ and two sections of different, known temperatures, C can be calculated as followed:

$$\ln C = \frac{[\ln R(z_1) - \Delta\alpha z_1]\, T(z_1)}{T(z_1) - T(z_3)} - \frac{[\ln R(z_3) - \Delta\alpha z_3]\, T(z_3)}{T(z_1) - T(z_3)} \tag{3.4}$$

The last parameter necessary to solve Equation 3.1 for $T(z)$ is γ. In the extended calibration method, it is derived through:

$$\gamma = [\ln C - \ln R(z_1) + \Delta\alpha z_1]\, T(z_1) \tag{3.5}$$

Measurements

The measurements were conducted using the FO-DTS instrument *AP Sensing N4386A* with the fibre-optical cable *LLK-BSTE 2FG5* by *BRUGG* of 600 m length. The cable included 2 fibres which where connected at the end and a fibre of 1,200 m length was generated. The resolution of the DTS instrument was 0.11 °C, according the the manufacturer (AP Sensing GmbH, 2009).
To calibrate the FO-DTS device after the method described by Suárez et al. (2011a), a section of the cable was put in a bath with warm water and the temperature was recorded using two temperature loggers *HOBO UA-002-08 Pedant*. Since the optical fibre in the cable formed a loop, the bath included two sections of the fibre, z_1 and z_2, as required for the extended calibration method. An illustration of the set-up is shown in Figure 3.2. The temperature of the stream water at the end of the cable, the middle of the optical fibre, was also recorded using two *HOBO* loggers.
The cable was buried manually in the sediment in about 10 cm depth. It was not possible to bury the cable in the sediment at some locations due to obstacles. The end of the cable was not buried since it served as a reference point for the calibration. It was assumed that the recorded temperatures would better coincide with temperature of the fibre when submerged in flowing water. The duration of the measurement was 67 min and values of $R(z)$ were recorded in intervals of 60 s at a spatial resolution of 1 m.
The recorded data were post-processed using the *GNU R* software (R Core Team, 2016). The temperatures along the cable were calculated, along with the span of the 95% confidence interval for the calculated temperatures.

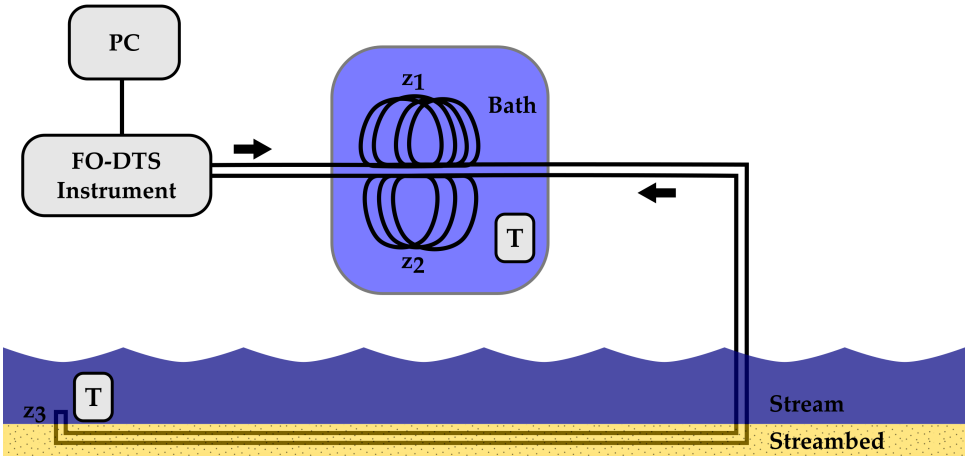

FIGURE 3.2: Set-up of the FO-DTS device for the measurements. Temperatures of the bath and of the stream water at z_3 were logged. Black arrows indicate the direction of the incident light. For clarification, the two fibres in the cable are depicted separately.

3.1.2 Sediment temperature profiles

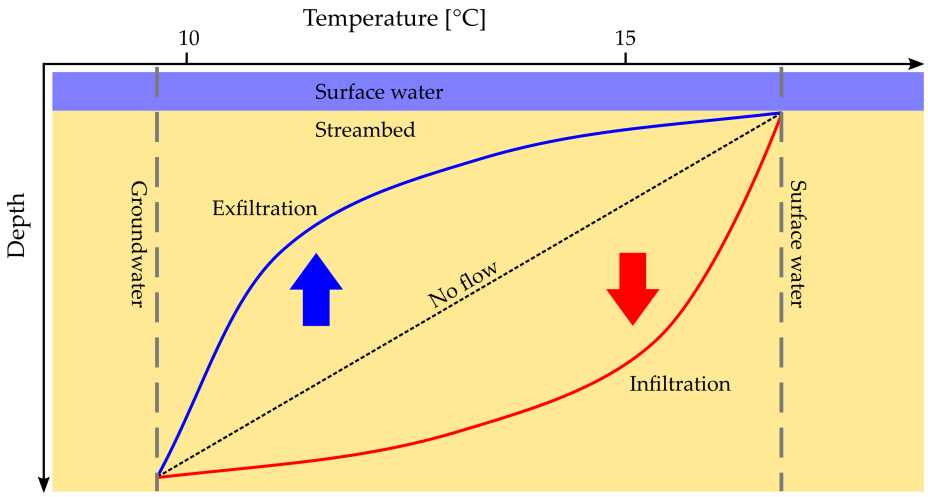

FIGURE 3.3: Conceptual illustration of hypothetic temperature gradients in a streambed in summer

Background

The exfiltration of groundwater into a stream or lake can be quantified by the measurement of temperature profiles in the sediment. Heat is transported through saturated porous media via conductive and advective mechanisms. Conduction is the propagation of heat through the medium based on the thermal conductivity of the matrix-fluid mixture. The transport of heat by advection is tied to the movement of a fluid through the porous medium and depends on the volumetric heat capacity of the fluid and the Darcy velocity of the fluid. The temperature gradient derived through the measurement of temperatures in different sediment depths is the result of heat movement by conduction and advection through the sediment. The characteristics of the temperature gradient in this transition zone between surface water and groundwater depend on the degree of vertical movement of water through the porous matrix. A conceptual illustration of steady-state temperature gradients in the sediment is shown in Figure 3.3. With no vertical movement, the temperature gradient between groundwater and surface water is linear since the conductive mechanism dominates the heat transport. Any vertical water movement through the streambed transports heat via advection. Vertical flow leads to a characteristic shape of the gradient as the advective transport mechanism is added to the conductive term. The exfiltration of groundwater into the surface water (the upward movement of water) leads to a steeper gradient near the interface between streambed and surface water in comparison to the no-flow case, as shown in Figure 3.3 in blue. The downward movement of water (surface water infiltration into the streambed) leads to smoother gradients near the interface and steeper gradients in greater depths compared to no-flow conditions, as shown in Figure 3.3 in red.

The variation of temperatures with increasing depth can be expressed mathematically as given in Equation (3.6) (Schmidt et al., 2006):

$$\frac{\partial T(z)}{\partial t} = \underbrace{\frac{K_{\mathrm{fs}}}{\rho_{\mathrm{c}}}\nabla^2 T(z)}_{\substack{\text{Conductive}\\ \text{transport}}} - \underbrace{\frac{\rho_{\mathrm{f}} c_{\mathrm{f}}}{\rho_{\mathrm{c}}}\nabla(T(z)q)}_{\substack{\text{Advective}\\ \text{transport}}} \tag{3.6}$$

where:

$T(z)$ = Temperature at depth z [°C]
t = Time [s]
q = Darcy velocity in vertical direction [m s^{-1}]
ρ_{c} = Volumetric heat capacity of of the sediment-water mixture [J m^{-3} K^{-1}]
$\rho_{\mathrm{f}} c_{\mathrm{f}}$ = Volumetric heat capacity of the fluid [J m^{-3} K^{-1}]
K_{fs} = Thermal conductivity of the sediment-water mixture [J s^{-1} m^{-1} K^{-1}]

Based on this equation, it is possible to determine the velocity of vertical water movement by the inverse modelling of sediment temperatures. However, Equation (3.6) describes the non steady-state case as a differential equation and requires time series of streambed temperatures and numerical methods to determine the velocity. The measurement of temperature profiles is not difficult. However, these measurements only provide point measurements and any attempt to quantify exfiltration to a stream reach will require the installation of many probes and the simultaneous measurement of temperatures. This is mostly not practicable due to the lack of resources.
Bredehoeft and Papaopulos (1965) developed an analytical solution of Equation (3.6), assuming steady-state vertical flow and vertically homogeneous streambed properties. They applied following boundary conditions on Equation (3.6): $T = T_0$ for $z = 0$ and $T = T_L$ for $z = L$ and yielded Equation (3.7) as a solution of Equation (3.6):

$$\frac{T(z) - T_0}{T_L - T_0} = \frac{exp\left(\frac{q\rho_{\mathrm{f}} c_{\mathrm{f}}}{K_{\mathrm{fs}}} z\right) - 1}{exp\left(\frac{q\rho_{\mathrm{f}} c_{\mathrm{f}}}{K_{\mathrm{fs}}} L\right) - 1} \tag{3.7}$$

where:

T_L = Groundwater temperatue [°C]
T_0 = Surface water temperature [°C]
L = Sediment depth at which $T = T_L$ [m]

Based on Equation (3.7) the flux q can be determined for a given L by comparing calculated to measured temperatures. Hence, Equation (3.7) is transformed to:

$$T(z) = \frac{exp\left(\frac{q\rho_{\mathrm{f}} c_{\mathrm{f}}}{K_{\mathrm{fs}}} z\right) - 1}{exp\left(\frac{q\rho_{\mathrm{f}} c_{\mathrm{f}}}{K_{\mathrm{fs}}} L\right) - 1}(T_L - T_0) + T_0 \tag{3.8}$$

The vertical Darcy velocity of water movement in the streambed can now be determined by fitting the calculated temperature profile to a measured profile by altering the Darcy velocity q. The sum of the squared deviations between measured and computed temperatures at different depths can be calculated

using Equation (3.9) (Schmidt et al., 2006):

$$\text{Error} = \sum_{j=1}^{j=n} \left[T_j - \left(\frac{exp\left(\frac{q\rho_f c_f}{K_{fs}} z_j\right) - 1}{exp\left(\frac{q\rho_f c_f}{K_{fs}} L\right) - 1} (T_L - T_0) + T_0 \right) \right]^2 \tag{3.9}$$

where:

q = Darcy velocity which minimizes the deviation $Error$ for a given L
n = Number of observations

The best fit is defined as the lowest deviation between measured and calculated temperatures which can be achieved based on the given data and property parameters.
This method is relatively simple to apply. However, some limitations and uncertainties have to be considered. The assumptions underlying the analytical solution of Equation (3.6) are mostly not valid under field conditions, due to heterogeneous sediments, lateral flow components, and the violation of the steady-state assumption. Furthermore, values for the parameters describing the material properties are taken from literature in most cases since they are difficult or impracticable to determine in the field. The parameter L, which describes the distance between the streambed surface water interface and the depth of the constant groundwater temperature T_L, is estimated by trial and error since this zone is not captured by the measurements in most cases.

Measurements

Measurements of temperature profiles in the streambed were conducted by the use of a device build by the Leibniz-Institute of Freshwater Ecology and Inland Fisheries, Berlin. The device includes a lance which was installed in the streambed and a handheld PC to read and store data, which was connected to the lance by a cable. A conceptual illustration of the temperature lance is shown in Figure 3.4. The lance was made from aluminium and included 16 thermistors of the type NTC 10 K, which were installed in a distance of 7 cm to each other. The accuracy of the thermistors was ±0.2 °C. By the use of a heat conductive glue in the drilling between thermistor and the surrounding, the thermistors were protected from the mechanical stress during the installation process and measured the temperature of the adjacent sediment without substantial influences related to the lance itself. With the configuration used for the measurements, profiles of up to 105 cm depth could be captured. The frequency of the data recording was 1 min^{-1}, while the temperatures were continuously displayed on the handheld PC in real-time. The thermistors did not provide absolute temperatures. Hence, it was necessary to calibrate the lance at the beginning of the measurements and between measurements frequently. In order to calibrate it, the lance was placed in the stream horizontally and the measurement of temperatures was started and constantly monitored, assuming the water temperature around the thermistors was stable and homogeneous. The absolute water temperature was measured using a PT1000 thermistor. After the values were stable, all temperature values of the lance were set to zero. Since the water temperature was recorded, the calculation of absolute temperatures was possible. To account for changes of the surface water temperature and the drift of the temperature values provided by the lance, this procedure was repeated frequently.

TABLE 3.1: Parameter values applied to the heat transport equation (3.8) during the analysis process.

Parameter	Value
K_{fs}	$1.5\,\mathrm{J\,s^{-1}\,m^{-1}\,K^{-1}}$
$\rho_f c_f$	$4.19 \times 10^6\,\mathrm{J\,m^{-3}\,K^{-1}}$
L	2 m
T_L	11.7 °C

To measure sediment temperature profiles the lances were installed in the streambed along the investigated stream reach in a distances of 5 m to each other, and about 0.5 m from the stream bank. To account for the surface water temperature for the boundary condition T_0, the lances were pushed into the sediment until only the uppermost thermistor was in direct contact with the surface water. The second thermistor was situated at the interface between streambed and surface water. Since the installation of the lance in the streambed was a disruption, the measurements were monitored until the temperatures were stable and assumed to be steady-state. These final temperature values were recorded and used for the estimation of the exchange flux between surface and subsurface.

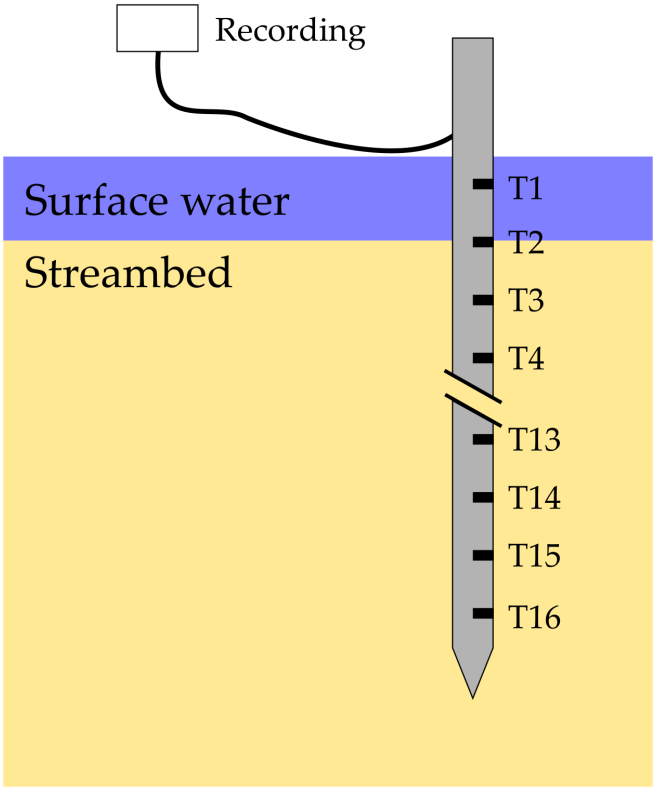

FIGURE 3.4: Conceptual illustration of the device used to obtain sediment temperature profiles; 16 thermistors were implemented with a distance of 7 cm between

Analysis

The recorded temperature profiles were analysed using the statistical software *GNU R* (R Core Team, 2016). The results were plotted using the *GNU R* package *ggplot2* (Wickham, 2016). The absolute temperatures at different depths were calculated by adding the water temperature obtained during the previous calibration to the relative temperature values recorded by the lance. Due to erroneous measurements, it was necessary to revise the obtained temperature profiles. Values below 10 °C or above 20 °C were rejected. In a visual inspection, outliers were also excluded from the data.
The boundary conditions of the temperature were applied by setting the uppermost temperature value as surface water temperature T_0. The groundwater temperature T_L was considered to be 11.7 °C. However, if the lowermost temperature recorded was below this value, the groundwater temperature T_L was set to the temperature reading of the lowermost thermistor. The depth z was set in reference to the second thermistor located at the interface between surface water and streambed, where the depth was set $z = 0$. The thermal conductivity K_{fs} of the streambed was not determined in this work. However, the range of realistic values is quite narrow (Stonestrom and Blasch, 2003) and errors in discharge are proportional to errors in the parameter K_{fs} (Schmidt et al., 2006). A value of $K_{\mathrm{fs}} = 1.5\,\mathrm{J\,s^{-1}\,m^{-1}\,K^{-1}}$ was chosen, since the stream reach under investigation exhibited similar streambed characteristics with medium to fine sands, as the sites in Schmidt et al. (2007).
The parameter set is shown in Table 3.1. The adjustment of the Darcy velocity in order to fit calculated to measured temperatures was done by using the nonlinear least square solver provided by *GNU R*. The algorithm requires boundary values for the altered parameter as well as a start value. The lower boundary of the Darcy velocity was set to $8.64 \times 10^{-3}\,\mathrm{l\,d^{-1}\,m^{-2}}$, the upper boundary was set to $8.64 \times 10^{2}\,\mathrm{l\,d^{-1}\,m^{-2}}$. The start value was set to $8.64 \times 10^{-1}\,\mathrm{l\,d^{-1}\,m^{-2}}$.

3.2 Numerical models

The measures used to evaluate the quality of the models will be presented in this section, followed by descriptions of the numerical models which have been used in this work. The description of the model includes the theoretical background of the models and the configuration used in this work. As far as possible the descriptions of the models have been aligned to each other in matters of variable denotation and the layout of governing equations.

3.2.1 Measures for model quality and model comparison

Statistical measures such as Pearson correlation coefficient and Nash-Sutcliffe efficiency coefficient can be used to asses a model's quality and will be introduced in the following section. Both coefficients are applied to the simulated and observed head and discharge data.

Pearson correlation coefficient

The correlation between two sequences of values can be quantified by calculating the Pearson correlation coefficient. The coefficient is based on the covariance of two variables, which describes the relation of the variability between these variables. In order to normalize the covariance and thus make it comparable, the covariance is divided by the standard deviation of the variables.
The coefficient is calculated as:

$$r = \frac{\sum_{i=1}^{n} (x_i - \bar{x}) \times \left(y_i - \bar{y}\right)}{\sqrt{\sum_{i=1}^{n} (x_i - \bar{x})^2 \times \sum_{i=1}^{n} \left(y_i - \bar{y}\right)^2}} \tag{3.10}$$

where:

r = Pearson correlation coefficient [-]
y_i = Observation value at time i
$\bar{y}$ = Mean value of observations
x_i = Simulated value at time i
$\bar{x}$ = Mean value of simulations

The coefficient ranges between -1 and 1. The latter value indicates a perfect correlation between observed and simulated variables. A correlation value of 0 indicates no correlation at all. A perfect negative correlation between the variables is indicated by a correlation coefficient of -1, meaning that the dynamics of the variables are contrary to each other. However, the Pearson correlation coefficient relies on the joint variance of the variables and does not account for any offset between the absolute values of the variables. Hence, a constant offset between observed and simulated values would result in a "perfect fit". Therefore, caution is advised when assessing model quality on the basis of this measure. However, it is suitable for the evaluation of the ability of models to simulate the general dynamics of a variable. In this work, the Pearson correlation coefficient is applied to the simulated and observed hydraulic heads and stream discharges.

Nash-Sutcliffe efficiency coefficient

The calculation of the Nash-Sutcliffe efficient coefficient (NSE) after Nash and Sutcliffe (1970) provides a statistical measure which overcomes the limitation of the coefficient previously described. It is used in hydrology to compare simulated to observed discharge data. Contrary to the correlation coefficient, the NSE coefficient accounts for the deviation of the simulated from the observed value at a point in time in proportion to the deviation of the observed value at this point in time from the mean value of all observations. The NSE is calculated as:

$$\mathrm{NSE} = 1 - \frac{\sum_{i=1}^{n} \left(y_i - \hat{y}_i\right)^2}{\sum_{i=1}^{n} \left(y_i - \bar{y}\right)^2} \tag{3.11}$$

where:

NSE = Nash-Sutcliffe efficiency coefficient [-]
y_i = Observation value at time i
$\hat{y}_i$ = Simulated value at time i
$\bar{y}$ = Mean value of observations

The NSE can range from $-\infty$ to 1. The latter value would be the result of a perfect fit of the simulated to the observed data. A NSE of 0 implies that the mean value of the observations is an evenly suitable predictor of the observed values as the simulated values. Hence, if NSE < 0 the mean value of the observations is a better predictor than the simulated data.

Water balance error

The absolute water balance error of a model can be defined generally as:

$$\mathrm{Error}_{\mathrm{abs}} = (\mathrm{Inflow} - \mathrm{Outflow}) - \Delta S \tag{3.12}$$

where:

Inflow = Sum of the flow of water into the model domain [L^3]
Outflow = Sum of the flow of water leaving the model domain[L^3]
ΔS = Total storage change within the model domain [L^3]

In order to compare the errors of models with each other, it is necessary to normalize the absolute error to the area of the catchment with:

$$\mathrm{Error}_{\mathrm{norm}} = \frac{\mathrm{Error}_{\mathrm{abs}}}{\mathrm{Area}_{\mathrm{Catchment}}}$$

or to calculate a percentage of the error proportionally to the sum of outflows of the model as:

$$\mathrm{Error}_{\mathrm{percentage}} = \frac{|\,\mathrm{Error}_{\mathrm{abs}}\,|}{\mathrm{Outflow}} \times 100\%$$

3.2.2 ArcEGMO

In this section the modeling system ArcEGMO (Becker et al., 2002) is presented and information about the configuration and parameter sets of the model of the Lietzengraben catchment are given. The model was prepared by Mey (2011) in the context of a doctoral thesis. It was kindly provided by the "Büro für Angewandte Hydrologie", Berlin for the comparison with the model HydroGeoSphere in this work. Since the development, calibration and validation was not part of this thesis, this section focuses on the components relevant for this work and the comparison to HydroGeoSphere. For any further information on the ArcEGMO-ASM model of the Lietzengraben catchment, the reader may be referred to the comprehensive work of Mey (2011).

Theory

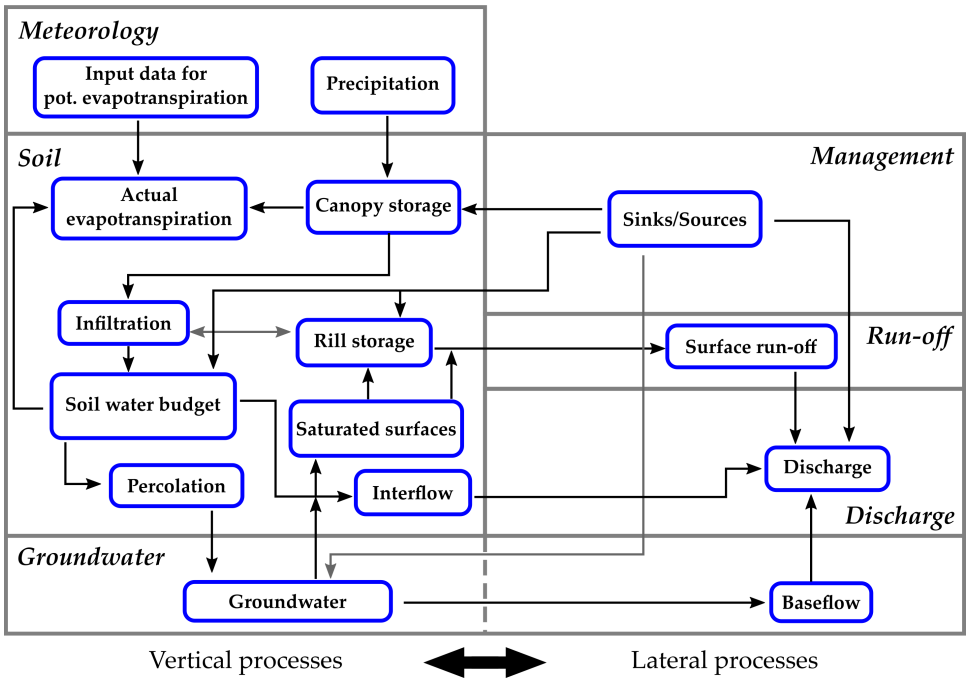

FIGURE 3.5: Model layers of ArcEGMO; modified from BAH (2011)

ArcEGMO was designed as an open modelling system. It provides various options to account for different hydrological processes in a modular structure. In general, the model is separated into six layers which represent either vertical or lateral processes. Lateral processes include the movement of water as surface run-off, stream discharge, and the subsurface movement of groundwater. Precipitation, infiltration of water into the soil, evaporation of soil water, percolation, and groundwater recharge are considered as vertical processes. An illustration of the general model structure and its components is shown in Figure 3.5.
For most of the model layers multiple options on the representation of hydrolocial processes are available, based on different physical approaches. Potential evapotranspiration, for example, can be described using the Penman equation, the grass reference evapotranspiration, the approach after Turc/Ivanov, or others

(BAH, 2011). The soil water budget layer also provides various options, as well as the groundwater layer, and the discharge layer. The choice of the used layers depends on the purpose of the simulations and the available input data. The spatial discretisation of the model domain is variable. The data handling in ArcEGMO is mostly done using geographic information systems and the spatial discretisation is flexible and can be chosen based on data availability. This approach is referred to as “hydrotopes”, the largest spatial units including the same combination of properties respectively parameter values.

Mey (2011) used the Plant-Soil-Carbon-Nitrogen model (PSCN) (Klöcking et al., 2012) for the representation of the soil, vegetation cover, percolation, groundwater recharge and the discharge generation by surface run-off. The PSCN module provides a detailed representation of the soil by the definition of distinct soil layers. The vegetation cover was represented dynamically, the depths of roots and the temporal variation of the leaf area index (LAI) were given as pre-defined time series. The calculation of the potential evapotranspiration was executed based on the approach after Turc/Ivanov. The stream discharge was calculated using a linear storage cascades approach. The groundwater domain was represented by the groundwater model ASM (Kinzelbach and Rausch, 1995) in two dimensions. Since only the upper aquifer was considered, this was sufficient for the goals of the work of Mey (2011).

The various model layers, each accounting for one component of the hydrologi-

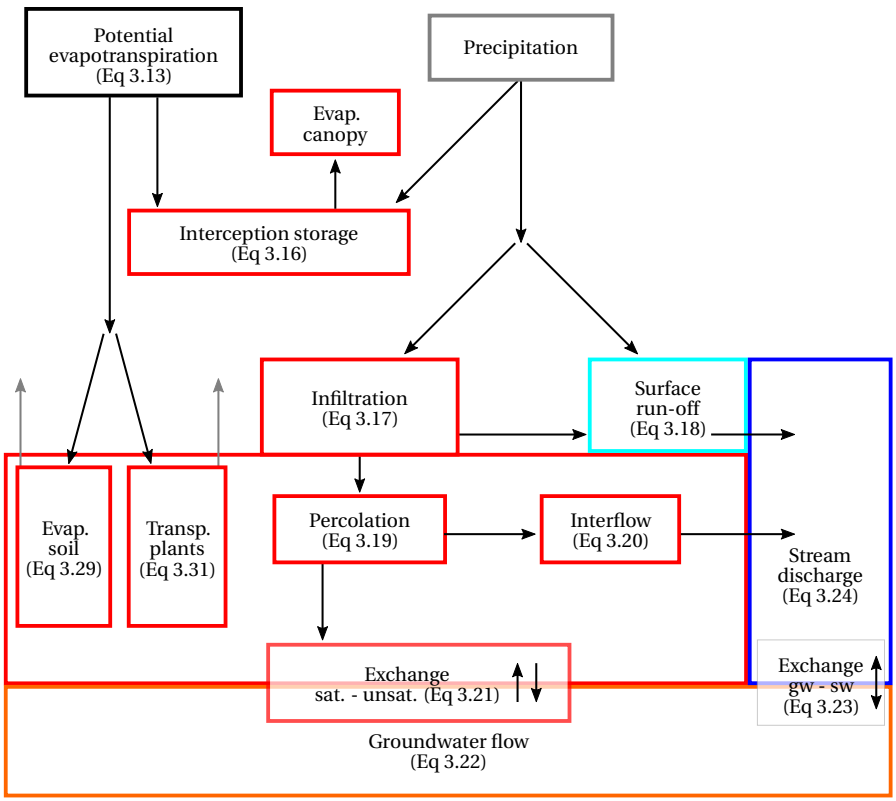

FIGURE 3.6: Simplified structure of the hydrological iterative model ArcEGMO-ASM; governing equations are refered to as numbers in brackets

cal cycle, include mathematical descriptions of the process they represent. In the following paragraphs the mechanisms and mathematical descriptions of model

layers are presented. In Figure 3.6 a simplified illustration of the model structure is given with references to the governing equations. The layout corresponds to Figure 3.9, which shows the structure of HydroGeoSphere in a similar fashion.

Potential evapotranspiration The potential evapotranspiration is calculated after Turc/Ivanov (DVWK, 1996), corrected after Glugla and König (1989). The potential evapotranspiration is given as:

$$ET_{\text{pot}} = \begin{cases} \frac{a\ \Omega\ C(\phi)\ (R_{\text{g}}+b)\,T_{\text{air}}}{T_{\text{air}}+15} & \text{for } T_{\text{air}} \geq 5\,^{\circ}\text{C} \\ 0.000036\,(25+\ T_{\text{air}})^2\,(100-\phi) & \text{for } T_{\text{air}} < 5\,^{\circ}\text{C} \end{cases} \tag{3.13}$$

$$C = \begin{cases} 1+\frac{50-\phi}{70} & \text{for } \phi < 50\% \\ 1 & \text{for } \phi \geq 50\% \end{cases} \tag{3.14}$$

where:

Ω = Correction factor after Glugla and König (1989)
ϕ = Relative humidity [%]
R_{g} = Global radiation [J cm^{-2} d^{-1}]
$a,\ b$ = Parameter ($a = 3.1 \times 10^{-3},\ b = 209.4$ for $\Delta t = 1$d)
T_{air} = Daily mean of air temperature [°C]

Interception The interception of precipitation by the vegetation cover on the surface is accounted for dynamically by linking the leaf area index (LAI) to the interception storage capacity as:

$$S_{\text{I}}^{\text{max}} = \begin{cases} k_{\text{S}}\left(0.935 + 0.498\ \text{LAI} - 0.00575\ \text{LAI}^2\right) & \text{for LAI } > 0 \\ 0 & \text{for LAI } = 0, \text{ not forested} \\ k_{\text{S}} S_{\text{I}}^{\text{min}}\, d_{\text{plant}} & \text{for LAI, forested} \end{cases} \tag{3.15}$$

where:

$S_{\text{I}}^{\text{max}}$ = Interception storage capacity [L]
k_{S} = Correction parameter for precipitation in forested areas [-]
$S_{\text{I}}^{\text{min}}$ = Minimum interception storage capacity [L]
d_{plant} = Density of plants [-], $0 \leq d_{\text{plant}} \leq 1$

The storage content $S_{\text{I}}(t)$ of the canopy is then calculated as:

$$S_{\text{I}}(t) = \begin{cases} S_{\text{I}}(t-\Delta t) + P(t) & \text{for } S_{\text{I}}(t-\Delta t) + P(t) < S_{\text{I}}^{\text{max}} \\ S_{\text{I}}^{\text{max}} & \text{for } S_{\text{I}}(t-\Delta t) + P(t) \geq S_{\text{I}}^{\text{max}} \end{cases} \tag{3.16}$$

where:

$P(t)$ = Precipitation [L]
$S_{\text{I}}^{\text{max}}$ = Interception storage capacity [L]

Infiltration The soil water dynamics, including infiltration, percolation, discharge generation, and groundwater exchange are represented in the model by the PSCN-module (Klöcking et al., 2012). Vertical movement is calculated on the basis of a multi-layer capacity model after Koitsch (1977) and Glugla (1969).

The infiltration of precipitation water into the subsurface is modelled in respect to the proportion of sealed surfaces at the affected spatial unit. The rate of infiltration is calculated as:

$$q_{\text{inf}} = (1 - \Psi)\min\{P_0,\ F_{\text{pot}}\} \tag{3.17}$$

where:

q_{inf} = Infiltration $[LT^{-1}]$
Ψ = Proportion of sealed surfaces [-], $0 \leq \Psi \leq 1$
P_0 = Effective precipitation $[LT^{-1}]$
F_{pot} = Infiltration capacity $[LT^{-1}]$

The effective precipitation is the amount of precipitation available for infiltration or surface run-off after accounting for the interception storage and evaporation. The proportion Ψ of the effective precipitation is processed as surface run-off. The infiltration capacity of the soil depends on the available storage capacity in the soil and the hydraulic conductivity of the soil.

Surface run-off The amount of effective precipitation which does not infiltrate into the soil is stored in the depression storage of the surface. The content of this storage is potentially available for infiltration in the next time steps of simulation. However, as soon as the depression storage capacity is depleted, surface run-off is generated. The calculation of surface run-off in ArcEGMO-ASM is based on the kinematic wave approximation of the Saint Ventant equation and the Manning-Strickler equation (Gupta and Sinclair, 1976; Willgoose et al., 1991). The surface run-off is given as:

$$q_{\text{ro}} = \frac{h^{2/3} \times S^{1/2}}{n} \tag{3.18}$$

where:

q_{ro} = Surface run-off $[LT^{-1}]$
h = Thickness of the water column $[L]$
S = Slope of the surface [-]
n = Manning roughness coefficient $[TL^{-1/3}]$

The surface run-off is routed to the adjacent surface stream and distributed among the stream reaches of the sub-catchment proportional to their length.

Soil water movement The vertical movement of infiltrated water from a layer within the soil to the layer beneath depends on the water content, with the exception of water flow through macro-pores in the soil. The module PSCN accounts for macro-pores on basis of an empirical equation. The proportion of the infiltrated water equal to the proportion of macro-pores is transported to underlying soil layer instantly. This process can be repeated over several layers. The equation to calculate the amount of macro-pores is not presented here. In order to transport water not affected by macro-pores to the underlying soil layer, a saturation greater than the field capacity must be reached. Furthermore, a soil temperature smaller 0 °C inhibits any movement of water since it is considered frozen. The amount of percolation from the soil layer z_j to the soil layer z_{j+1} is

described as:

$$q_{\text{perc}}(z_j,\ t) = \begin{cases} 0 & \text{for } \theta(z_j,\ t) \leq \theta_{\text{fc}}(z_j) \vee T_{\text{soil}}(z_j, t) < 0\,^{\circ}\text{C} \\ \lambda(\max(0,\ \theta(z_{j,t}) - \theta_{\text{fc}}(z_j))^2) & \text{for } \theta(z_j,\ t) > \theta_{\text{fc}}(z_j) \wedge T_{\text{soil}}(z_j, t) \geq 0\,^{\circ}\text{C} \end{cases} \tag{3.19}$$

where:

$q_{\text{perc}}(z_j,\ t)$ = Percolation in soil layer z_j at time t $[LT^{-1}]$
θ = Soil water content [-]
θ_{fc} = Water content at field capacity [-]
λ = Parameter accounting for hydraulic conductivity $[L^{-1}T^{-1}]$
T_{soil} = Soil temperature [°C]

The model includes the consideration of interflow. The occurence of interflow is coupled to the inclination of the soil layer and requires full saturation, which often is linked to a lower hydraulic conductivity of the underlying soil layer. The amount of soil water discharged as interflow is calculated in the PSCN module as:

$$q_{\text{int}}(z_j,\ t) = \begin{cases} 0 & \text{for } \theta(z_j,\ t) \leq \theta_{\text{fc}}(z_j) \vee T_{\text{soil}}(z_j,\ t) < 0\,^{\circ}\text{C} \\ k^{\text{h}} \sin(\arctan\alpha)\lambda(\max(0,\ \theta(z_j,\ t) - \theta_{\text{fc}}(z_j))^2 & \text{for } \theta(z_j,\ t) > \theta_{\text{fc}}(z_j) \wedge T_{\text{soil}}(z_j,\ t) \geq 0\,^{\circ}\text{C} \end{cases} \tag{3.20}$$

where:

$q_{\text{int}}(z_j,\ t)$ = Interflow in soil layer z_j at time t $[LT^{-1}]$
α = Inclination of the soil layer [-]
λ = Parameter accounting for hydraulic conductivity $[L^{-1}T^{-1}]$
T_{soil} = Soil temperature [°C]
k^{h} = Correction factor [-]

Consequently, the change of the water content of a soil layer j in the course of one time step is calculated as the result of percolation into the soil layer, the percolation out of the soil layer, the loss due to evapotranspiration, and the loss due to interflow.

$$\frac{\Delta\theta(z_j,\ t)}{\Delta t} = q_{\text{perc}}(z_{j-1},\ t) - E_{\text{soil}}(z_j,\ t) - q_{\text{perc}}(z_j,\ t) - q_{\text{int}}(z_j,\ t)$$

Interaction saturated - unsaturated zone The interaction between the saturated zone (groundwater) and the unsaturated zone is controlled by the opposing processes of capillary rise of groundwater into the unsaturated zone due to capillary forces and the percolation of soil water due to water contents exceeding the field capacity, also denoted as groundwater recharge. The capillary rise is considered in ArcEGMO-ASM on the basis of tabulated values, the groundwater recharge is calculated as percolation (see Equation 3.19). The exchange q_{ex} between saturated and unsaturated zone is the given as:

$$q_{\text{ex}} = \left(q_{\text{perc}} - q_{\text{capillary}}\right) \times S_{\text{s}} \tag{3.21}$$

where:

q_{perc} = Groundwater recharge $[L]$
$q_{\text{capillary}}$ = Capillary rise $[L]$
S_{s} = Specific storage [-]

Subsurface flow The groundwater is represented in the model system ArcEGMO-ASM by the finite difference code ASM (Kinzelbach and Rausch, 1995). The flow of groundwater is accounted as two dimensional flow and formulated as:

$$\frac{\partial\left((h-b)k_{\mathrm{f}}\frac{\partial h}{\partial x}\right)}{\partial x}+\frac{\partial\left((h-b)k_{\mathrm{f}}\frac{\partial h}{\partial y}\right)}{\partial y}+q=n_e\frac{\partial h}{\partial t} \tag{3.22}$$

where:

$\frac{\partial h}{\partial x}$, $\frac{\partial h}{\partial y}$ = Hydraulic gradient in x- and y-direction [-]
$h-b$ = Thickness of the saturated part of the aquifer $[L]$
k_{f} = Hydraulic conductivity $[LT^{-1}]$
q = Sources and sinks $[LT^{-1}]$
n_e = Effective porosity [-]

Interaction stream - groundwater The interaction between surface streams and the groundwater is an important process for the accurate representation of stream discharge, especially in lowland catchments, where groundwater baseflow dominated the discharge generation. The coupling between the model layer accounting for the stream discharge and the groundwater layer is described in ArcEGMO-ASM as:

$$q=\begin{cases}\Delta h\times l_{\mathrm{f}}\times A & \text{for } h_{\mathrm{gw}}\geq h_{\mathrm{sb}}\\ h_{\mathrm{sw}}-h_{\mathrm{sb}}\times l_{\mathrm{f}}\times A & \text{for } h_{\mathrm{gw}}<h_{\mathrm{sb}}\end{cases} \tag{3.23}$$

where:

q = Exchange flux $[LT^{-1}]$
Δh = Difference between groundwater head and surface water level $[L]$
l_{f} = Leakage factor $[L^{-2}T^{-1}]$
A = Area available for exchange $[L^2]$
h_{gw} = Groundwater head $[L]$
h_{sb} = Elevation of the streambed $[L]$
h_{sw} = Surface water level $[L]$

ArcEGMO-ASM accounts for the geometry of surface streams. The banks of channels are included in the exchange process and contribute to the exchange area, depending on the water level. The exchange flux is incorporated into Equation 3.22 for the groundwater layer and into Equation 3.24 for the stream discharge.

Stream discharge Surface streams are represented in ArcEGMO-ASM as discrete stream reaches in a cascade of linear storages. The stream discharge of a stream reach is calculated as the sum of the input by surface run-off, drainage flow, interflow, groundwater exchange, and the inflow to the stream reach from the adjacent stream reach upstream.

$$Q=Q_{\mathrm{ro}}+Q_{\mathrm{drain}}+Q_{\mathrm{int}}+Q_{\mathrm{gw}}+Q_{\mathrm{up}} \tag{3.24}$$

The retention of water within a stream reach is accounted for as:

$$\begin{aligned}Q_k^t-Q_k^{t-\Delta t}=C_1\left[Q_{k-1}^{t-\Delta t}-Q_k^{t-\Delta t}\right]+C_2\left[Q_{k-1}^{t}-Q_{k-1}^{t-\Delta t}\right]+\\ Q_{\mathrm{ro},k}+Q_{\mathrm{gw},k}+Q_{\mathrm{drain},k}+Q_{\mathrm{int},k}\end{aligned} \tag{3.25}$$

where:

Q_k^t = Discharge in stream reach k at time t $[L^3T^{-1}]$
Q_{ro} = Surface run-off inflow $[L^3T^{-1}]$
Q_{gw} = Groundwater baseflow $[L^3T^{-1}]$
Q_{drain} = Drainage inflow from adjacent cells $[L^3T^{-1}]$
Q_{int} = Interflow $[L^3T^{-1}]$

The coefficients

$$C_1 = 1 - e^{-t/K_\tau}$$

and

$$C_2 = 1 - C_1 \times \frac{K_\tau}{t}$$

incorporate the retention parameter of the stream reach, K_τ, into the equation. The occurrences of backwaters in surface streams are accounted for based on the height of the water column in a stream reach. Water is not transported to the downstream stream reach, if the water level in the current reach is lower or equal to the water level of the downstream reach.

Actual evapotranspiration The calculations of the actual evaporation and actual transpiration are executed separately. The evaporation of water stored in the interception storage is calculated as:

$$E_{\text{can}} = ET_{\text{pot}} - \max(0,\ ET_{\text{pot}} - S_{\text{I}}) \tag{3.26}$$

The proportion of the potential evapotranspiration which is available for soil evaporation and plant transpiration is distributed amongst them based on the coverage of the the surface. The coverage is calculated as:

$$B = 1 - e^{-0.5\ \text{LAI}} \tag{3.27}$$

The potential soil evaporation is then calculated as:

$$E_{\text{soil}}^{\text{pot}} = ET_{\text{pot}} - E_{\text{can}} - E_{\text{snow}} - E_{\text{dep}} \tag{3.28}$$

where:

E_{snow} = Actual evaporation of snow $[L]$
E_{dep} = Actual evaporation from the depression storage at the surface $[L]$

It is assumed that the evaporation from the uppermost soil layer is only limited by the water content of this layer. After the water storage of this layer is depleted, the model allows for evaporation from the underlying soil layer if there is still potential for evaporation. This process is repeated until the potential evaporation is fully exhausted. The consumption of water from the lower soil layers is given as:

$$E_{\text{soil}}(z,\ t) = E_{\text{soil}}^{\text{pot}}(t) \times R_{\text{se}}(z,\ t) \times \frac{\left[1 - e^{-20\lambda_1 \frac{z}{z_{\max}}}\right]}{\left[1 - e^{-20\lambda_1}\right]} \tag{3.29}$$

$$R_{\text{se}}(\theta) = \begin{cases} 1 & \text{for } \theta \geq \theta_{\text{fc}} \\ \frac{\theta - \theta_{\text{wp}}}{\theta_{\text{fc}} - \theta_{\text{wp}}} & \text{for } \theta_{\text{wp}} \leq \theta < \theta_{\text{fc}} \\ 0 & \text{for } \theta < \theta_{\text{wp}} \end{cases} \tag{3.30}$$

where:

$E^{\text{pot}}_{\text{soil}}$ = Potential soil evaporation [L]
λ_1 = Parameter for the hydraulic conductivity of the top soil layer [$L^{-1}T^{-1}$]
R_{se} = Function accounting for the decrease of evaporation with depth [-]
z_{max} = Maximum depth for evaporation [L]
θ = Water content [-]
θ_{fc} = Water content at field capacity [-]
θ_{wp} = Water content at the wilting point [-]

Hence, the consumption of water through evaporation is limited by the maximum depth at which evaporation is allowed, the water content, and the parameter accounting for hydraulic conductivity of the uppermost soil layer. Evaporation of water from surface water bodies is not incorporated in the PSCN module. This is compensated by tying time series of potential evapotranspiration to water bodies like lakes separately. Actual evaporation is then calculated accordingly to the surface areas of the water bodies.

The consumption of soil water by transpiration of plants is calculated as:

$$T_{\text{plants}}(z,\ t) = T^{\text{pot}}_{\text{plants}}(t) \times R_{\text{trans}}(z,\ t) \times \frac{\left[1 - e^{-\beta \frac{z}{z_{\text{root}}}}\right]}{1 - e^{-\beta}} \tag{3.31}$$

$$R_{\text{trans}}(\theta) = \begin{cases} 0 & \text{for } \theta \leq \theta_{\text{wp}} \\ 1 - \frac{0.9\theta_{\text{fc}} - \theta}{0.9\theta_{\text{fc}} - \theta_{\text{wp}}} & \text{for } \theta_{\text{wp}} < \theta < 0.9\theta_{\text{fc}} \\ 1 & \text{for } 0.9\theta_{\text{fc}} \leq \theta \leq 0.9\theta_{\text{fc}} \\ 0.3 + 0.7 \frac{\theta_{\text{sat}} - \theta}{\theta_{\text{sat}} - 0.9\theta_{\text{wp}}} & \text{for } \theta > 0.9\theta_{\text{fc}} \end{cases} \tag{3.32}$$

where:

$T^{\text{pot}}_{\text{plants}}$ = Potential transpiration by plants[L]
β = Parameter [-]
R_{trans} = Function accounting for the decrease of root density with depth [-]
z = Depth [L]
z_{root} = Maximum rooting depth [L]
θ = Water content [-]
θ_{wp} = Water content at wilting point [-]
θ_{fc} = Water content at field capacity [-]
θ_{sat} = Water content at full saturation [-]

Physical model

Catchment The boundaries of the subsurface Lietzengraben catchment were implemented in ArcEGMO-ASM as shown in Figure 3.7. Pfützner (2005) determined that the subsurface catchment differs from the extent of the surficial catchment (shown in Figure 2.1).
The topography was implemented in the model based on a digital elevation model (DEM) with a horizontal resolution of 25 m × 25 m. Based on the elevations, the steepness of slopes and the direction of the slopes were calculated. The horizontal discretisation of the model was chosen as 25 m × 25 m, accordingly to the resolution of the DEM (Mey, 2011).

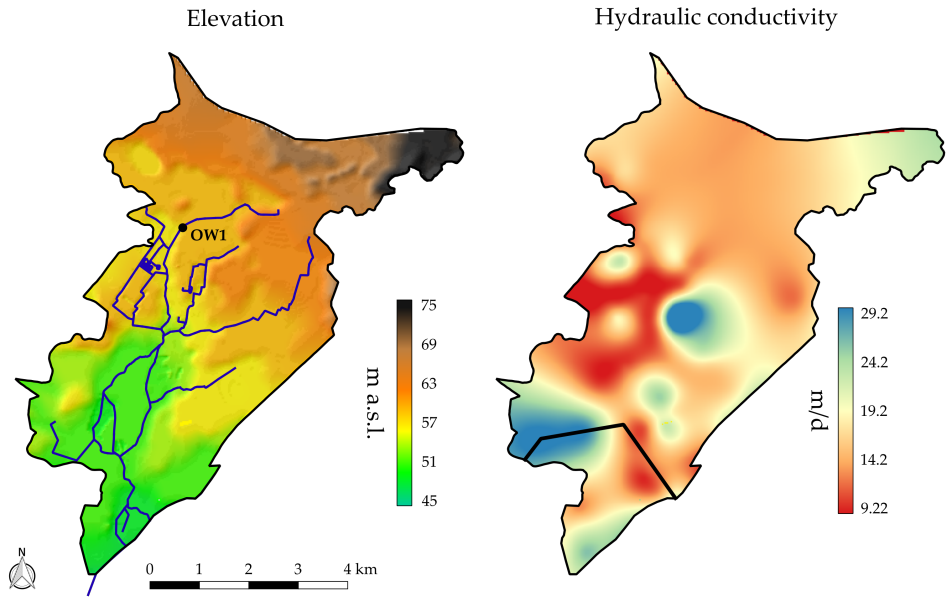

FIGURE 3.7: Left: Catchment of the ArcEGMO-ASM model and implemented streams; Right: Hydraulic conductivities of the aquifer as calibrated for ArcEGMO-ASM, the boundary between the southern and northern porosity zone of the aquifer is shown as black line

Hydrogeology The relevant aquifer for the model was the upper, unconfined aquifer. Mey (2011) described the aquifer as a sandy aquifer which is closed to the eastward and westward end of the catchment by the underlying marl since the sandy aquifer is completely eroded in this area. A description of the aquifer is given in Section 2.5. The hydraulic conductivities of the aquifer were estimated on the basis of results by Wachholz (2005) and included in the calibration process. Pfützner (2005) separated the aquifer into two zones of porosities. This distinction was chosen accordingly to the spatial separation of the aquifer into a northern part, located on a glacial plateau with inclusions of marls in the aquifer, and a southern part of sand in a former glacial valley. The estimation of the porostiy was part of the calibration process and yielded a porosity of $\phi = 0.1$ for the northern part and $\phi = 0.25$ for the southern part of the aquifer. The boundary which separates the two zones of uniform porosities is shown in Figure 3.7.

Land use In order to include surface properties like the surface roughness, the proportion of sealed surfaces, and vegetation properties (maximum rooting depth, leaf area index (LAI), canopy storage capacity) in the model, various types of land use were defined. The parameters representing the rooting depth of plant and the LAI were varied annually. For the temporal variation of these parameters, two types were chosen. One for agricultural areas, one for forested areas.

Soil The PSCN model used in the ArcEGMO model to account for the soil water budget and the calculation of runoff generation, discharge generation, groundwater recharge, and evapotranspiration offers the possibility to include detailed information about the soil in the model. Hence, the quality of the input data is important. The classification of the catchment into zones of soil types was based on soil maps and the linked description of parameters. At some locations

field investigations were undertaken and the results were included in the soil parametrisation. In order to immobilize pollutants in the upper soil, at some locations in the central catchment marl has been brought into the upper soil layer, as described in Section 2.2. For these areas the upper 30 cm of the soil were assumed to have the properties of marl with decreased hydraulic conductivity and porosity.

Surface water The ArcEGMO-ASM model included streams, lakes, and irrigation ponds. Streams and ponds were represented as stream elements which were predefined in the model and parametrized by the bed elevation, width, and geometry. The Lake Bogenseekette was represented as linear storage connected to the stream system with a volume and a surface area in dependence of the water volume currently stored. Weirs were represented in the model by the use of modules accounting for management measures. For every weir, the type of weir, the streambed elevation, the height of the weir and the width of the weir were parametrized. The discharge at weirs was calculated based on the equation after Poleni (Bollrich, 2000).

Updates The model of the Lietzengraben catchment built and described by in the previous paragraphs did include the time period from 1995 to 2007. It did not include the irrigation pond "Teich 11". To account for the start of the irrigation of treated wastewater into "Teich 11" in the beginning of 2007, the input time series were extended to the end of 2012. Furthermore, the irrigation pond "Teich 11" was added to the model by "Büro für Angewandet Hydrologie", Berlin. A re-calibration of the model was not performed. Pfützner (2013) found no substantial changes of the model quality. However, the fit of simulated to observed hydraulic heads at an observation well located between the new pond and a stream was not satisfactory. This was explained by the spatial discretisation of 25 m × 25 m since the distance between pond and stream is only about 170 m by (Pfützner, 2013).

Boundary conditions

Meteorology The input data for the model were the daily mean temperature, daily precipitation sums, daily sunshine duration, and daily mean humidity. The effective precipitation available to the model was calculated on the basis of several meteorological stations in the vicinity of the catchment. Precipitation values for each cell were interpolated on the basis of the daily precipitation sums at these stations. The remaining meteorological input data, needed for the calculation of the potential evapotranspiration, were taken from the station in Berlin Buch.

Hydrology At several locations in the catchment sinks and sources of water were included as time series. The discharge of treated wastewater into the irrigation ponds was included as time series. The treated wastewater was discharged into more ponds than realized in HydroGeoSphere. At OW1 (see Figure 3.7) water was discharged into the Lietzengraben as a source, accounting for the upper catchment. The evaporation from the water surfaces of the Lake Bogenseekette and the Karower Teiche was represented as a point sink of water. The time series contained rates of potential evapotranspiration. The actual volume of evaporation from the free water surfaces was calculated based on the area of the water body, which was derived from tabulated relationships between lake volume and surface. The surface water exited the catchment through the Lietzengraben

stream and the stream originating in the Karower Teiche and discharging to the river Panke south of the Lietzengraben.

Hydrogeology The subsurface boundary condition at the outer boundary of the catchment was chosen as a no-flow boundary.

Calibration procedure The calibration of the model was conducted manually. Parameters for the calibration were the hydraulic conductivity of the aquifer, the specific storage, which was assumed to be the effective porosity due to the unconfined aquifer, and the a leakage coefficient describing the coupling of streams to the subsurface. The surface water layer of the model was not calibrated since previous works showed that the predefined parameter sets were sufficient (Mey, 2011).
The calibration was conducted step wise from global to local values. On the basis of the values and their spatial distribution determined by Wachholz (2005) for the hydraulic conductivity the hydraulic conductivity was altered globally. Hence, the spatial patterns were preserved. After the global hydraulic gradient of the catchment, the slope of the groundwater table in the catchment was simulated reasonable, local hydraulic conductivity was altered locally to fit the simulated mean hydraulic heads at observation wells to observed heads. The amplitude of the dynamics of the hydraulic heads were fit to observed data in a further step by the alteration of the porosity. As in the previous steps, the calibration process went from global changes to local changes. Mey (2011) chose lower and upper boundaries for this parameter of $\phi = 0.1$ and $\phi = 0.3$, respectively. In order to get reasonable results for this parameter, the time period for the calibration included several years and the chosen observation wells were not influenced by nearby streams. Groundwater observation wells in the vicinity of streams are often heavily influenced by these. By the alteration of the leakage coefficient of the streambed, which controls the exchange of surface and subsurface water, simulated hydraulic heads at these observation wells were fit to observed heads. Mey (2011) used different leakage coefficients for the exfiltration of groundwater to the stream and the infiltration of stream water into the subsurface in order to account for clogging layer at the streambed. These clogging layers are considered to decrease the infiltration rate due a increased low resistance.
The data availability for the calibration process was inconsistent due to irregular measurements of hydraulic heads at observation wells. Hence, the calibration to hydraulic head data of observation wells was conducted for the period from 1994 to 1999. The calibration to observed discharge data was conducted for the period 1997 to 1999.

Post-processing for analysis of groundwater - surface water interaction

As presented in Equation (3.23), the exchange volume between a surface stream and the aquifer is governed by the head difference, the leakage factor, and the area available for the exchange. The model provides the calculated discharge of groundwater to the spatial units of the streams as volume per time per discrete stream feature (or stream reach). Therefore, in order to compare the results of the measurements (Section 4.1) with results obtained by ArcEGMO-ASM, the volume must be transformed into a flux rate.
The area which contributes to the exchange term is related to the level of the the

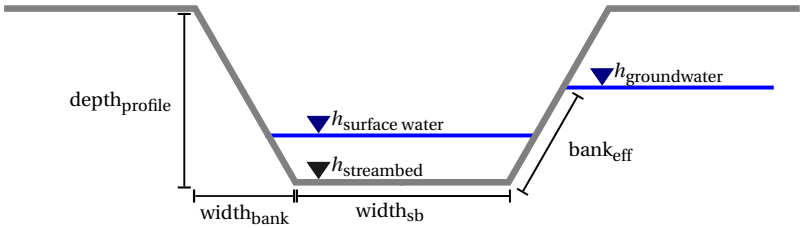

FIGURE 3.8: Profile of a stream feature as represented in ArcEGMO-ASM

adjacent groundwater, since not only the streambed, but also the stream banks are relevant during effluent conditions. A conceptual illustration of stream features, as represented in ArcEGMO-ASM, is shown in Figure 3.8. For every discrete stream feature, ArcEGMO-ASM provides the possibility to define geometric properties of the stream reach. Along with the depth of the profile, the width of the streambed and the length of the stream reach, the slope of the banks is pre-defined for every stream feature. The slope of the stream banks is given as:

$$s_{bank} = \frac{\text{depth}_{profile}}{\text{width}_{bank}}$$

The the lateral length of the bank surface, which is involved in the exfiltration of groundwater to the stream, is then calculated as:

$$\text{bank}_{eff} = \sqrt{(h_{groundwater} - h_{streambed})^2 + \left(\frac{h_{groundwater} - h_{streambed}}{s_{bank}}\right)^2} \tag{3.33}$$

where:

bank$_{eff}$ = Lateral length of the banks surface $[L]$
s_{bank} = Bank slope [-]
$h_{groundwater}$ = Groundwater head $[L]$
$h_{streambed}$ = Elevation of the streambed $[L]$

For every stream feature, the area contributing to the exfiltration of groundwater at the specific time step can then be calculated as:

$$A_{reach} = l_{reach} \times (\text{width}_{sb} + 2 \times \text{bank}_{eff}) \tag{3.34}$$

where:

l_{reach} = Length of the stream reach $[L]$
width$_{sb}$ = Width of the streambed $[L]$

The discharge rate of groundwater to the stream reach, normalised to the area, is therefore given as:

$$q = \frac{Q_{reach}}{A_{reach}} \tag{3.35}$$

where:

q = Flux rate of groundwater to the stream $[LT^{-1}]$
Q_{reach} = Discharge volume of groundwater to the stream reach $[L^3T^{-1}]$

3.2.3 HydroGeoSphere

HydroGeoSphere originates from the numerical model FRAC3DVS (Therrien, 1992), a robust numerical model which simulates variably saturated subsurface flow in three dimensions with the ability to simulate transport processes as well. However, the model lacked the integration of the fully integrated interaction between subsurface and surface flow. Further development of the model in order to overcome this limitation led to HydroGeoSphere, a fully integrated, physically based model.
This section gives a brief overview on the theoretical background of HydroGeoSphere. However, only the aspects relevant for the functionalities used in this work are considered. The transport of solutes or heat is possible but was not used. The version of HydroGeoSphere being used in this work is revision 1183, released in 2012. The model was and is still under development. The description of the model and the governing equations are taken from the manual of HydroGeoSphere published on April 23th, 2012 (Therrien et al., 2012).

Theory

Corresponding to Figure 3.6 in the previous section on ArcEGMO-ASM, Figure 3.9 shows a simplified illustration of HydroGeoSphere with governing equations. In the following paragraphs the equations will be described in detail.

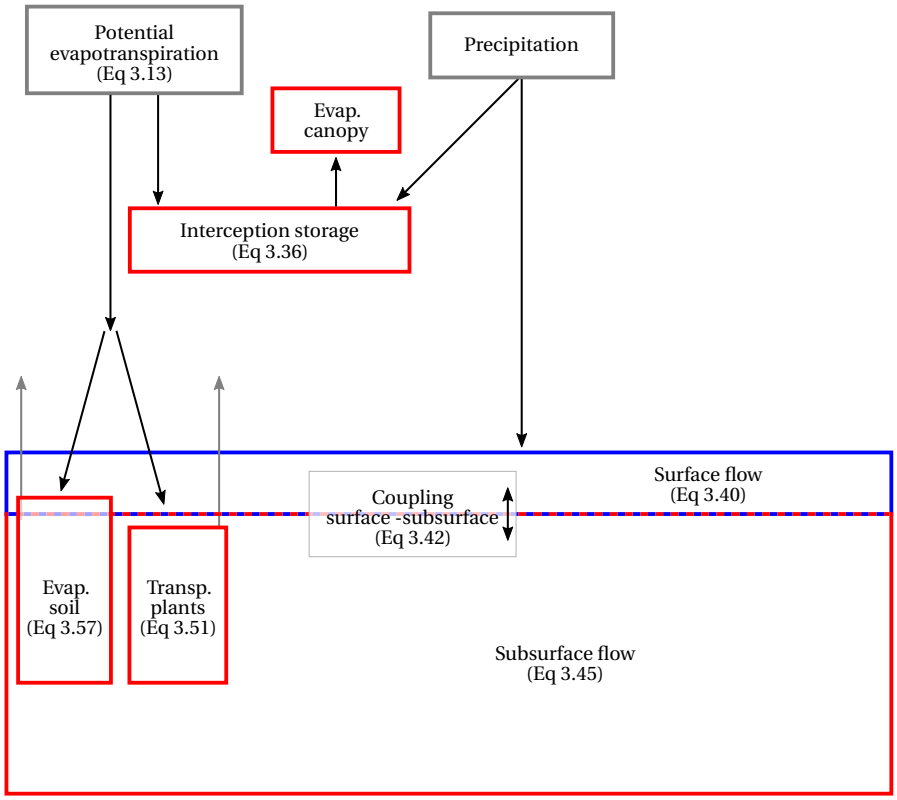

FIGURE 3.9: Simplified structure of the fully integetrated model HydroGeoSphere; Governing equations are refered to as numbers in brackets

Potential evapotranspiration HydroGeoSphere does not provide the calculation of the potential evapotranspiration.

Interception The interception of precipitation by the canopy of the vegetation cover is represented in HydroGeoSphere as a bucket model. In the beginning of a precipitation event the canopy storage is filled. Any precipitation exceeding the storage capacity of the canopy is passed to the surface. In HydroGeoSphere, the interception storage capacity is implemented after Kristensen and Jensen (1975) as:

$$S_{\mathrm{I}}^{max} = c_{\mathrm{int}} \times \mathrm{LAI} \tag{3.36}$$

where:

$S_{\mathrm{I}}^{\mathrm{max}}$ = Interception storage capacity $[L]$
LAI = Leaf area index [-]
c_{int} = Canopy storage parameter $[L]$

Since the interception storage capacity depends on the LAI, it is possibly subject to changes during the annual cycle of vegetation.

Surface flow The surface flow in HydroGeoSphere is driven by the topography and accounts for the interaction between subsurface and surface water. The surface flow is simulated in two dimensions based on the diffusive-wave approximation of the Saint Venant equations for surficial water flow. For the two dimensional Saint Venant equations, the flow is assumed to be dominated by bottom shear stress and to exhibit a vertically hydrostatic pressure distribution. Furthermore, flow velocities are calculated as depth averaged for mild slopes. In order to simplify the Saint Venant equations, the terms accounting for inertia in the description of the flow momentum are neglected and the Manning's formula for the calculation of friction slopes is used. This leads to the diffusive wave approximation of the Saint Venant equation, which is formulated in HydroGeoSphere as:

$$\frac{\partial \phi h_{\mathrm{o}}}{\partial t} - \frac{\partial}{\partial x}\left(d_{\mathrm{o}} K_{\mathrm{ox}} \frac{\partial h_{\mathrm{o}}}{\partial x}\right) - \frac{\partial}{\partial y}\left(d_{\mathrm{o}} K_{\mathrm{oy}} \frac{\partial h_{\mathrm{o}}}{\partial y}\right) + d_{\mathrm{o}}\Gamma_{\mathrm{o}} \pm Q_{\mathrm{o}} = 0 \tag{3.37}$$

where:

ϕ_{o} = Surface flow domain porosity [-]
h_{o} = Water surface elevation $[L]$
d_{o} = Depth of flow $[L]$
K_{ox}, K_{oy} = Surface conductance in x- and y-direction $[LT^{-1}]$
Γ_{o} = Flow between the surface and subsurface domain $[L^3 L^{-3} T^{-1}]$
Q_{o} = Volumetric flow rate of external sources and sinks $[LT^{-1}]$

The surface conductance in x-direction is calculated as:

$$K_{\mathrm{ox}} = \frac{d_{\mathrm{o}}^{2/3}}{n_{\mathrm{x}}} \frac{1}{[\partial h_{\mathrm{o}}/\partial s]^{1/2}} \tag{3.38}$$

and for the y direction as:

$$K_{\mathrm{oy}} = \frac{d_{\mathrm{o}}^{2/3}}{n_{\mathrm{y}}} \frac{1}{[\partial h_{\mathrm{o}}/\partial s]^{1/2}} \tag{3.39}$$

where:

n_x, n_y = Manning roughness coefficients in x and y direction $[L^{-1/3}T]$
s = Slope in the direction of maximum slope [-]

Equation 3.37 can be rewritten as:

$$\nabla \times \left(d_o q_o\right) - d_o \Gamma_o \pm Q_o = \frac{\partial \phi_o h_o}{\partial t} \tag{3.40}$$

The fluid flux q_o [-] is given as:

$$q_o = -K_o \times k_{ro} \nabla \left(d_o + z_o\right) \tag{3.41}$$

k_{ro} [-] describes the reduction of horizontal conductance due to the exclusion of obstruction storage. z_o is the elevation of the streambed which leads to the elevation of the water surface being $h_o = d_o + z_o$.
The surface flow under natural conditions is influenced by obstacles and surface depressions, especially in urban and agricultural environments. To simulate surface flow in a realistic manner these factors have to be considered. In HydroGeoSphere this is realized by the implementation of parameters accounting for rill storage and obstruction height. The rill storage is the depth of small scale surface depressions which act as storage and inhibit surface flow. After the rill storage is filled, lateral flow over the surface is induced. Obstacles like trees or buildings decrease the area on the surface available for surface flow, e.g. the storage capacity, and increase the roughness due to additional frictional forces. The area available for surface flow ranges from 0 at the land surface to unity at elevations higher than the obstruction storage height. This is incorporated in the porosity parameter ϕ_o in Equation 3.37 and Equation 3.40. The effects of rill storage and exclusion of obstruction storage can occur simultaneously.

Surface-subsurface coupling The coupling between the subsurface and the surface domain can be represented by one of two approaches. The common node approach assumes the continuity of the hydraulic heads between the subsurface and the surface. This implies an instant equilibrium between the domains and hence does not imply the evaluation of the exchange term Γ_{ex} in Equation 3.44 and Γ_o in Equation 3.40 within the model. The second approach, denoted as dual node approach does not assume the continuity of hydraulic heads. The exchange between surface and subsurface domain is then calculated on basis of the Darcy equation. The exchange term is implemented in HydroGeoSphere as:

$$d_o \Gamma_o = \frac{k_r k_{f,z}}{l_{coupl}} \left(h - h_o\right) \tag{3.42}$$

where:

h = Subsurface water head $[L]$
h_o = Surface water head $[L]$
$k_{f,z}$ = Saturated hydraulic conductivity of the subsurface$[LT^{-1}]$
k_r = Relative permeability [-]
l_{coupl} = Coupling length $[L]$

The relative permeability k_r is the same as in Equation 3.49 in the porous medium for water flowing from the subsurface to the surface domain. However,

HydroGeoSphere accounts for the exclusion of obstruction storage and hence the relative permeability for flow of water from the surface to the subsurface is related to the obstruction height. This relationship is formulated as:

$$k_r = \begin{cases} S_{ex}^{2(1-S_{ex})} & \text{for} \quad d_o < H_s \\ 1 & \text{for} \quad d_o > H_s \end{cases} \tag{3.43}$$

with

$$S_{ex} = \frac{d_o}{H_s}$$

where:

d_o = Depth of flow $[L]$
H_s = Obstruction height $[L]$

Subsurface flow The flow of water within the porous medium is represented in HydroGeoSphere as fully saturated or variable saturated flow in three dimensions. It is assumed that the fluid is incompressible, the matrix of the porous medium is not deformable, and isothermal conditions are applied.
The three-dimensional, variable saturated flow in the subsurface is described in HydroGeoSphere by a modified form of the Richard's equation:

$$-\nabla \times (w_m q) + \sum \Gamma_{ex} \pm Q = \omega_m \frac{\partial}{\partial t}(\theta_{\text{sat}} S_{\text{w}}) \tag{3.44}$$

where:

w_m = Volumetric fraction of the total porosity occupied by the porous medium [-]
q = Fluid flux $[LT^{-1}]$
Γ_{ex} = Volumetric fluid exchange rate $[L^3L^{-3}T^{-1}]$
Q = Fluid exchange with the outside of the model domain $[L^3L^{-3}T^{-1}]$
θ_{sat} = Water content at full saturation [-]
S_{w} = Degree of water saturation [-]

The volumetric fraction w_m is 1.0 as long only one porous medium is considered in the simulation. The saturated water content of the medium θ_{sat} is considered to be equal to the porosity of the medium. The term Q accounts for boundary conditions leading to inflow or outflow of water into or out of the subsurface domain while Γ_{ex} stands for the exchange of water between the subsurface domain and other domains which can be considered in HydroGeoSphere. These include wells, tile drains, discrete fractures, and surface water. The fluid flux in a variable saturated porous medium q can be described as:

$$q = -k_{\text{f}} \times k_r \nabla(\psi + z) \tag{3.45}$$

where:

k_{f} = Hydraulic conductivity $[LT^{-1}]$
k_r = Relative permeability of the medium [-]
ψ = Pressure head $[L]$
z = Elevation head $[L]$

The relative permeability k_r depends on the degree of water saturation S_{w}. The water saturation describes the content of water in the medium in relation to

the water content under fully saturated conditions as:

$$S_{\mathrm{w}} = \frac{\theta}{\theta_{\mathrm{sat}}} \tag{3.46}$$

where:

θ = Water content [-]

Therefore, the range of values of S_{w} is between 0 and 1. Hence, it is independent from the porosity of the medium. In any porous medium the water content, e.g. the saturation, is linked to the water pressure. This relationship is highly non-linear and is represented in HydroGeoSphere by the models of Brooks and Corey (1964) or Van Genuchten (1980). In the following, the model of the latter is described since it was used in this work. The relation between saturation and pressure after Van Genuchten (1980) was formulated as:

$$S_{\mathrm{w}} = \begin{cases} S_{\mathrm{res}} + (1 - S_{\mathrm{res}}) \left[1 + \mid \alpha\psi \mid^{\beta}\right]^{-\nu} & \text{for } \psi < 0 \\ 1 & \text{for } \psi \geq 0 \end{cases} \tag{3.47}$$

where:

S_{w} = Water saturation [-]
S_{res} = Residual water saturation [-]
α, β = Van Genuchten-Mualem parameters [L^{-1}], [-]
ψ = Pressure head [L]

ν can be derived by:

$$\nu = 1 - \frac{1}{\beta}, \quad \beta > 1 \tag{3.48}$$

The parameters α and β, denoted as van Genuchten-Mualem parameters, are often estimated by the inverse modeling of results from laboratory experiments or by the use of models which rely on information about the soil texture composition. The relative permeability k_r in Equation 3.45 is then given as:

$$k_r = S_e^{(l_p)} \left[1 - \left(1 - S_e^{1/\nu}\right)^{\nu}\right]^2 \tag{3.49}$$

where:

S_e = Effective saturation [-]
l_p = Pore connectivity parameter [-]

The effective saturation S_e is given by:

$$S_e = \frac{S_{\mathrm{w}} - S_{\mathrm{res}}}{1 - S_{\mathrm{res}}}$$

The pore connectivity parameter in Equation 3.49 was determined as $l_p = 0.5$ by Mualem (1976) for most soils. In HydroGeoSphere the estimation of $S_{\mathrm{w}}(\psi)$ and $k_r(S_e)$ can be executed by the use of pre-defined tabulated data or the calculation of tables based on a given set of parameter values.
The storage term on the right hand side of Equation 3.44 is calculated in HydroGeoSphere similar to Cooley (1971) and Neumann (1973). The impact of the matrix compressibility of the porous medium on the storage properties is considered to be negligible, even under unsaturated conditions. The storage term is

then formulated as:

$$\frac{\partial}{\partial t}(\theta_{\text{sat}} S_{\text{w}}) \approx S_{\text{w}} S_s \frac{\partial \psi}{\partial t} + \theta_{\text{sat}} \frac{\partial S_{\text{w}}}{\partial t} \tag{3.50}$$

where:

S_s = Specific storage coefficient $[L^{-1}]$

Actual Evapotranspiration HydroGeoSphere calculates actual evapotranspiration from a given potential evapotranspiration. The calculation is strictly separated into transpiration by plants and evaporation.
The calculation of water withdrawal due to transpiration by plants affects the rooting zone of plants in the subsurface domain. Transpiration rates are modeled after Kristensen and Jensen (1975), given as:

$$T_{\text{plants}} = f_1(\text{LAI})\, f_2(\theta) \text{RDF} \left[ET_{\text{pot}} - E_{\text{can}} \right] \tag{3.51}$$

where:

T_{pot} = Transpiration rate $[LT^{-1}]$
$f_1(\text{LAI})$ = Function of the LAI [-]
$f_2(\theta)$ = Function of the water content [-]
RDF = Root distribution function [-]
ET_{pot} = Potential evapotranspiration $[LT^{-1}]$
E_{can} = Canopy evaporation $[LT^{-1}]$

As shown in Equation 3.51, the potential transpiration rate is dependent on multiple functions, accounting for the mechanism controlling the transpiration. The dependency on the vegetation cover is formulated as:

$$f_1(\text{LAI}) = \max\{0,\ \min[1,\ (C_2 + C_1\ \text{LAI})]\} \tag{3.52}$$

The dependency on the water content θ is given as:

$$f_2(\theta) = \begin{cases} 0 & \text{for} \quad 0 \le \theta \le \theta_{\text{wp}} \\ f_3 & \text{for} \quad \theta_{\text{wp}} \le \theta \le \theta_{\text{fc}} \\ 1 & \text{for} \quad \theta_{\text{fc}} \le \theta \le \theta_{\text{ox}} \\ f_4 & \text{for} \quad \theta_{\text{ox}} \le \theta \le \theta_{\text{an}} \\ 0 & \text{for} \quad \theta_{\text{an}} \le \theta \end{cases} \tag{3.53}$$

with:

$$f_3 = 1 - \left[\frac{\theta_{\text{fc}} - \theta}{\theta_{\text{fc}} - \theta_{\text{wp}}} \right]^{C_3} \tag{3.54}$$

and:

$$f_4 = 1 - \left[\frac{\theta_{\text{an}} - \theta}{\theta_{\text{an}} - \theta_{\text{ox}}} \right]^{C_3} \tag{3.55}$$

where:

C_1, C_2, C_3 = Fitting parameters [-]
θ = Water content [-]
θ_{wp} = Water content at wilting point [-]
θ_{fc} = Water content at field capacity [-]
θ_{ox} = Water content at the oxic limit for transpiration [-]
θ_{an} = Water content at the anoxic limit of transpiration [-]

Equation 3.53 formulates four distinct zones for the transpiration of water by plants. At saturations below the wilting point, water uptake and hence transpiration is not possible. Above the anoxic limit the transpiration is also 0. The optimum zone is with water contents between the field capacity and the oxic limit of plant transpiration. Between the saturation zones with no transpiration and the optimum zone, the transpiration is gradually increased or decreased, respectively. The root density function in Equation 3.51 describes the abundance of roots with varying depth. The RDF is implemented as:

$$\mathrm{RDF} = \frac{\int_{z_1'}^{z_2'} r_F(z')\,dz'}{\int_0^{z_{\max}} r_F(z')\,dz'} \tag{3.56}$$

where:

$z_{\max}$ = Effective root length [L]
z' = Depth below the soil surface [L]
$r_F(z')$ = Root extraction function [L^3T^{-1}]

At default, the root density distribution is linear correlated with the depth. However, HydroGeoSphere provides options to account for the distribution as a constant, as a quadratic decay function, or a cubic decay function. In this work, the quadratic decay function was applied.

The evaporation of water from the surface and subsurface domain is calculated as:

$$E_{\text{soil, surf}} = \alpha^* \left(ET_{\text{pot}} - E_{\text{can}}\right)\left[1 - f_1(\mathrm{LAI})\right]\ \mathrm{EDF} \tag{3.57}$$

where:

α^* = Wetness factor [-]
EDF = Evaporation distribution function [-]

The evaporation is limited by the vegetation cover, expressed as LAI, which controls the amount of radiation reaching the land surface. This limitation is given as $\left[1 - f_1(\mathrm{LAI})\right]$, which is the counterpart to $f_1(\mathrm{LAI})$ in Equation 3.51. The evaporation from the soil and the surface is limited by the penetration depth of radiation energy and the water content, which is expressed as a wetness factor α^* given as:

$$\alpha^* = \begin{cases} \frac{\theta - \theta_{e2}}{\theta_{e1} - \theta_{e2}} & \text{for} \quad \theta_{e2} \le \theta \le \theta_{e1} \\ 1 & \text{for} \quad \theta > \theta_{e1} \\ 0 & \text{for} \quad \theta < \theta_{e2} \end{cases} \tag{3.58}$$

where:

θ_{e1} = Water content at the end of the energy limiting stage [-]
θ_{e2} = Limiting water content [-]

As expressed in Equation 3.58, a soil water content greater than θ_1 allows the full evaporation potential to occur while a soil water content smaller than θ_{e2} inhibits any evaporation in the subsurface.
The evaporation process also affects the surface flow domain. The implementation of the evaporation process in HydroGeoSphere accounts for surface depressions, e.g. rill storage. The surface area available for evaporation is 0 at the soil surface and gradually increases until the water depth on the surface is equal to or greater than the rill storage height, where the available area becomes unity. The evaporation distribution function is formulated as an equivalent to the root density function described above. Different functions are available to account for the decrease of available energy with depth. In this work, the quadratic decay function was chosen.

Physical model

The physical model of the Lietzengraben model was set up on the basis of interpolated data from measurements, geographical maps, literature, and the model of the catchment set up by Mey (2011) with ArcEGMO-ASM.

Catchment

Boundaries & topography The surface catchment boundaries were derived by the analysis of a digital elevation model with a horizontal resolution of 10 m × 10 m and a vertical accuracy of 2 m. However, the catchment was extended at the southern boundary to a channel, which cuts deep into the adjacent terrain. Due to this extension, the catchment area was greater than the area of the ArcEGMO-ASM model, but did coincide well. The surficial catchment was chosen to avoid the accumulation of surface water at the boundaries. The topography was corrected for features like elevated road and railways to avoid steep gradients and hence unnecessary risk of numerical difficulties. However, the outer boundary of the area simulated in this study was extended to the south-west to a drainage channel about 10 m below the surrounding terrain. The aim of this extension was to account for potential groundwater exfiltration to this channel. The channel discharges into the river Panke at the southern corner of the simulated catchment. The total area of the catchment modelled with HydroGeoSphere in this study is 42 km^2, while the area of the model set up with ArcEGMO-ASM is about 37 km^2. The HydroGeoSphere catchment, the streams and surface water bodies in the catchment, and the observation wells and stream gauges are shown in Figure 3.10.

Discretisation The discretisation of the model domain was an important part of the model set-up. On the one hand, a fine discretisation of the model area would induce a high number of cells, which would lead to long computational times. On the other hand, the size of cells determines the numerical stability of the model and provides the possibility to get results in a higher spatial resolution. The finite element methods provides the possibility to define an irregualar grid, with a finer mesh in areas of interest. Hence, a mesh which was finer in the area adjacent to the the irrigation ponds (20 to 30 m) and relatively coarse in the remaining catchment (70 to 100 m) was chosen. The geometry of surface water features was implemented in the process of mesh generation to ensure the accurate representation of streams, lakes, and irrigation ponds. The mesh was

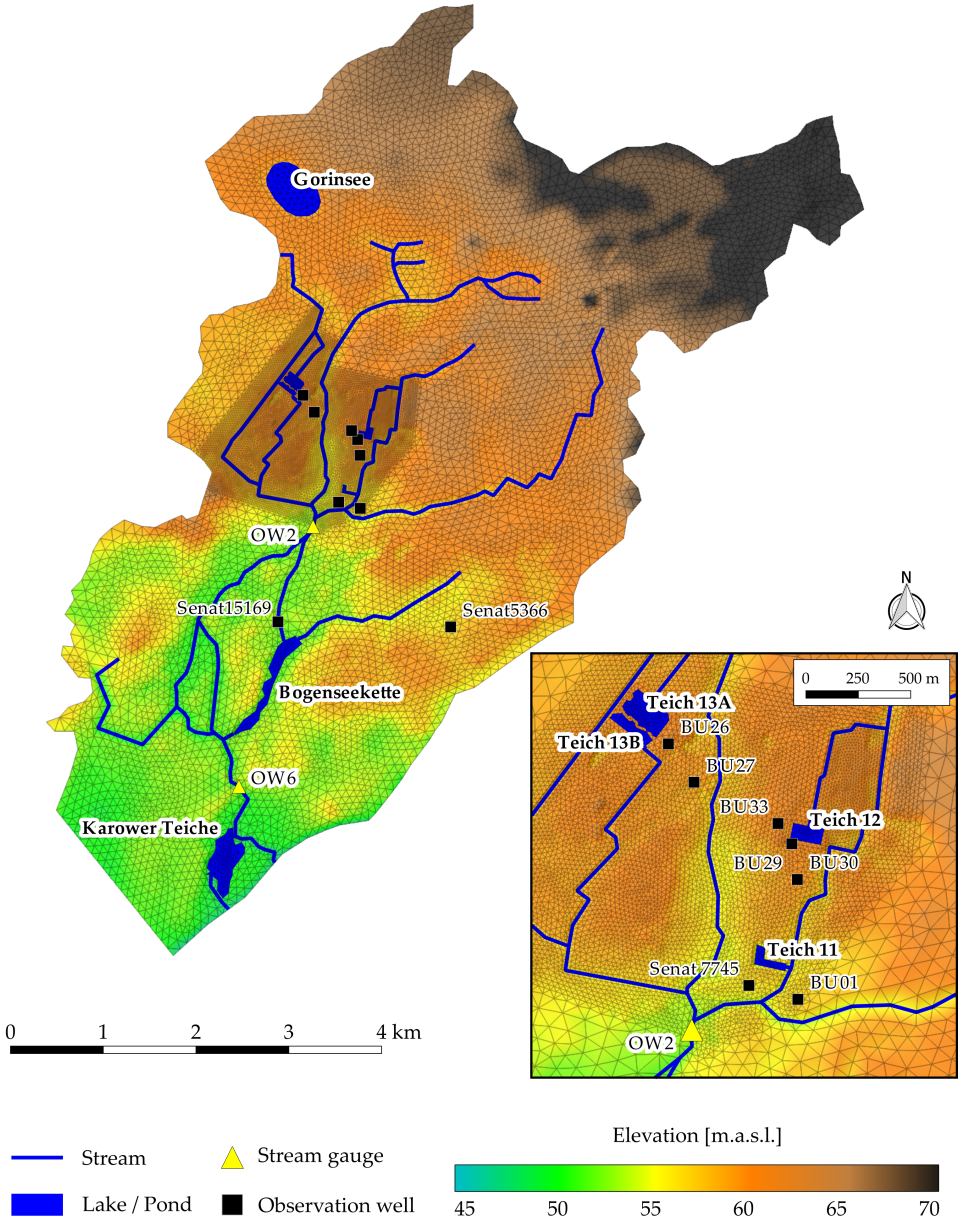

FIGURE 3.10: Lietzengraben catchment as represented in HydroGeoSphere

generated with the pre-proccesing software Grid Builder (McLaren, 2011). The mesh configuration was the result of a processs beginning with a fine mesh and test for computational effort needed to run the model. Since the calibration of the model was done automatically by the use of the calibration algorthm PEST (Doherty, 2010), it was crucial to achieve a result with low computational effort. The vertical discretisation was done in the same manner. As a result, the aquifer was divided into 8 layers with increasing thickness from the top to the bottom. The thickness of each layer was defined by relative values describing the proportions of the layers to each other. The layers were divided using thickness values of 0.2, 0.2, 0.3, 0.5, 1, 1, 1 and 2, proportional to each other, for mesh generation. The soil was considered by the definition of one layer at the top of the subsurface domain which was 0.43 m thick. The spatial discretisation lead to a total number of 243,864 elements.

The temporal discretisation was handled dynamically by the model within pre-defined restrictions. An upper limit of 1 d and a lower limit of 1×10^{-6} d were defined.

Surface water bodies In many applications of HydroGeoSphere on a catchment scale, it is not necessary to pre-define surface streams since the model generates surface water bodies based on topography and hydraulic conditions. However, the stream network in the Lietzangraben catchment is human made and the streambed elevations were much lower than the adjacent terrain. Therefore, the stream network was included in the set-up process. The stream network used in ArcEGMO-ASM was implemented, with the given streambed elevations used in ArcEGMO-ASM. The nodes of the surface of the mesh were altered along the streams. The irrigation ponds were represented by the adaptation of site maps of the ponds. The ponds "Teich 13" and "Teich 12" were sealed at the bottom by a layer of relatively impermeable marl, the pond "Teich 11" has not been sealed. In the following, the first named group is referred to as sealed ponds, the latter as unsealed pond. Weirs in the catchment were represented by increasing the streambed elevation to the desired water level elevations. HydroGeoSphere did not provide features accounting for management measures like weirs.

Observation points Based on available data, stream gauges and groundwater observation wells were chosen for the calibration and validation of the model. Discharge gauge OW2 is located in the central catchment, downstream of the confluence of the Lietzengraben stream and the streams discharging the irrigated treated wastewater. Discharge gauge OW6 is located near the outlet of the Lietzengraben stream from the catchment. While OW2 represents the upper catchment, OW6 gives the integrated response of the whole catchment.
Several groundwater observation wells were integrated into the model. The majority of the wells is located in the surrounding of the irrigation ponds. Observation ponds Senat15169 and Senat5366 were further downstream and near the eastern boundary of the catchment, respectively. The locations of the stream gauges and the groundwater observation wells are shown in Figure 3.10.

Surface properties The classification of the catchment area into zones of distinct land use was done by the adaptation and reclassification of land use classes integrated in ArcEGMO-ASM. Additionally, land use was checked and completed where no data was available by the use of colour infrared images. The type of land use determines the properties governing the surface water flow. However, many of the surface parameters where involved in the calibration process. Therefore, the number of surface types was reduced to decrease the number of parameters. Since the catchment is dominated by forests and grasslands, this reduction seemed justified. The types of surfaces were defined as land, streams, irrigation ponds with a sealed bed, lakes, and ponds. Goderniaux et al. (2009) reported the coupling length l_{coupl} to be an insensitive parameter. Due to the chatchment characteristics with drainage channels and artificial ponds, the coupling length of streams and ponds were estimated during calibration. The roughness of streambeds, expressed as the Manning's roughnesss $n_{\text{x,y}}$, is of great importance for the discharge behaviour in a catchment (Sciuto and Diekkrüger, 2010). First model runs during the model set-up showed that the parameter values reported

in literature of 0.005 s m$^{-1/3}$ to 0.04 s m$^{-1/3}$ (Arcement and Schneider, 1989; Hornberger, 1998; Li et al., 2008; Jones et al., 2008; Alaghmand et al., 2014) led to insufficient dynamics of the simulated discharge. The simulations were characterised by the very quick response of stream discharge to precipitation events and very high peak discharge volumes. Hence the parameter was included into the calibration process.

The distinction between different vegetation types influences the depth of water consumption. Despite numerous efforts, it was not possible to realize different zones of evapotranspiration properties. Due to unknown reasons, the simulation was not able to achieve convergence of the numerical solution and the hydraulic heads at several points on the land surface dropped with increasing speed down to $<< -1{,}000$ m. As a result, the time steps chosen by the model dropped below the pre-defined lower limit of 1×10^{-6} d. This lead to the termination of the simulation run. Therefore, the classification of the evapotranspiration properties were reduced to land and water. Major parts of the catchment consist of rural grasslands and forested areas. The set of parameter values differed in the chosen leaf area index (LAI) and rooting depth $z_{\max}$ of these vegetation classes. The values were taken from literature as given in Table 3.2. Parameters for water contents were altered. Values for θ_{wp}, θ_{fc}, θ_{ox}, and θ_{an} were originally taken from Therrien et al. (2012). However, the parameter value was increased to avoid non-convergence of the solution on the surface. The LAI was chosen lower than reported in literature for trees. However, the function $f_1(LAI)$ as in Equation 3.52 yields a value of 1 for every LAI ≥ 2, given the parameters C_1 and C_2 as in Table 3.2. The calculation of actual transpiration given Equation 3.51 is hence not decreased by $f_1(LAI)$. Therefore, the value chosen for LAI is irrelevant, if the LAI is kept > 2. The LAI would eventually become < 2 during the winter months when potential evapotranspiration is very low and thus is not substantial for the annual sum of evapotranspiration.

TABLE 3.2: Evapotranspiration parameter values

Parameter	Source	Land	Water
LAI	altered after Therrien et al. (2012)	3	0
$z_{\max}$	altered after Therrien et al. (2012)	3 m	0.2 m
C_1	Goderniaux et al. (2009)	0.5	
C_2	Goderniaux et al. (2009)	0	
C_3	Goderniaux et al. (2009)	10.0	
c_{int}	Goderniaux et al. (2009)	0 m	
z_{evap}	Goderniaux et al. (2009)	2 m	
θ_{e1}	Therrien et al. (2012)	0.5	
θ_{e2}	Therrien et al. (2012)	0.1	
θ_{wp}	-	0.1	
θ_{fc}	-	0.15	
θ_{ox}	-	1.01	
θ_{an}	-	1.02	

Hydrogeology As described in section 2.5, the uppermost aquifer was considered to be isolated from the underlying aquifer by a thick layer of marl. The

thickness and hydraulic conductivities of the aquifer were derived from borehole data, which had been used as a basis in previous studies (Wachholz, 2005; Mey, 2011). The thickness data were interpolated using a thin plate spline algorithm (Nychka et al., 2015) processed in *GNU R*. The thickness of the aquifer was implemented in the model. Hydraulic conductivities were interpolated in *GNU R* by ordinary kriging (Pebesma, 2004; Gräler et al., 2016). The interpolated hydraulic conductivity of the aquifer was used as the starting point in the calibration process, while the distribution of the hydraulic conductivity remained unaltered. The raster map of the distributed hydraulic conductivity was normalized to its maximum value. This distribution was used for the calibration process. The hydraulic conductivities in vertical direction have not been included in the borehole data. The values have been obtained through calibration. A map of the aquifer thickness is shown in Figure 3.11. The porosity of the aquifer was also included in the calibration process. However, based on the findings by Mey (2011), the aquifer was divided into two zones of uniform porosity. Mey (2011) estimated a distinction between the northern and southern part of the aquifer with the porosity being substantially higher in the southern part with $\phi = 0.25$ in comparison to the northern part with $\phi = 0.01$. This boundary was implemented in the HydroGeoSphere model and is shown in Figure 3.11.

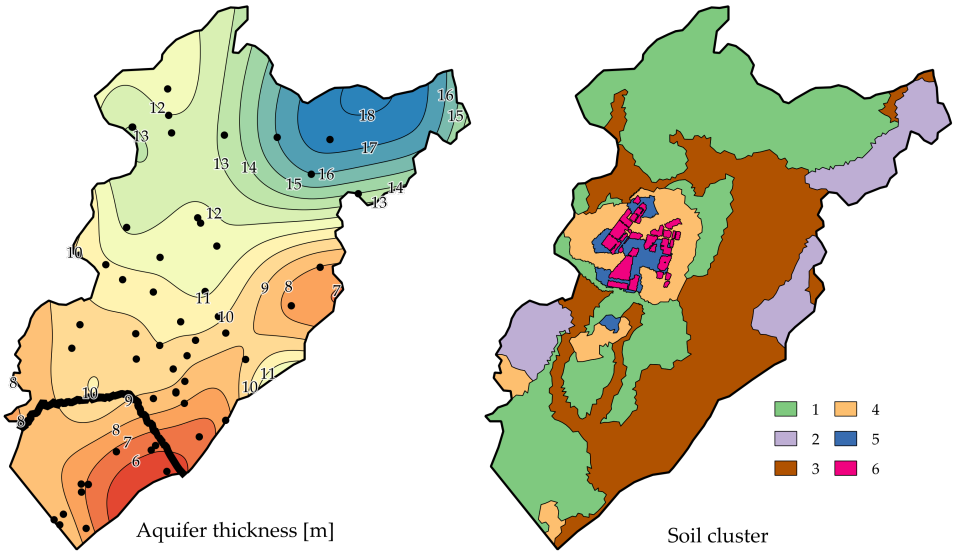

FIGURE 3.11: Left: Interpolated thickness of the unconfined aquifer; boreholes are shown as black dots, the black line indcates the boundary between the northern and southern part of the aquifer. Right: Distribution of soil clusters in the catchmenet as implemented in HydroGeoSphere

Soil In comparison to the ArcEGMO-ASM model, a simplified approach to represent different soil properties was used. The spatial differentiation of distinct soil layers and the number of different soil types were reduced. The goal of this approach was to avoid numerical instabilities due to a large number of parameter transitions between neighbouring soil types. Furthermore, only one layer was used to represent the soil layer overlying the aquifer, which made it necessary to aggregate soil data.

Data source Basis for the parametrisation of the soil layer, was soil data used in the existing ArcEGMO-ASM model. Mey (2011) combined data derived from maps with analysis of field samples to gain meaningful soil parameters and spatial distribution of different soil types. This dataset included information about saturated hydraulic conductivity, residual saturation, porosity, fractions of sand, silt, and clay (amongst others). The values provided in these tables were used in the parametrisation process of the HydroGeoSphere model. Since the model boundaries of ArcEGMO-ASM and HydroGeoSphere do not coincide for some parts, the missing information about spatial distribution of soil types outside the ArcEGMO-ASM model domain was derived from additional soil information (*Grundkarte der BÜK 300 im Onlinekatalog*). The Van Genuchten parameters needed for the parametrisation of soil layers in HydroGeoSphere have not been provided and were estimated based on the content of sand, silt and clay in the parametrisation process described below.

Vertical aggregation Soil data in ArcEGMO-ASM are organised in soil profiles which consist of a distinct sequence of soil layers of different properties. The uppermost layers of every profile have been used in the parametrisation process. For every soil profile, layers up to a depth of 43 cm below surface or layers of the soil type "Sl3" (medium loamy sand) have been included in the aggregation process. This choice was made based on the areas in the catchment, where marl/loam was ploughed into the top layer of the soil. In these areas, the medium value of thickness of this layer was 43 cm, described as "Sl3". For the same reason, the thickness of the top layer in HydroGeoSphere is 43 cm. The parameters of the included soil layers were calculated using a weighted mean with respect to the thickness of the particular soil layer.

Parameter estimation Based on the sand, silt, and clay content, values for the Van Genuchten parameters were calculated using the Rosetta model (Schaap et al., 2001). North of the Lietzengraben stream in the upper catchment, and at the south-eastern boundary of the model domain, small areas of peat soils exist. These areas could not be represented by meaningful parameter sets, since in these zones macro-pore flow is dominant, which can hardly be described by the Van Genuchten model (Vereecken et al., 2010). Parameter sets from neighbouring soil types were used since these peat areas were comparatively small.

Soil parameter clusters To obtain reasonable parameter values and spatial differentiation while reducing the numbers of soil types and their corresponding parameter sets, soil types with similar parameter sets have been grouped into clusters. To preserve areas with marl/loam ploughed into the top layer these were excluded from clustering and added afterwards as an additional soil parameter cluster. A cluster analysis in *GNU R* yielded an optimum number of 5 different clusters for the remaining soil types. As selection criterion the sum of squares of the differences between the cluster value and the "original" value of the parameters was set. The larger the number of clusters, the smaller the sum of square gets. At a number of 5 clusters, the decrease of the sum of squares declines rapidly. Using more clusters does reduce the sum of squares significantly. The spatial distribution of the six soil parameter clusters is shown in Figure 3.11. Note the areas with marl/loam, denoted as "Soil cluster 6". The parameter sets for the soil parameter clusters are noted in Table 3.3. The deviations between the original

parameter values and the corresponding cluster value were between -10% and +10%. Only for the saturated hydraulic conductivity K_f the maximum deviation has been almost 200% in one case. Since the value of hydraulic conductivity is a highly uncertain parameter and the affected areas are located nearby the model boundaries, this error seemed acceptable.

TABLE 3.3: Parameter values of the soil parameter clusters

Cluster	k_f [m d^{-1}]	θ_{res} [-]	θ_{sat} [-]	α [m^{-1}]	β [-]
1	3.9	0.068	0.499	3.3	2.9
2	0.4	0.073	0.394	4	1.5
3	3.1	0.056	0.439	3.7	2.5
4	6.7	0.062	0.399	3.6	3.8
5	10	0.046	0.29	3.6	4
6	0.7	0.16	0.551	3	1.4

Boundary conditions

Meteorological boundary conditions Precipitation data with a temporal resolution of one day was obtained from the meteorological station Buch, located south-east of the catchment. The location of the station is shown in Figure 2.1. Potential evapotranspiration input was derived by ArcEGMO-ASM, which calculated the potential evapotranspiration after Turc/Ivanov, corrected after Glugla (DVWK, 1996; Glugla and König, 1989). Therefore, the same input of potential evapotranspiration was used for HydroGeoSphere and ArcEGMO-ASM.

Discharge of treated wastewater The discharge volumes of treated wastewater were taken from data provided by "Büro für Angewandte Hydrologie", Berlin. However, due to the simplification of the irrigation ponds during the set-up of the HydroGeoSphere model, the discharge was evenly distributed among irrigation pond "Teich 13", which actually consists of several ponds.

Outer boundaries The base of the aquifer was considered impermeable and hence a no-flow boundary condition was applied. The outer boundaries of the aquifer were also implemented as no-flow boundaries. Groundwater could leave the catchment after the exfiltration to the river Panke in the south-east of the catchment or exfiltration to the deep channel along the south-west boundary of the catchment. A critical depth boundary was applied along the surficial edges of the catchment, which allowed surficial water to exit the catchment inhibited.

Calibration procedure

The initial state of the calibrated model was obtained by applying an average annual groundwater recharge of 80 mm on the surface until discharge and groundwater heads did not change during time significantly and hence steady state conditions were assumed . The hydraulic conductivity of the aquifer was slightly adjusted in order to be in range of the mean hydraulic heads. The aquifer was assumed as isotropic at this stage of the calibration process. The Manning's coefficient n was also adjusted in order to achieve discharge volumes in the range of the observed discharge.
The calibration process was carried out by applying the PEST algorithm (Doherty,

2010). The parameters used for calibration and their spatial affiliation are shown in Table 3.4. Due to the computational effort and the resulting long computational times, and the number of parameters used for the automated calibration, the time period for the calibration process was limited to the year 2007. In 2007, the discharge of treated wastewater to irrigation pond "Teich11" started and hence all irrigation ponds were operational. Simulated discharge volumes and groundwater heads were compared to observed values during the calibration process. The stream discharge gauges and the groundwater observation wells represented in the model were described in the previous paragraphs and are shown in Figure 3.10. To account for the locations of observation wells in the catchment and in order to emphasise the importance of the area adjacent to the irrigation ponds, the deviations between simulated and observed data were weighted by multiplication to a weighting factor. In general, the observation wells Senat15169 and Senat5366 in the southern part of the catchment were weighted by the factor 0.8, the remaining wells and the stream gauges were weighted by a factor of 1. The number of available data points was accounted for, too. Hence, the summarised deviation of simulated to observed heads at an observation well with only 13 available observation points over the calibration period had the same impact on the calibration process as the summarised deviation at observation wells with 365 available data points.
In order to validate the calibrated model, simulated discharge and groundwater heads for the period 2008 to 2012 were compared to observed data and evaluated based on the calculated Nash-Sutcliffe efficiency coefficients, Pearson correlation coefficients, and a visual inspection of the results. For most of the groundwater observation wells data were only available until the mid of 2011. In order to support the analysis of the field measurements undertaken in 2012, however, the validation period was extended to the end of 2012.

TABLE 3.4: Parameters included in the calibration process

Description	Parameter	Zones
Manning's roughness	$n_{x,y}$	Streams, ponds & lakes, land
Coupling length	l_{coupl}	Streams, unsealed pond, sealed pond
Porosity	ϕ	Aquifer north, aquifer south
Hyd. conductivity	k_f^{xy}	Aquifer
Hyd. conductivity	k_f^{z}	Aquifer

4 Results and discussion

4.1 Estimation of groundwater discharge

In 2012 several measurements campaigns were undertaken to estimate groundwater - surface water interaction along a stream reach. The overall goal was to determine spatial and temporal patterns of groundwater discharge to the stream and to compare results obtained by different methods. Furthermore, field measurements have been compared to the outcome of simulations. In this section results from field measurements are presented and discussed. The comparison of these results to simulations will be discussed in section 4.2.2.

4.1.1 Location of field measurements

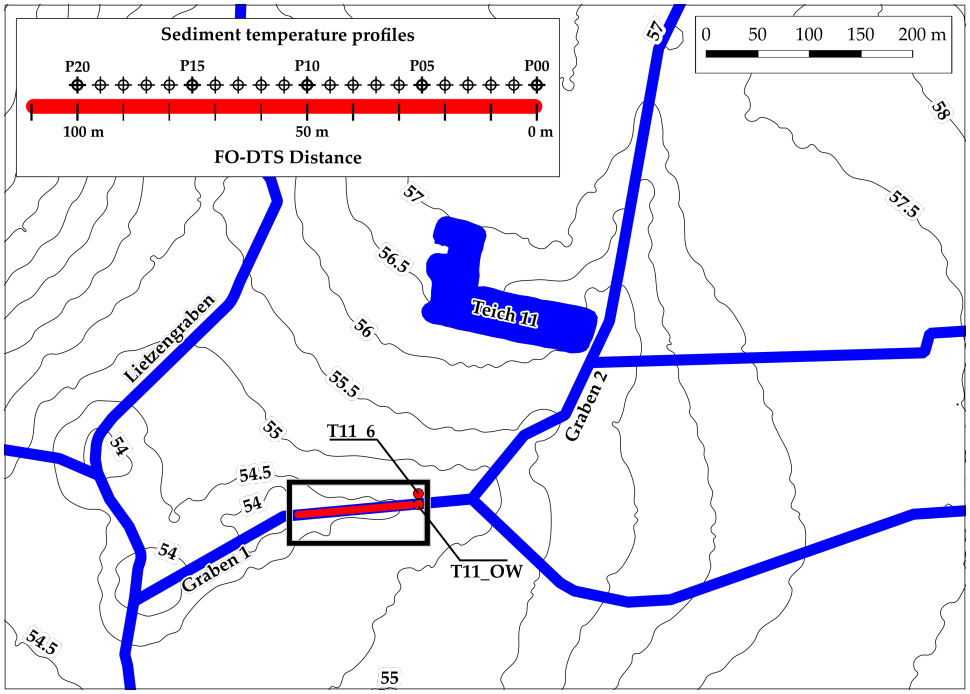

FIGURE 4.1: Location of the stream reach where measurements were conducted (black box). In the upper left the arragnement of the FO-DTS measurements and sediment temperature profiles are shown. The observation well T11_6 and the water level gauge T11_OW were located upstream of the measurements (red dots). Elevation contour lines are shown in black, with elevations in m.a.s.l

Sediment temperature measurements were made alongside a 110 metre long section of the stream “Graben 1” as shown in Figure 4.1. On 28/02/2012 and on 30/07/2012 measurements using the FO-DTS device were conducted. On 08/08/2012 profiles of sediment temperatures were recorded using the temperature profile device. Measurements in Februrary will be referred to as winter

measurements, measurements in July/August as summer measurements.

4.1.2 Fibre-optical temperature sensing

The results from the two measurement campaigns with the FO-DTS device are shown in Figure 4.2 and Figure 4.3. Mean sediment temperatures are shown together with the 95% confidence interval and accuracy of the measurement. The average of the surface water temperature over the measurement period is shown as well. This allows the identification of section with sediment temperatures deviating from surface water temperature. The figures include locations of possible deviations or erroneous measurements due to obstacles in the sediment, which inhibited the proper installation of the cable.

Winter measurements

In Figure 4.2 the results of the measurements on 28/02/2012 are shown. Two sections with increased temperatures, indicating groundwater discharge, are clearly distinguishable from the average surface-water temperature (5.3 °C). One is located between 30 m and 35 m. The second zone is located between 56 m and 70 m with a local minimum in temperature at 60 m, which is above the surface-water temperature. The maximum temperatures measured in the stream bed sediments were 6.1 °C (at 33 m), 6.2 °C (at 56 m), and 6.0 °C (at 67 m). The effects of obstacles, which inhibited a proper placement of the cable in the sediment, are also visible. Obstacles between 35 m and 47 m prevented the installation of the cable in the sediment, the same applied for the section between 89 m and 99 m. Thus, the temperatures in these sections represent the surface water temperatures. The good agreement between average temperatures in these sections and average surface water measurements validates the quality of the calibration. Some sections have been buried in the sediment insufficiently due to small-scale obstacles (e.g. roots). At these points, temperatures were lower than surface water temperature (position 14 m) or higher than surface water temperature (at positions 6 m and 28 m). This is most likely an artefact of the FO-DTS method, which averages temperatures over cable sections each one metre long.
Sections with increased sediment temperatures were interpreted as spots of exfiltration of groundwater, which was warmer than surface water. Sections of the cable which were buried in the sediments and did not show increased temperatures and were not disturbed by obstacles showed temperatures around the surface water temperature (section 76 m to 88 m) or lower (section 8 m to 24 m). These sections can be interpreted as follows: The infiltration of stream water into the sediment lead to temperatures that are similar to the surface water temperatures. In sections with temperatures below the stream temperatures, the lateral (hyporheic) flow of water in the sediment could lead to an advective transport of the diurnal signal of temperature. When no flow is occurring, the conductive transport of heat could lead to the same result. This means that lower temperatures could originate from the night before the measurement. The possibility that no flow is occurring should also be considered. This means that water may be present that was introduced into the sediment while the cable was installed. As a consequence, it is not possible to determine the sections of the cable that showed infiltration with sufficient certainty, as there are several mechanisms that

could lead to temperatures lower or equal to the stream temperature. On the other hand, sections of the cable that exhibited temperatures significantly higher than the stream water temperature can with sufficient certainty be interpreted as exfiltration of groundwater to the stream.

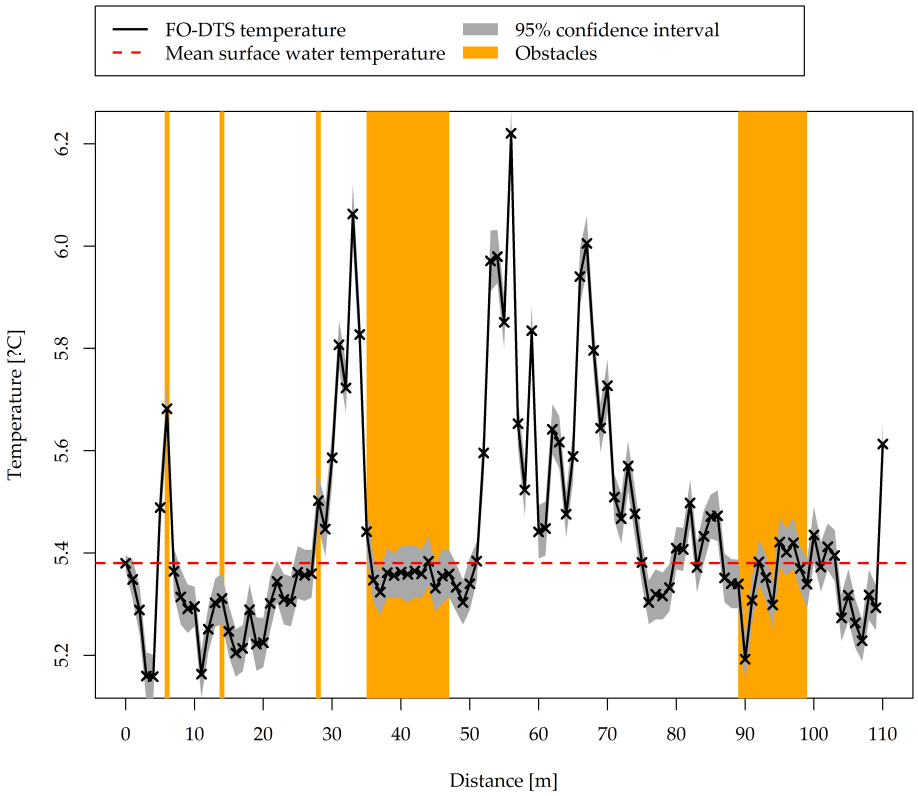

FIGURE 4.2: Temperatures measured along the stream reach during the winter measurements on 28/02/2012

Summer measurements

Figure 4.3 shows the results of the measurements on 30/07/2012. Two sections with temperatures lower than the surface water temperatures can be identified. One is located between 15 m and 41 m. The second zone is located between 55 m and 90 m. The minimum temperatures measured in the stream bed sediments were 14.5 °C (32 m) and 15.3 °C (68 m) for these two zones. Due to obstacles, it was not always possible to bury the cable in the sediment. The affected sections of the cable are marked in Figure 4.3. The temperatures measured in these sections should hence be discarded. Despite the fact that the cable was not buried in the sediment or or submerged in the surface water, the temperatures measured in the affected sections were similar to the stream temperature or even lower. This could be an artefact caused by the measuring technique. Since values are integrated over sections of 1 m instead of providing point measurements, the temperatures shown in Figure 4.3 represent rather an average over those sections. If the cable section next to the obstacle was buried in the sediment, and groundwater exfiltration occurred in this spot, the temperature can exhibit values below or similar to the surface water temperature. In the final section of the cable (behind 90 m), the measured temperatures were higher than the surface water temperatures. The

reason for this could not be identified. Most likely, the cable was close to the sediment surface, which heated up due to exposure to sunlight. While the rest of the stream reach is located within forest, this section of the stream may have been exposed to sunlight, especially during late afternoon when measurements were conducted. As in the case of the winter measurements, we only attribute longer sections where temperatures were below the surface water temperature to zones of groundwater exfiltration to the stream.

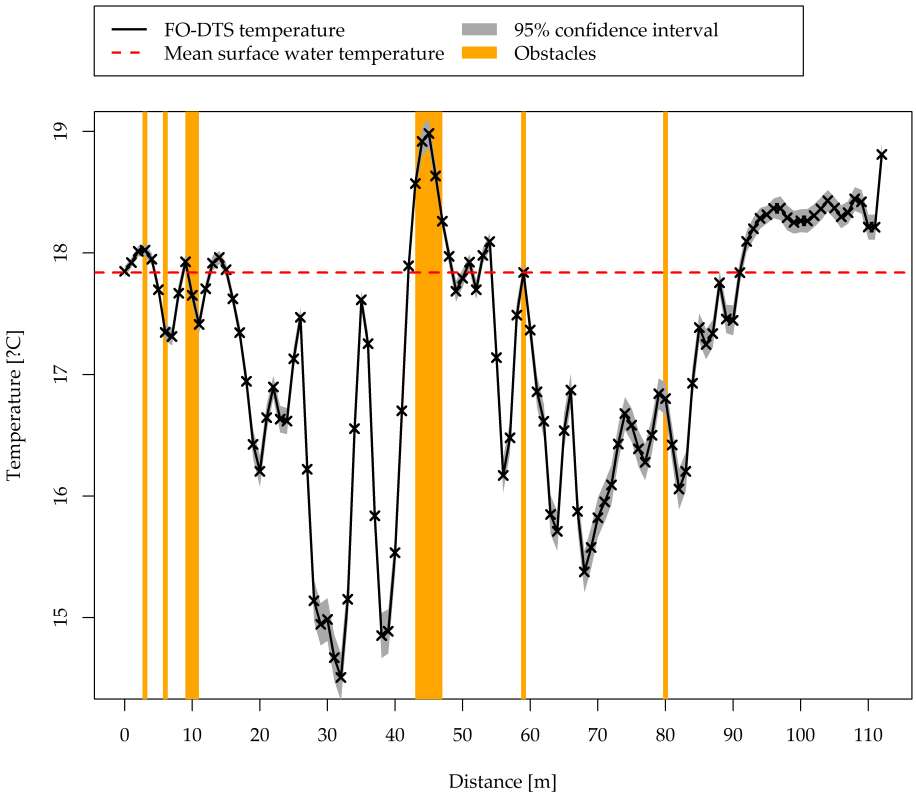

FIGURE 4.3: Temperatures measured along the stream reach during the summer measurements on 30/07/2012

Comparison of winter and summer measurements

To check for differences in the location of exfiltration zones in the stream reach between winter and summer conditions, we compared results from these two measurement campaigns. Generally, the differences between sediment temperatures and surface water temperatures were greater in summer than in winter as can been seen in Figures 4.3 and 4.2. This could be the result of the greater difference in temperature between groundwater and stream water during summer (summer: stream water about 18 °C; winter: stream water about 5.5 °C, annual mean groundwater temperature 9 °C). Another explanation would be a higher groundwater discharge in summer. Measurements of groundwater heads at observation well T11_6 and surface water levels “Graben 1”, however, showed a mean hydraulic gradient of -0.034 m/m on 28/02/2012 and -0.028 m/m on 30/07/2012 between well and stream. Since the gradient during the winter measurements was steeper than it was during the summer measurements, this explanation must be excluded.

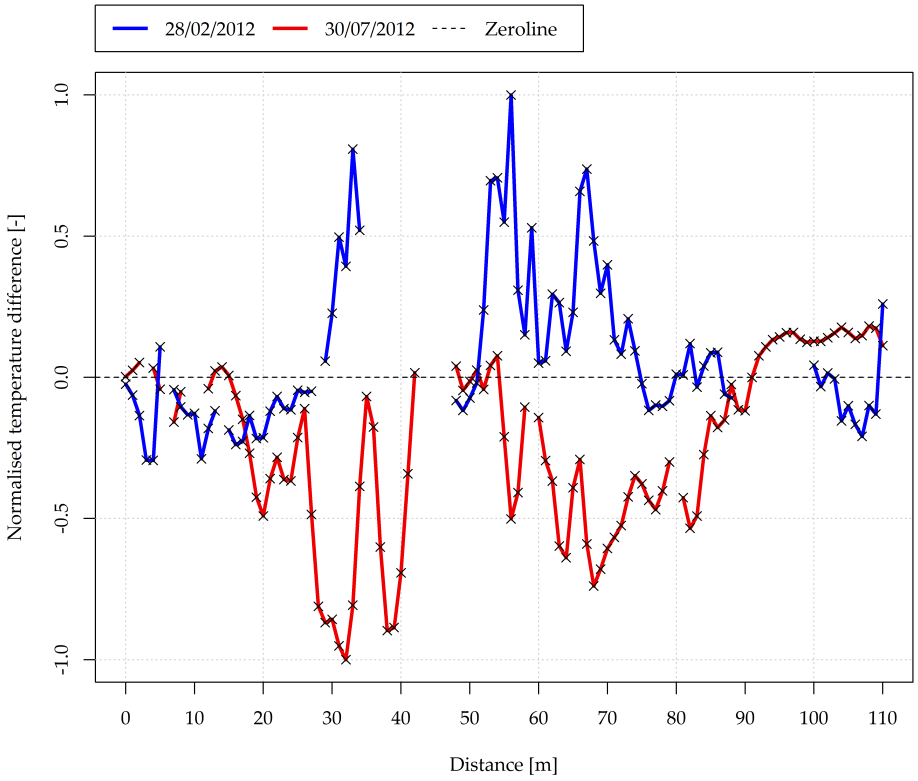

FIGURE 4.4: Normalised temperature differences between sediment and surface water for the winter and the summer FO-DTS campaign; sections of the FO-DTS affected by obstacle have been removed

To compare the spatial patterns of exfiltration, we normalized the measured temperature differences to their maximum values. The results are shown in Figure 4.4. The spatial distribution of temperature anomalies are very similar in both measuring campaigns. The first hot spot seems to be expanded during the summer measurements, if one neglects the steep decrease in temperature difference around 37 m. Since it was not possible to bury the cable at this part of the stream during the winter measurements, the end of the exfiltration zone is not clear. Therefore, the boundary of this exfiltration zone is blurry in both cases. The second exfiltration zone is also existent on both measurement dates.
It can be assumed that the spatial patterns of groundwater exfiltration in this stream reach is independent of seasonal changes. One possible reason for this can be found in the irrigation of treated wastewater in the pond “Teich 11” north of the stream, which leads to an elevation of the adjacent groundwater table. Another reason is the morphology of the stream. “Graben 1” was built as a drainage channel hence cuts into the surrounding terrain. The elevated groundwater table and the low stream bed elevation lead to groundwater gradients in direction of the stream. The aquifer is not homogeneous between pond “Teich 11” and the stream. Drill logs show fine to coarse sands on the top of the aquitard and suggest the existence of clay lenses. This aquifer heterogeneity on the metre scale and small scale heterogeneities in the stream bed lead to spatially uneven discharge of groundwater to the stream.

4.1.3 Estimation of exfiltration rates based on sediment temperature profiles

On 08/08/2012, temperature profiles were measured in the sediment along the stream. The locations are shown in Figure 4.1. The aim was to compare the qualitative patterns of groundwater exfiltration determined by the FO-DTS device with the quantitative results from analysing sediment temperature profiles and to examine if there is a correlation between the results. The measurements were taken one week after the FO-DTS campaign and we assumed that the general hydraulic conditions did not change significantly since the time lag was only 7 days. However, on 02/08/2012 and on 03/08/2012 precipitation of 7 mm per day occurred. A comparison of the hydraulic gradients between observation well T11_6 and the stream level at T11_OW (Figure 4.1) showed a difference of -0.004 m/m. Hence, the gradient was slightly steeper at the time of sediment temperature profile measurements.
The measured sediment temperatures are plotted in Figure 4.5. The red lines indicate the fitted curve of the heat transport equation after Schmidt et al. (2006). In general, good agreements between measured and calculated temperatures were obtained. The temperature profile P06 was excluded from further interpretation as the difference between the uppermost point and the lowest point in the profile was only 1.2 °C. The temperature at the sediment-water interface of 12.3 °C was about 3 °C lower compared to the other profiles, and hence considered as not plausible.
The profiles P07, P08, P10, P11, P12, and P13 yielded temperatures at the lowest point that were lower than the assumed groundwater temperature. Since these profiles were located next to each other and we used two devices for the measurements, it is assumed that these are not erroneous measurements. One possible reason for this effect could be that the source of exfiltrating groundwater is different from the rest of the measured profiles. If the heat content of the aquifer is not distributed evenly with depth, it is possible that water originating from groundwater recharge during winter, is colder than the shallow groundwater. Hence the observation of deeper sediment temperatures could be a hint for the discharge of groundwater from the lower layer of the aquifer. Since the scope of this study is the spatial pattern of discharge of groundwater to the stream, the chosen methods do not provide sufficient information to validate this assumption. The fluxes obtained by fitting the analytical solution of the heat transport equation to measured temperatures ranged from $15\,l\,d^{-1}\,m^{-2}$ at profile P00 to $158\,l\,d^{-1}\,m^{-2}$ at profile P07 with a mean value of $84\,l\,d^{-1}\,m^{-2}$ and a median of $77\,l\,d^{-1}\,m^{-2}$. All analysed profiles showed exfiltration, and no infiltration zone was determined. This seems plausible considering the morphology of the stream and the discharge of treated wastewater nearby. All profiles with temperatures at the lowermost point lower than the assumed groundwater temperature of 11.7 °C yielded flux rates of discharging groundwater greater than the mean value respectively the median. This could suggest that a local subsurface flow system brings colder groundwater to the stream in this reach of the stream, resulting in lower temperatures and higher discharge rates. This is most likely caused by local changes in aquifer characteristics or by small scale heterogeneity patterns in the aquifer which focus streampaths to hotspots of groundwater discharge.

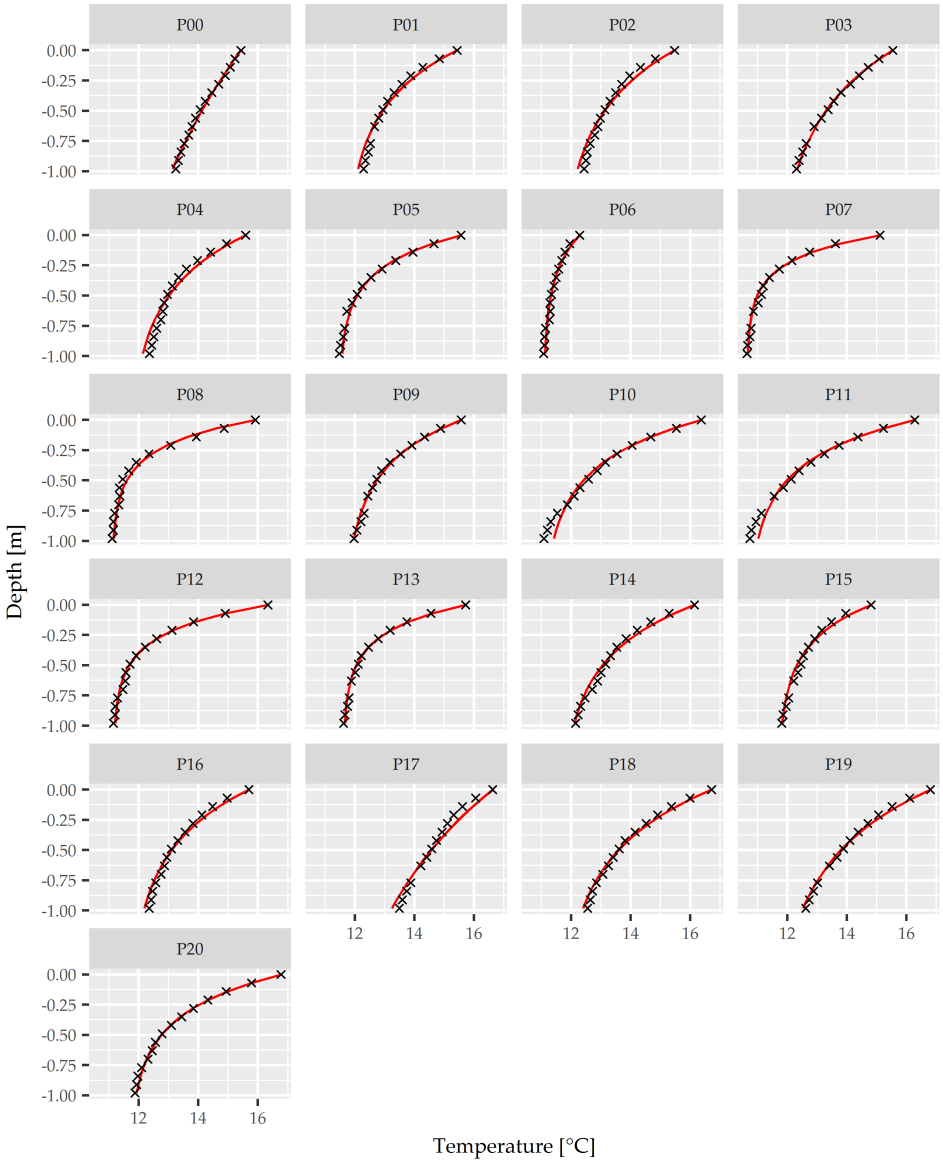

FIGURE 4.5: Sediment temperature profiles along the stream reach, indicated as crosses. The best fit of the analytical solution of the heat transport equation is plotted as red line.

4.1.4 Comparison of quantitative and qualitative results

To discuss the qualitative results of the FO-DTS and the sediment temperature profiles in general as well as some of the features observed in particular, a comparison of the results from FO-DTS and sediment temperature profiles are shown in Figure 4.6 (summer measurements).
In general, there is a weak correlation between the results from FO-DTS and temperature profiles. Zones with increased temperature differences match roughly with zones where higher flux values were calculated from the temperature profiles. It should be mentioned, however, that results from temperature profiles suggest exfiltration of groundwater at every measurement location while there are zones with no differences in temperatures measured by FO-DTS suggesting no flow or infiltration of surface water. It remains unclear if this is a result from

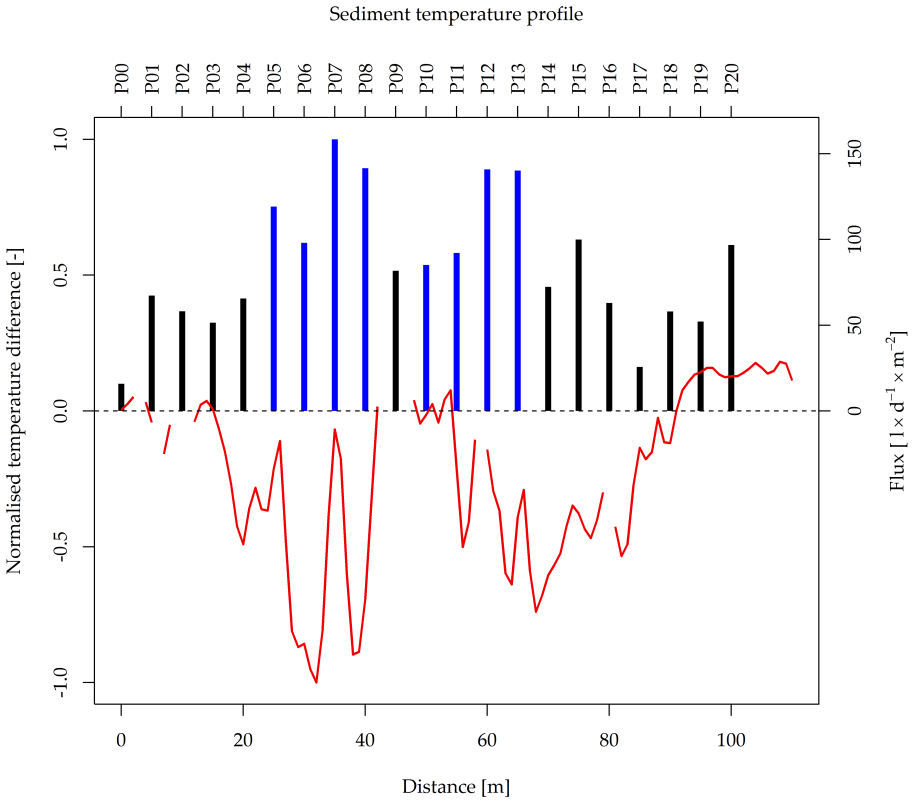

FIGURE 4.6: Comparison between normalised temperature differences of the FO-DTS summer measurement (red line) and calculated fluxes based on the temperature profiles. Blue bars indicate changed temperature values for the lower boundary condition of the analytical solution of the heat transport equation. The boundary conditons were not changed for black bars. Sections of the FO-DTS affected by obstacle have been removed.

disturbance of the sediments while installing the FO-DTS cable or if the fit of calculated temperature profiles to the measured temperature profiles overestimate the flux rates in general. Anibas et al. (2009) suggested that the method tends to overestimate flux rates if the assumption of steady state is violated. Furthermore, it should be noted that point measurements are compared with measurements integrated over a (short) section of the FO cable. There is a slight shift of the patterns derived with FO-DTS compared to temperature profiles. This may be a result of inaccurate GPS measurements and cable placement. The fact that the temperature profiles with adjusted lower boundary condition temperatures match with sections where increased temperature differences were observed, supports the conclusion that the same patterns were observed yet with deviating results. In summary, we conclude that the observed patterns have their origin in geologic features since all three measurement campaigns (FO-DTS in winter, FO-DTS in summer and temperature profiles in summer) show similar patterns of exfiltration zones.

4.2 Numerical modelling

4.2.1 HydroGeoSphere

The results of the calibration of HydroGeoSphere to observed stream discharge and groundwater head data, and the validation of the model are presented and discussed below. In a following paragraph, the parameters which were derived during the calibration process are discussed along with possible explanations for the model behaviour.

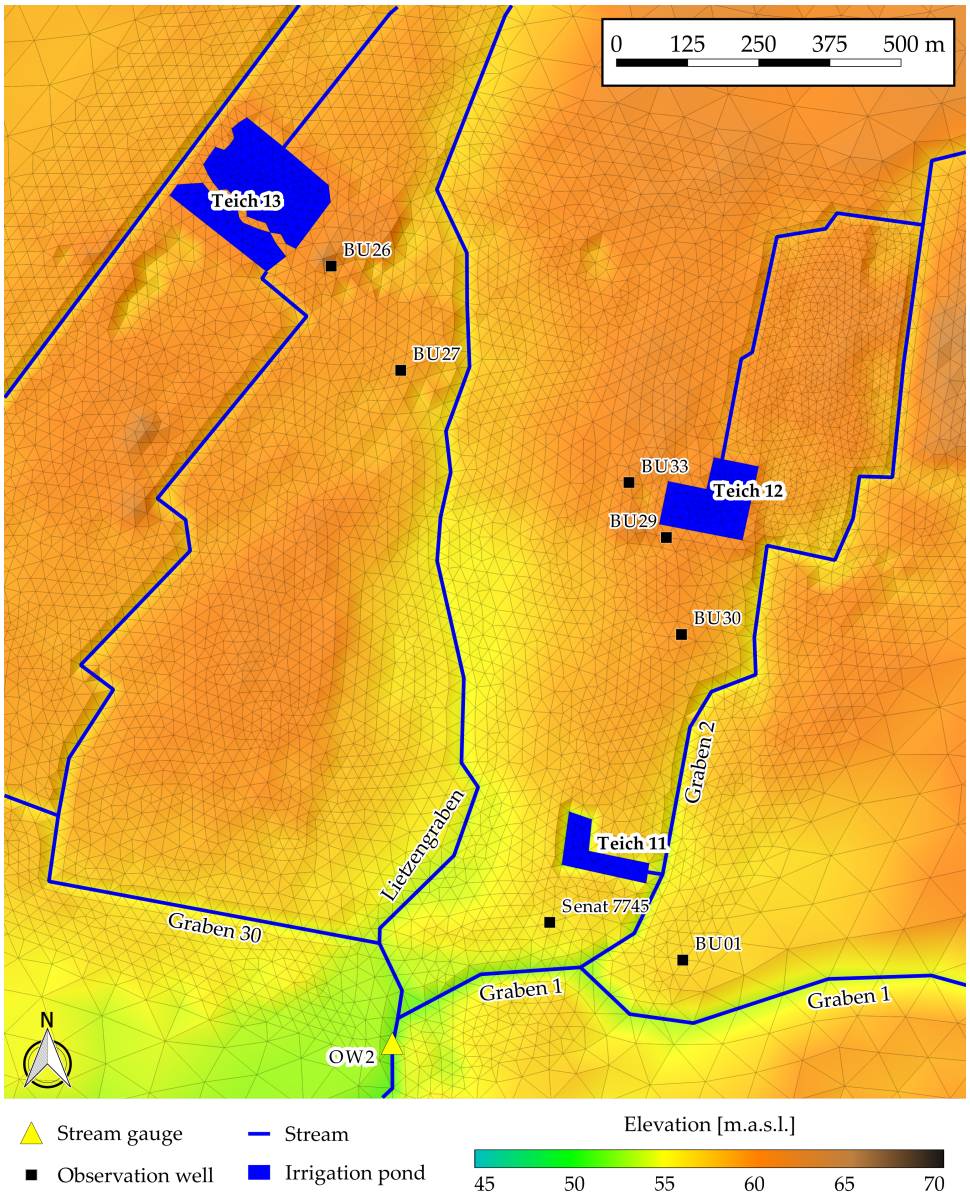

FIGURE 4.7: Map of the central catchment area. Streams and ponds are shown as represented in HydroGeoSphere. The horizontal discretisation of the model is shown in grey.

Calibration period 2007

The calibration results for stream discharge and groundwater head data are presented in the following paragraph.

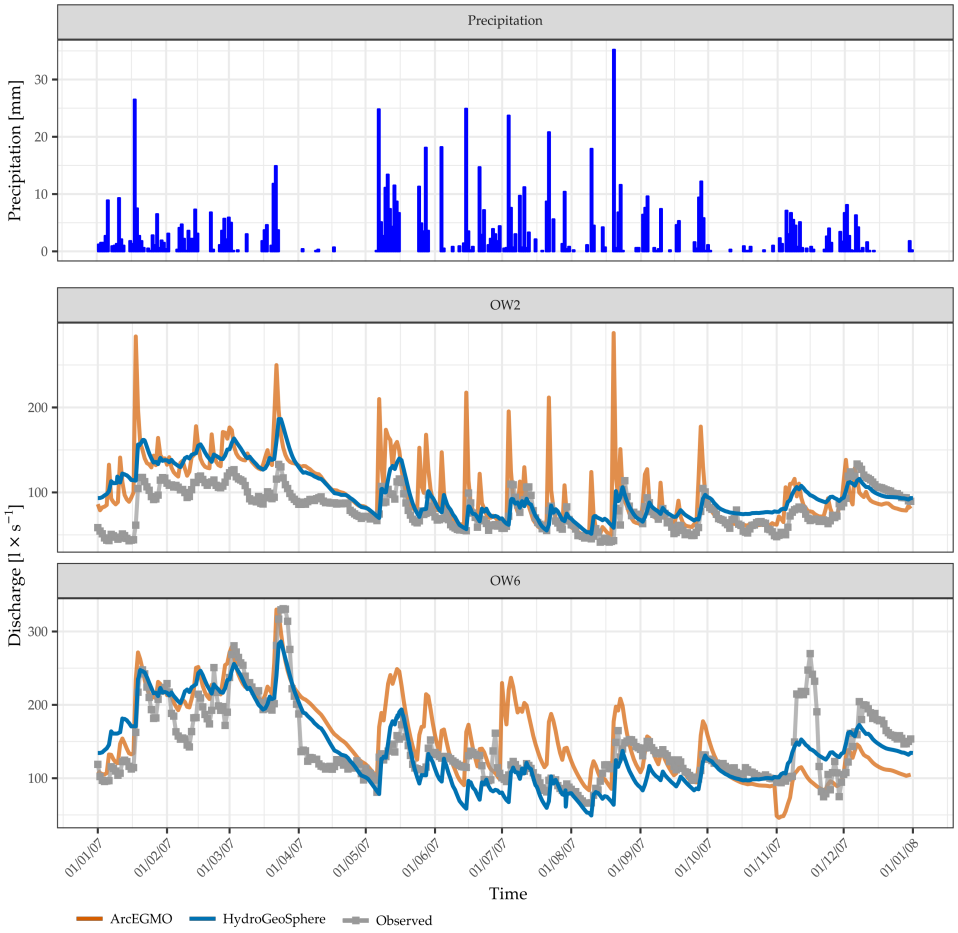

FIGURE 4.8: Simulated discharge during the 2007 calibration period with ArcEGMO-ASM, HydroGeoSphere, and observed discharge; blue bars indicate daily precipitation sums

Discharge The simulated stream discharge during the calibration period 2007 is plotted in Figure 4.8 in comparison to the observed discharge at two stream gauges (Figure 3.10). Additionally, the daily precipitation sums during 2007 are shown. Calculated Nash-Sutcliffe efficiency coefficients for the calibration period are shown in Table 4.1. The general fit of simulated to observed discharge is reasonable, but the quality differs over the course of the calibration period.

At OW2, the discharge volume is overestimated in the first 4 months of 2007. For the remaining time, simulated and observed discharges coincide well. The Nash-Sutcliffe efficiency of -0.45, however, suggests that the mean value of observed discharge is a better predictor of the discharge behaviour at OW2 than the results of HydroGeoSphere. The low Nash-Sutcliffe efficiency can be explained by the discrepancy of around 40 l s^{-1} between observed and simulated values within the first 4 months of 2007.
The period between May and October is captured very well and shows the response of the system upstream OW2 to various precipitation events. However, the values of observed run-off peaks during single events are underestimated by the model. The subdivision of model performance in a better fit during the period from March to October and a poor fit in comparison to the rest of the

calibration period matches with the increased evapotranspiration rates during summer. Besides the overestimation of discharge, the model was not able to reproduce the steep decrease of discharge after precipitation events, for example by the end of March or beginning of November.

OW6, however, shows a slightly different behaviour. As shown in Figure 4.8, the observed and simulated discharges accord well with each other. A Nash-Sutcliffe efficiency coefficient of 0.55 (Table 4.1) is satisfactory and indicates a good model performance. In contrast to the discharge time series of OW2, a distinct differentiation of the calibration period into phases of good and poor model fit is not possible. At the beginning of February, the model clearly overestimates discharge rates, while during most of the year, discharge is underestimated. During the growing season with increased evapotranspiration the underestimation is very distinct. Still, the general dynamics are captured well. In general, the dynamic discharge response of HydroGeoSphere to precipitation events (in the following denoted as discharge events) resembles to be relatively slow.
The difference in model performance between OW2 and OW6 is most likely caused by the differences in land use, the geometry of the water bodies, and the influence of management measures. In the catchment upstream of OW2 forest, grasslands and scrubs dominate the landscape. Forested areas have a high potential of evapotranspiration due to a dense vegetation cover and deeper roots, which enhances the water availability to the plants.
Upstream of OW6, however, the Lietzengraben stream runs through some wetlands and Lake Bogenseekette. Wetland areas and lakes can dampen discharge responses to precipitation events and act as a reservoir during dry periods. Since the model topography could not reflect the lake morphology and wetland areas in detail, this is a possible source of additional deviation between observed and calculated discharge. A large discharge event in the mid of November with a peak discharge of about $270\,\mathrm{l\,s^{-1}}$ was not represented well. Both the observed peak discharge and the temporal pattern were not captured by the model. This discharge event is linked to a management activity in the stream network. Weir 11, upstream of OW6 was opened to avert damage from its structure due to storm flow (Pauli et al., 2008). This measure, the opening of a weir, could not be represented in the model due to the fixed surface elevation.
The calculated mean discharge at OW6 is only about 3% higher than the mean observed discharge. This is another indicator for a good model performance.

Hydraulic heads Groundwater heads at nine observation wells were used for calibration. One can distinguish between observation wells adjacent to the ponds (Figure 4.7) where treated wastewater is discharged (BU01, BU26, BU27, BU29, BU30, BU33, and Senat7745) and observation wells in the lower catchment, further away from the ponds (Senat15169 and Senat5366). Well Senat5366 is located near the eastern boundary of the model domain; Senat15169 is located at the stream which discharges into the Lake Bogensee.
To evaluate the model's performance on simulating the temporal patterns of hydraulic heads in the catchment, a comparison of simulated and observed hydraulic heads at the observation wells is shown in Figure 4.9. The calculated Pearson correlation coefficients r for simulated and observed groundwater heads at the observation wells is shown in Table 4.2 along with the results for the stream gauges. As described in Section 3.2.1, this measure is an indicator for a model's

TABLE 4.1: Calculated Nash-Sutcliffe efficiency coefficients of simulated and observed stream discharge and groundwater heads in the calibration period (2007) and validation period (2008 - 2012) for HydroGeoSphere(HGS) and ArcEGMO-ASM.

	2007		2008 - 2012	
	HGS	**ArcEGMO-ASM**	**HGS**	**ArcEGMO-ASM**
OW2	-0.45	-1.79	0.39	0.05
OW6	0.55	0.19	0.65	0.65
BU01	-11.47	-3.9	-0.87	0.6
BU26	-5.04	-6.88	-0.88	-5.01
BU27	0.62	-68.83	0.66	-17.28
BU29	0.05	-1.04	-0.47	-0.87
BU30	-0.77	-32.94	0.87	-15.32
BU33	-0.42	-3.24	-1.79	-0.39
Senat15169	-20.98	-52.45	-3.56	-12.39
Senat5366	-37.69	-47.66	-7.55	-15.4
Senat7745	-39.87	-96.98	-11.3	-29.19

TABLE 4.2: Calculated Pearson correlation coefficients r of simulated and observed stream discharge and groundwater heads in the calibration period (2007) and validation period (2008 - 2012) for HydroGeoSphere(HGS) and ArcEGMO-ASM.

	2007		2008 - 2012	
	HGS	**ArcEGMO-ASM**	**HGS**	**ArcEGMO-ASM**
OW2	0.72	0.56	0.79	0.77
OW6	0.79	0.64	0.83	0.81
BU01	0.84	0.78	0.9	0.78
BU26	0.77	0.42	0.7	-0.07
BU27	0.86	0.87	0.88	0.86
BU29	0.89	0.8	0.76	0.65
BU30	0.9	0.82	0.94	0.85
BU33	0.89	0.88	0.84	0.85
Senat15169	0.61	0.62	0.84	0.89
Senat5366	0.25	0.1	0.66	0.39
Senat7745	0.53	0.57	0.82	0.81

ability to reproduce the dynamics of observed variables. Additionally, the calculated Nash-Sutcliffe efficiency coefficients for the groundwater heads are shown (Table 4.1). However, the calculated values were below zero for the most wells. At BU01, in comparison to observed values, HydroGeoSphere underestimates heads about 0.15 m to 0.2 m. This is shown in Figure 4.9. The general dynamic over the annual cycle is reproduced well, except for the increase in head by the end of the year. BU01 is located south-east of pond “Teich 11”, between two streams (Figure 4.7). The well is close to both of the streams, which could explain the deviation. A coarse spatial discretisation could lead to a faulty calculation of hydraulic gradients since only a small number of elements lies between well and stream. An overestimation of the water exchange between stream and aquifer by the model could boost this effect. The reproduction of the annual cycle with an offset is also reflected in the r of 0.84.
BU26 is located directly south-east of pond “Teich 13”. The model overestimates

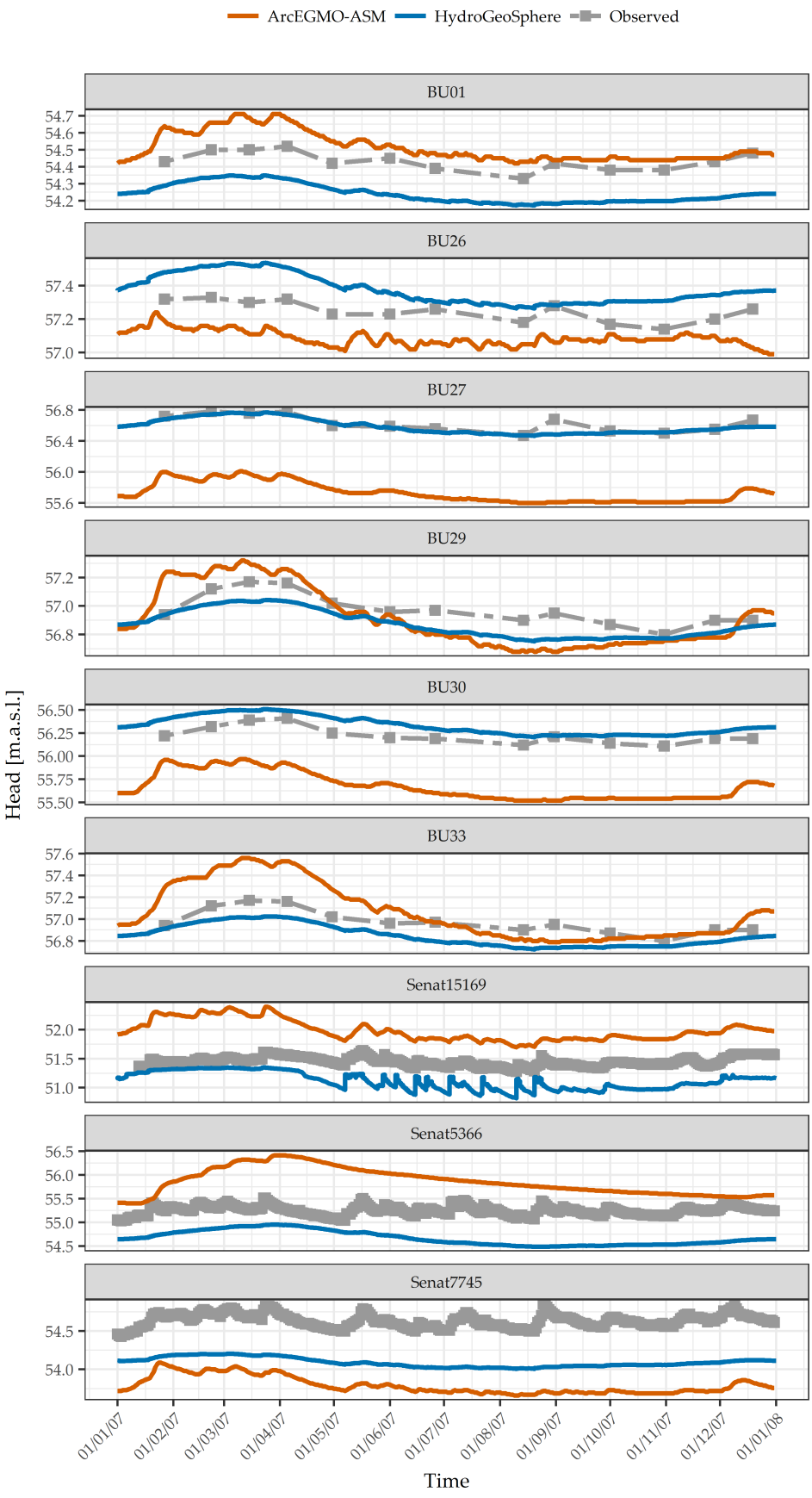

FIGURE 4.9: Calibration period 2007: Simulated and observed groundwater heads at the observation wells during the 2007 calibration period

groundwater heads and also exaggerates the annual dynamics. There is a significant increase in groundwater heads in the first quarter of the year, which cannot be found in observed data. Since the geometry of irrigation ponds is represented in a very simplified way in the model, it is possible that this is also the reason for deviations.
The best fit of simulated heads to observed data was achieved at BU27 with a coefficient of determination $r = 0.86$ and a Nash-Sutcliffe efficiency coefficient of 0.62. BU27 is located south-east of pond "Teich 13" between the outlet and the Lietzengraben stream. The simulated and observed head values coincide very well. The temporal dynamics is reproduced well and the difference between observed and simulated values ranges between -0.03 m (overestimation) and +0.19 m (underestimation). The median of the difference is 0.02 m. The underestimation by 0.19 m is a single event by the end of August.
BU29, located directly south of pond "Teich 12", coincides quite well with observed data. The temporal dynamics over the annual cycle are captured well, which is reflected by the correlation coefficient $r = 0.89$. The heads are, however, generally underestimated by 0.1 m on average.
The calculations for BU30 ($r = 0.9$) reproduce the dynamics over the annual cycle very good, but tend to overestimate groundwater heads by 0.10 m on average. BU30 is located between BU29 and the adjacent stream to the south-east. In combination with the underestimation of heads at BU29, the results from BU30 suggest that the gradient between pond "Teich 12" and the stream, which receives water from pond "Teich 12" by groundwater discharge, is underestimated. This may be caused by an overestimation of lateral hydraulic conductivity.
BU33, west of pond "Teich 12", also fits the observed annual dynamics of groundwater heads but underestimates head values by around 0.12 m on average. The dynamics are reproduced well, with a relatively constant offset between observed and simulated values, as reflected in the high r of 0.89. Observation well Senat-7745 is located between pond "Teich 11" in the North and the ditch "Graben 1" in the south. Unfortunately, the calibration did not yield a satisfactory fit of calculated to observed heads here. The observed data show distinct dynamics in head values which have a similar shape as the discharge at OW2. Hence, aquifer and stream should be well connected in this area. The model was not able to reproduce these dynamics and underestimated groundwater heads by about 0.5 m on average.
Hydraulic heads at observation wells Senat5366 and Senat15169 in the lower part of the catchment were also not reproduced well. Senat15169 is heavily influenced by the stream "Seegraben". In the model, this stream falls dry occasionally and hence the simulated heads at the observation well are too low. Senat5366 lies within an urban area with wastewater drainage, sealed surfaces and little groundwater recharge. With the features of HydroGeoSphere it was not possible to reproduce this behaviour of an urban environment, although this was not the aim of this study.

Validation period 2008 - 2012

The validation of the calibrated model was conducted with data from the period 2008 to 2012.

Discharge In general, the comparison of observed and simulated discharge at OW2 and OW6 yielded similar results to the simulations performed for 2007. The

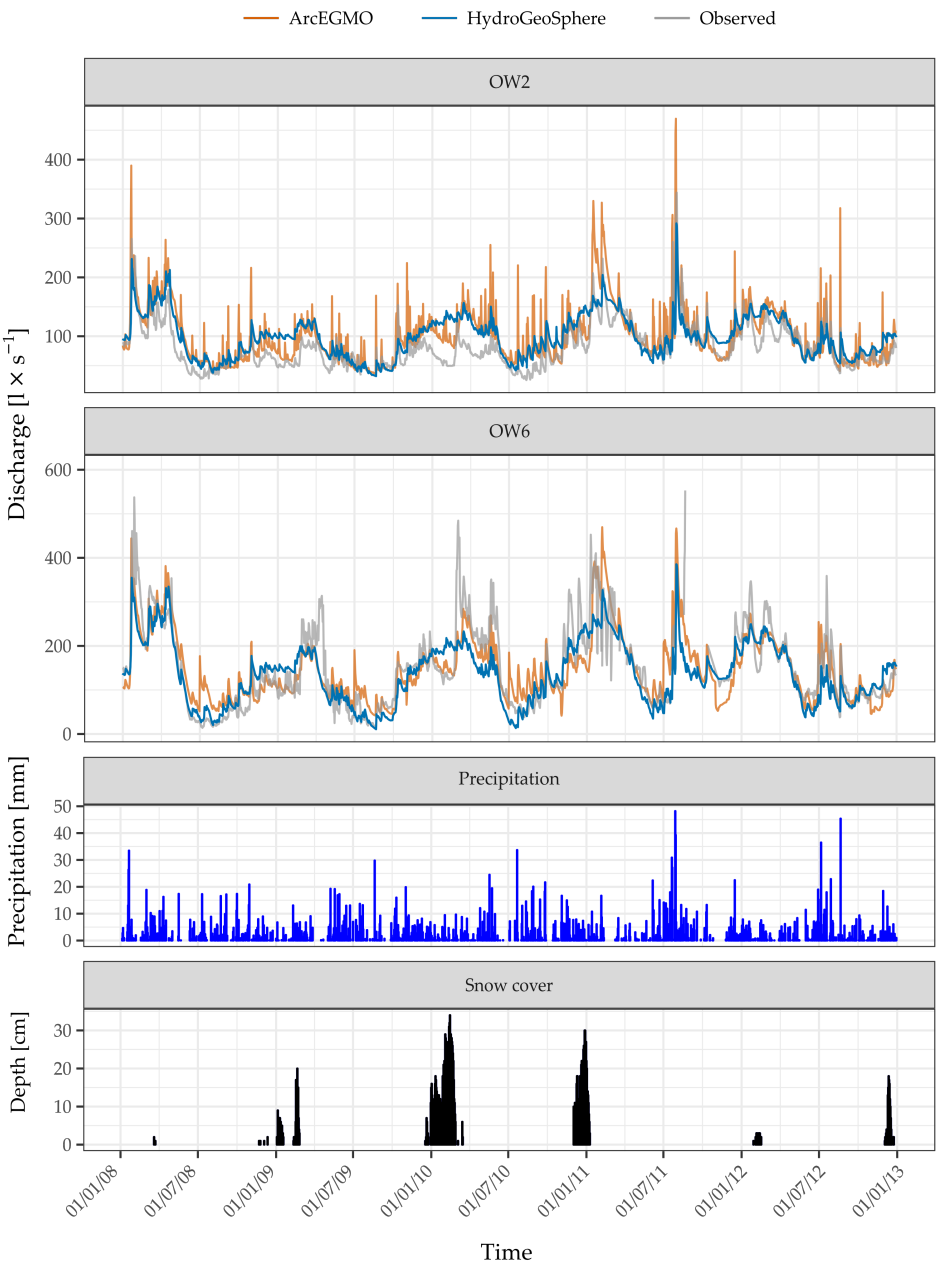

FIGURE 4.10: Simulated and observed discharge during the validation period 2008 - 2012 by ArcEGMO-ASM and HydroGeoSphere; recorded daily precipitation sums and observed snow depths at the meteorological station Berlin-Buch

dynamics of stream discharge at stream gauge OW2 were simulated reasonably well. The fit of simulated to observed data, however, was not consistent during the validation period. A visual inspection of simulated and observed discharge yielded a better agreement in summer than at the beginning and by the end of each year, as shown in Figure 4.10. In the beginning of each calendar year, the discharge was substantially overestimated, especially in the beginning of 2009 and 2010. While the observed discharge during these periods decreased, the simulation yielded increasing or stable discharge rates. This was observed by the end of 2011, too. Seemingly, the model performed better during low flow periods

TABLE 4.3: Precipitation and calculated actual evapotranspiration for HydroGeoSphere

	2007	**2008**	**2009**	**2010**	**2011**	**2012**
Precipitation [mm]	786	657	653	678	689	654
Evapotranspiration [mm]	723	548	581	565	638	622

during the growing season and overestimated discharge dynamics during wet periods with higher discharge. This is consistent to the results of the calibration, as described in the previous section. To investigate further explanations for the observed deviations, the recorded snow depths at the meteorological station Berlin-Buch (DWD Climate Data Center, 2018) have been included into Figure 4.10. The check of discharge deviations against the recorded snow depths yielded a plausible explanation for the overestimation of the discharge by the model in some cases. In the beginning of 2009 and the beginning and end of 2010, the records showed a snow cover of more than 10 cm over several days to weeks. As the input of precipitation in HydroGeoSphere does not account for snowfall, this precipitation is processed immediately in the model and leads to increased discharge rates. The precipitation of snow, however, impacts observed discharge only after the snow cover is melted. Hence, the observed discharge during these periods decreases. At OW6, the fit of simulated to observed discharge was good, in general. However, discharge at OW6 was substantially underestimated by the model in the beginning of 2009 and 2010. In both cases, it is very likely that the deviation originates in the melting of the snow cover. This process is not represented in HydroGeoSphere and hence leads to a underestimation of the discharge. At OW6, this underestimation of observed discharge is greater than at OW2 due to the larger upstream catchment. At the turn of the years 20010/2011, HydroGeoSphere fully failed to reproduce the observed fluctuations of the discharge. It remains unclear, however, if these observed fluctuations were based on valid discharge records. The discharge data were corrected for obviously erroneous measurements during this periods but without reference measurements, it was limited to check the plausibility of these data.
The comparison of simulated to observed discharge showed that the model is capable to reproduce discharge dynamics and levels reasonably despite the short calibration period. This is reflected in the high Nash-Sutcliffe efficiency coefficients of 0.39 for OW2 and 0.65 for OW6. However, the inability of HydroGeoSphere to account for snowfall and snowmelt clearly affects the model quality.

Hydraulic heads Similar to the validation results for discharge, the comparison of observed to simulated heads yielded minor changes in simulation quality compared to the calibration period. The longer period used for model validation, however, allowed for an improved comparison of simulated to observed heads since the dynamics observed in groundwater heads are not as distinct as in discharge data. The time series of observed and simulated groundwater heads are shown in Figure 4.11. As stated above, the general findings for the simulation of the calibration period are confirmed. However, some differences became more visible during the 5 year validation period.
In most cases, the general annual dynamics of the groundwater heads were simulated well, while the amplitude of the seasonal changes were underestimated. The level of the observed groundwater tables were simulated better adjacent to

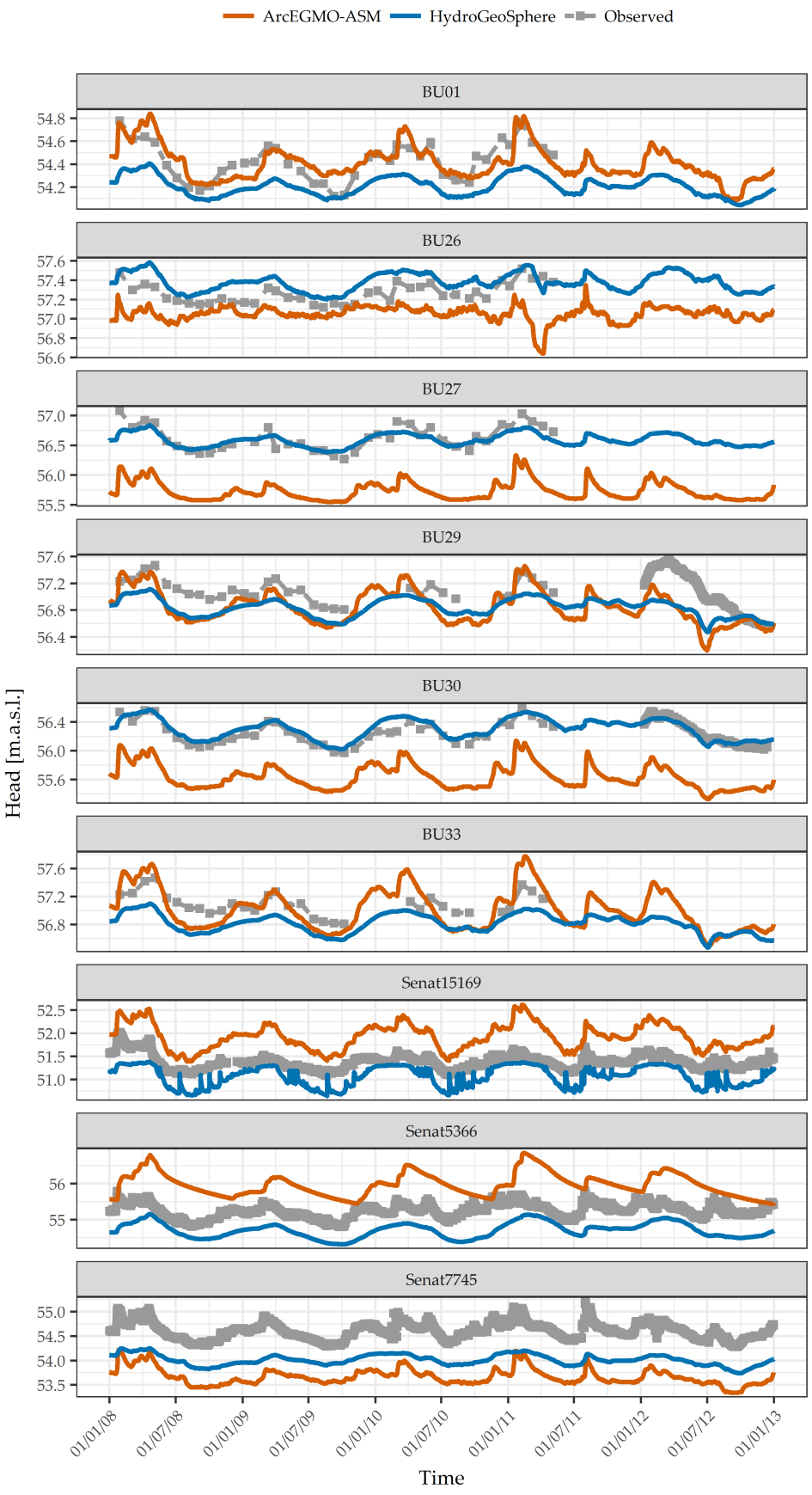

FIGURE 4.11: Validation period 2008 - 2012: Simulated and observed groundwater heads at the observation wells during the validation period

the irrigation ponds in comparison to observation wells located in the southern part of the catchment. This may be the result of the calibration process with emphasis on the area around the irrigation ponds. Heads at observation wells BU26 and BU27, located on a transect between irrigation pond “Teich 13” and the Lietzengraben stream, were reproduced very well. Also, the heads at the wells BU29 and BU30, on a transect between “Teich 12” and ”Graben 2” were simulated reasonably. On both transects, the fit of simulated to observed data was better at the wells located near the stream.
In general, the calculated Pearson correlation coefficients for observed and simulated groundwater heads were higher for the validation period than for the calibration period (see Table 4.2). Although, these results cannot be compared quantitatively, the model is clearly able to reproduce groundwater heads outside the calibration period.

Discussion of calibration quality

Meteorological conditions In the following, the meteorological conditions during the calibration period are discussed in comparison to the conditions during the validation period in order to further assess the quality of the calibrated model. The meteorological conditions applied to the model in 2007 and during the validation period 2008 to 2012 differed from each other in terms of annual precipitation sums.
The long-term mean annual precipitation sum for the catchment is about 610 mm (Gerstengarbe et al., 2003; Lahmer and Pfützner, 2003). In 2007, the precipitation sum of 786 mm highly exceeded the long term average. Thus, the model was calibrated during an abnormal wet period. The annual precipitation sums applied to HydroGeoSphere during the calibration and validation period are shown in Table 4.3. Due to the increased availability of water to evapotranspiration, the calculated actual evapotranspiration sum for the calibration period was also substantially higher than for the validation period (Table 4.3), despite similar calculated potential evapotranspiration inputs. A comparison of the occurrences of daily precipitation sums with respect to their amount yielded no significant differences between calibration and validation period. Therefore, as the quality of the fit of simulated to observed data was comparable between calibration and validation, it is likely that the calibration of the model during an exceptional wet period did not have a negative impact on the model quality. Therefore, it can be assumed that the deviation between simulated and observed data originated in the chosen and calibrated parameter values, respectively.

Irrigation of treated wastewater The management strategy for the discharge of treated wastewater to the irrigation ponds changed over the course of the years. While in the beginning the discharge volume was constant, it was regulated later. In Figure 4.12 the evolution of discharged volumes of treated wastewater in the period from 2007 to 2012 is shown. During the calibration period in 2007 the volume was constant after a decline in early February. Beginning in 2009, the discharge of treated wastewater was regulated seasonally. During the summer months, the discharge volumes were increased in comparison to the winter months. The annual sum of the discharge was nearly constant. It was not possible to identify any influence of the dynamics of irrigation volumes on the deviation between observed and simulated discharge. As described in section 4.2.1, the pattern of deviations is most likely linked to the temporal evolution of

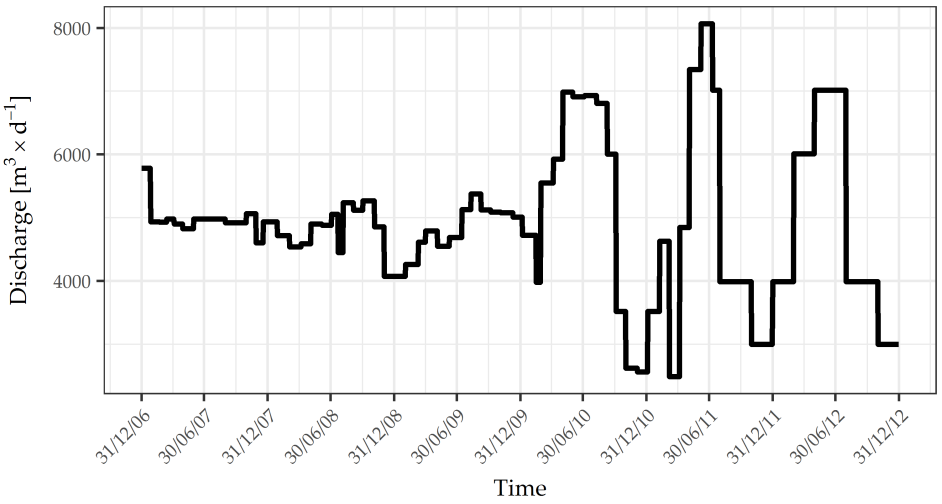

FIGURE 4.12: Total daily sums of discharged treated wastewater

evapotranspiration. The differences between observed and simulated hydraulic heads in the aquifer could also not be linked to variations in the discharge of treated wastewater. Hence the impact of the changed management strategy on the simulation quality was assumed to be negligible.

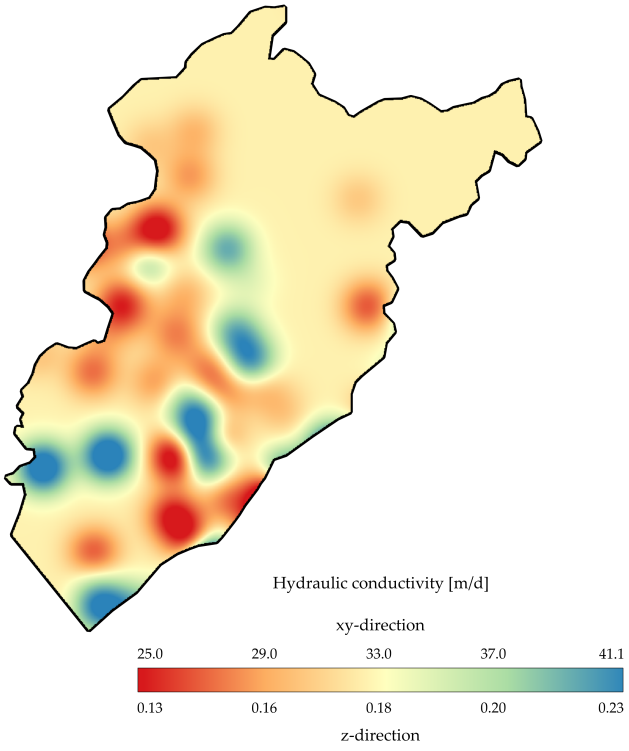

FIGURE 4.13: Distribution of the calibrated values of saturated hydraulic conductivity of the aquifer for both horizontal and vertical conductivity

Fitted parameters The calibration procedure yielded values for preassigned parameters, which are described in detail in section 3.2.3. The PEST algorithm

TABLE 4.4: Calibrated parameter values and composite scaled sensitivities (CSS); Values of calibrated hydraulic conductivity are maximum values. The table is ordered by *CSS overall* in descending order.

Parameter	**Type**	**Calibrated value**	**CSS discharge**	**CSS heads**	**CSS overall**
n_{stream}	Manning's roughness	$0.15\,\text{s}\,\text{m}^{-1/3}$	1.05×10^{6}	5.3×10^{6}	3.3×10^{6}
n_{land}	Manning's roughness	$0.91\,\text{s}\,\text{m}^{-1/3}$	1.8×10^{5}	2.2×10^{5}	1.5×10^{5}
$l_{\text{coupl}}^{\text{unsealed}}$	Coupling length	$1.44 \times 10^{-6}\,\text{m}$	2.1×10^{5}	2.0×10^{5}	1.5×10^{5}
$n_{\text{pond, lake}}$	Manning's roughness	$4.28\,\text{s}\,\text{m}^{-1/3}$	2.3×10^{5}	1.8×10^{5}	1.4×10^{5}
$l_{\text{coupl}}^{\text{stream}}$	Coupling length	$5.17 \times 10^{-3}\,\text{m}$	8.3×10^{1}	1.7×10^{2}	1.1×10^{2}
k_{f}^{z}	Saturated hydraulic conductivity	$0.3\,\text{m}\,\text{d}^{-1}$	7.4×10^{-1}	7.0	4.3
ϕ_{south}	Porosity	0.3	4.0	4.3	3.0
ϕ_{north}	Porosity	0.3	3.9	4.0	2.9
k_{f}^{xy}	Saturated hydraulic conductivity	$54.85\,\text{m}\,\text{d}^{-1}$	5.3×10^{-2}	4.6×10^{-1}	2.8×10^{-1}
$l_{\text{coupl}}^{\text{sealed}}$	Coupling length	3.23 m	1.4×10^{-2}	4.4×10^{-1}	2.7×10^{-1}

(Doherty, 2010) provided not only a combination of parameters which resulted in the smallest deviation between observed and simulated data, but also the relative sensitivity of the model output to these parameters. The relative sensitivities for the parameters, along with the estimated values for the parameters, are listed in Table 4.4. The sensitivity values were calculated with respect to the actual calibrated value and are hence comparable to each other. The table is ordered by the overall relative sensitivity of the parameters.

The most relevant parameter by far was the Manning's roughness of the stream network. The roughness was considered to be the same in x and y direction. Interestingly, the value for the calibrated Manning's roughness coefficient ($n_{\text{stream}} = 0.15\,\text{s}\,\text{m}^{-1/3}$) was much higher than values reported in the in literature. Values found for natural streams and rivers range from $0.005\,\text{s}\,\text{m}^{-1/3}$ to $0.04\,\text{s}\,\text{m}^{-1/3}$ (Arcement and Schneider, 1989; Hornberger, 1998; Li et al., 2008; Jones et al., 2008; Alaghmand et al., 2014). The default value provided by HydroGeoSphere is $0.054{,}8\,\text{s}\,\text{m}^{-1/3}$ (Therrien et al., 2012). However, the discharge dynamics were not represented well using these values and hence the parameter was included in the calibration process. The estimated values for the Manning's roughness of the land surface was much higher than values reported in literature, too. However, the calibrated values were consistent with streams having a lower Manning's n than the land surface. The value estimated for surface water bodies like ponds and lakes were between land and streams, which is plausible. Goderniaux et al. (2009) estimated Manning's n of 0.3, 3.0 and 6.0 $\text{s}\,\text{m}^{-1/3}$ for urban, rural, and forested areas, respectively. Goderniaux et al. (2009) explained these deviations between

literature and calibrated values as a result of a coarse spatial and temporal discretisation.

The coupling length of the streams was third most sensitive. The calibrated value for the stream network corresponded to the values reported in the literature (e.g. Alaghmand et al., 2014). The calibrated value for the unsealed irrigation pond was with 1.44×10^{-6} m much lower than literature values, and the calibrated value for the sealed irrigation ponds was with 3.23 m much higher than expected. This may be a result of the representation of the sealed beds by solely the coupling length. However, the sensitivity of the model output to these parameters was 3 and 6 orders of magnitude lower than the sensitivity to the coupling length of the unsealed ponds, respectively. The coupling length of the sealed irrigation ponds was the least sensitive parameter.

The calibrated value of aquifer porosity for both the northern and southern parts of the catchment of 0.3 was the upper limit, which was set before calibration and what is reported in literature (Hölting and Coldewey, 2005). The different formation history of these two parts of the aquifer is not reflected in this parameter set and differs from the choices made by Mey (2011) with 0.1 for the upper part of the catchment and 0.25 for the lower part of the catchment. The porosity of the aquifer greatly influences the amplitude of groundwater head fluctuations. Hence, the observed deviations between simulated and observed groundwater head dynamics described in Section 4.2.1 are most likely a consequence of the calibrated porosity values.

The relative sensitivity of the parameter describing the saturated hydraulic conductivity in x, y (k_f^{xy}) and z-direction (k_f^z) respectively, was surprisingly low. The saturated hydraulic conductivity in the vertical direction was more sensitive than in the horizontal directions. During the calibration process, the maximum value of saturated hydraulic conductivity within the raster of spatial distribution changed. This raster included areas outside the model domain. Hence, the maximum value in Table 4.4 is larger than the actual maximum value in the HydroGeoSphere model ($k_f^{xy} = 41.1\,\mathrm{m\,d^{-1}}$; $k_f^z = 0.23\,\mathrm{m\,d^{-1}}$). The distribution of the calibrated values within the model domain are shown in Figure 4.13. While the value for the xy-direction is within the range of values for a sandy aquifer (Heath, 1983; Bear, 1988; Hölting and Coldewey, 2005; Li et al., 2008), the calibrated anisotropy with a ratio of about 180 to 1 between k_f^{xy} and k_f^z is not realistic. Some authors reported a strong anisotropy within porous aquifers (Freeze and Cherry, 1979; Paradis and Lefebvre, 2013), but accounting for the formation history of the catchment under glacial influence (Benda, 1995), this ratio is not very likely in our case. The calibration algorithm, however, does not account for feasible alteration of parameter values, but strictly optimises. This can lead to unrealistic results in a model like HydroGeoSphere, which requires a high number of parameters.

The discussion of different aspects of the calibration and validation results of the HydroGeoSphere model lead to the conclusion that the model has some limitations and uncertainties, but can provide a basis for future investigations. The model performed under changing boundary conditions, such as different precipitation sums, evapotranspiration rates, and volumes of discharged treated wastewater with comparable and reasonable quality. Calibrated parameters, however, were not always meaningful from a physical point of view. Due to the high number of parameters required by the model, it is uncertain if perhaps another set of parameter values could yield the same model output. This equifinality is a

common criticism on models exhibiting this degree of complexity (Beven, 2002), but some authors argue that the complexity of hydrological procceses cannot be captured by simplified models (Brunner and Simmons, 2012). Furthermore, sensitivities of model parameters were surprising and differed from values reported by Goderniaux (2010), which could suggest an erroneous representation of hydrological processes within the model, in general.
However, it was not possible to identify specific sources of the deviations between observed and measured data within the parameter values. Due to the variety of parameters used in the model, an interaction between different parameters is most likely. This means that the model is able to reproduce the system behaviour to a certain degree, but it is not certain that this will be the case in further simulations under varying boundary conditions. Since the input data used for this model did not show striking changes in the general model behaviour, the use of the HydroGeoSphere model of the Lietzengraben catchment for further investigations is justified. However, results should always be analysed keeping the limitations and restrictions of the model in mind.

4.2.2 Comparison ArcEGMO-ASM - HydroGeoSphere

The discussion of the model calibration and validation of HydroGeoSphere in the previous section lead to the conclusion that the model provided a reliable basis for further investigations. Some limitations were, however, identified. The overall goal of this section is to discuss the differences between HydroGeoSphere and ArcEGMO-ASM regarding the model performance in the simulation of discharge, groundwater heads, and water balance. The ability of the models to account for management measures is discussed, along with advantages and limitations of the model concepts and model handling. At the end of this section the groundwater - surface water interaction simulated by HydroGeoSphere and ArcEGMO-ASM is compared to the empirical results as described in section 4.1.

Contrary to the previous section, the results are discussed separately for discharge and groundwater heads. The model ArcEGMO-ASM has been calibrated using data of the period from 1994 to 1999, the validation of the model has been conducted based on data of the period from 2000 to 2006 (Mey, 2011). Contrary to the calibration of HydroGeoSphere, ArcEGMO-ASM was calibrated during a period with no discharge of treated wastewater. The discharge of treated wastewater started in 2004 and was hence only included in the validation period of ArcEGMO--ASM. The irrigation pond "Teich 11" was not included in the original model described by Mey (2011). The modified model, provided by Pfützner (2013), included pond "Teich 11" and several new groundwater observation wells, but was not calibrated again. A detailed description of ArcEGMO-ASM, the calibration process, and the applied modifications can be found in section 3.2.2. The gauges OW2 and OW6 where not used originally in the ArcEGMO-ASM model, but were included for the comparison to HydroGeoSphere.

Discharge

2007 A comparison of the simulation results of ArcEGMO-ASM and HydroGeoSphere with the observed data during the year 2007 is shown in Figure 4.8. In Table 4.1 the calculated Nash-Sutcliffe efficiencies are tabulated. The most notable differences between HydroGeoSphere and ArcEGMO-ASM regarding discharge dynamics during 2007 were the peak values of the streamflow response to precipitation events. The peaks of the ArcEGMO-ASM simulations were generally higher than the results obtained from HydroGeoSphere and the observed discharge volumes. At OW2 this overestimation was more distinct than at OW6. The attenuated response of ArcEGMO-ASM to precipitation events at OW6 compared to OW2 was most likely linked to lakes and wetlands upstream, which served as buffers and hence reduced the peak discharge volumes. Since neither lakes nor wetlands exist upstream of gauge OW2, the response to precipitation was more immediate and not attenuated.
Another factor for the different reactions to precipitation events in the catchment between the two models may be found in the conceptual realisation of precipitation input. As described in Sections 3.2.2 and 3.2.3, the implementation of precipitation differs between ArcEGMO-ASM and HydroGeoSphere. In HydroGeoSphere, precipitation input was based on data of one meteorological station and was distributed uniformly across the catchment. ArcEGMO-ASM makes use of several precipitation gauges distributed around the catchment area. The amount of precipitation input at the spatial units was interpolated between

these stations and was therefore not distributed uniformly. This lead to significant differences in annual precipitation sums between the models, which will be discussed in more detail in section 4.2.2.
To assess differences regarding the discharge simulation, differences of daily precipitation volumes are shown in Figure 4.14 for the year 2007. The calculated differences between the models were not constant and were not evenly distributed temporally. At some occasions, the deviation added up to several mm of precipitation. Hence, using one station as source for precipitation input in HydroGeoSphere led to an underestimation or overestimation of precipitation in the catchment, depending on the location in the catchment. Single events with high precipitation intensity were missed, especially during the summer period. A linear correlation between the daily difference of input precipitation and the daily difference in simulated discharge at gauge OW2 was, however, not found. Since the generation of discharge from precipitation is highly non-linear, and since both models were calibrated using different precipitation input, this is not surprising. Hence, the precipitation data were most likely not the only reason for the differences between the simulated discharge of the models.
At OW2, both ArcEGMO-ASM and HydroGeoSphere overestimated the discharge

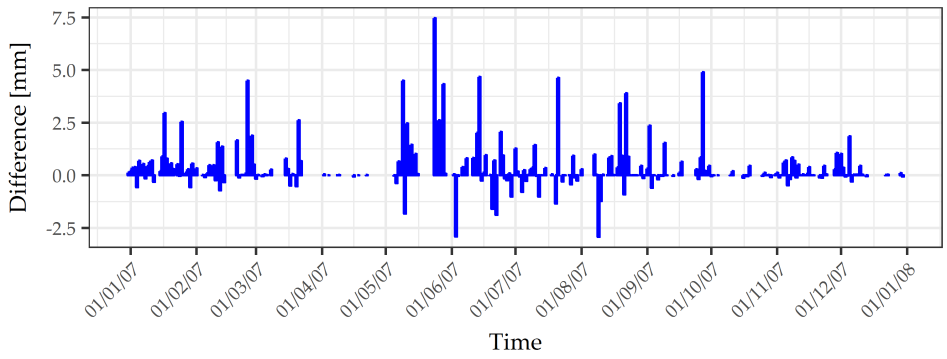

FIGURE 4.14: Differences between precipitation input in ArcEGMO-ASM and HydroGeoSphere in 2007

from the beginning of the year until mid of April (Figure 4.8). The discharge simulated by HydroGeoSphere for the first 4 months of the year overestimated some of the discharge events and the mean discharge in comparison to observed discharge. However, the dynamics of the observed discharge were met reasonably well by the simulation results. ArcEGMO-ASM, on the other hand, simulated discharge with a more distinct and also more realistic dynamic than HydroGeoSphere. The peak discharge volumes simulated by ArcEGMO-ASM ranged up to about $280\,l\,s^{-1}$ on 18/01/2007 and $250\,l\,s^{-1}$ on 22/03/2007 during this period, while HydroGeoSphere simulated discharge events with a maximum discharge of $160\,l\,s^{-1}$ and $185\,l\,s^{-1}$, respectively. Hence, both models overestimate the observed discharge substantially. Furthermore, the maximum discharge was reached with a time lag of 2 to 1 days by ArcEGMO-ASM and HydroGeoSphere, respectively. The corresponding observed discharge was $117\,l\,s^{-1}$ on 20/01/2007 and $132\,l\,s^{-1}$ on 23/03/2007. Both models overestimated the discharge response to the recorded precipitation events. A potential reason for this overestimation by the simulations may be the precipitation of snow which is handled differently in the models. While HydroGeoSphere interprets the precipitation of snow as rainfall, ArcEGMO-ASM interprets precipitation as snow if the daily mean temperature is below 0.1 °C. The

recorded daily mean temperature during the precipitation events was between 5 °C and 7 °C, and snowfall was therefore not included in either model. A review of the recorded snow depths at the meteorological station Berlin-Buch, however, yielded a snow cover during several days in January and February 2007. The overestimation of discharge by both models is hence caused by the erroneous input of precipitation. The melting of the snow cover in February caused an increase of discharge in the catchment which was consequentially not reproduced correctly by the models.

It was assumed that an additional reason for the diverging simulated discharge dynamics was the overestimation of the influence of mechanisms generating rapid discharge responses to precipitation events like for example surface run-off. To test this hypothesis, the observed discharge at gauge OW1 was compared to the discharge at OW2 simulated by ArcEGMO-ASM. The locations of gauges and streams are shown in Figure 4.7 and 3.7. The data of OW1 was used as a boundary condition in ArcEGMO-ASM to account for the discharge generation in the upper catchment. A comparison between observed discharge at OW1 and OW2, and the discharge simulated for OW2 by ArcEGMO-ASM is shown in Figure 4.15. While the observed discharge at OW2 clearly corresponded to the discharge observed at OW1, the discharge simulated by ArcEGMO-ASM was clearly overestimated. This suggests that the source areas of the overestimated discharge portions were not located in the upper catchment but upstream of the confluences of the stream "Graben 30" and the Lietzengraben and the confluence of stream "Graben 1" and the Lietzengraben, respectively. Stream "Graben 30" connects the pond complex "Teich 13" to the Lietzengraben, "Graben 1" connects the ponds "Teich 11" and "Teich 12" to the Lietzengraben. Furthermore, the outflows of the ponds to the streams, simulated by ArcEGMO-ASM, were examined to identify the source of the overestimated discharge portions. However, the discharge volumes were negligible with outflow <0.5 l s^{-1} for "Teich 11", ca. 10 l s^{-1} for "Teich 12", zero outflow and ca. 12 l s^{-1} for the southern and northern outlets of "Teich 13", respectively. This suggests that surface run-off and the fast response of groundwater heads and thus exfiltration to surface streams upstream of the confluences were most likely responsible for the overestimated simulated discharge response.

After the discharge event at the end of March both models failed to reproduce the decline in discharge volumes (Figure 4.8). The decrease of discharge volumes was simulated similarly by both models. The simulated discharge of both models reached the level of observed discharge in the beginning of May. During the vegetation period until the beginning of October the discharge dynamics and discharge volumes were simulated very well by both models. However, ArcEGMO-ASM overestimated the peak values, as described for the beginning of the year 2007 in the previous paragraph. In the period from October to end of December 2007, discharge was simulated reasonably well by ArcEGMO-ASM, while HydroGeoSphere overestimated the discharge volumes.

Overall, both models showed reasonable simulations of the discharge at gauge OW2 in 2007. Contrary to this visual evaluation of the simulation results, the calculated Nash-Sutcliffe efficiency coefficients (NSE) of –0.45 for HydroGeoSphere and –1.79 for ArcEGMO-ASM suggested a poor fit of simulated to observed data. The NSE below zero indicated that the mean value of observed data would be a better predictor of discharge than the simulated data. However, this statistical measure strictly penalises any deviation from the comparative data, even if the temporal variations are identical. Hence, a mere consideration of the calculated NSE is not useful and a visual comparison of simulated and observed data is an

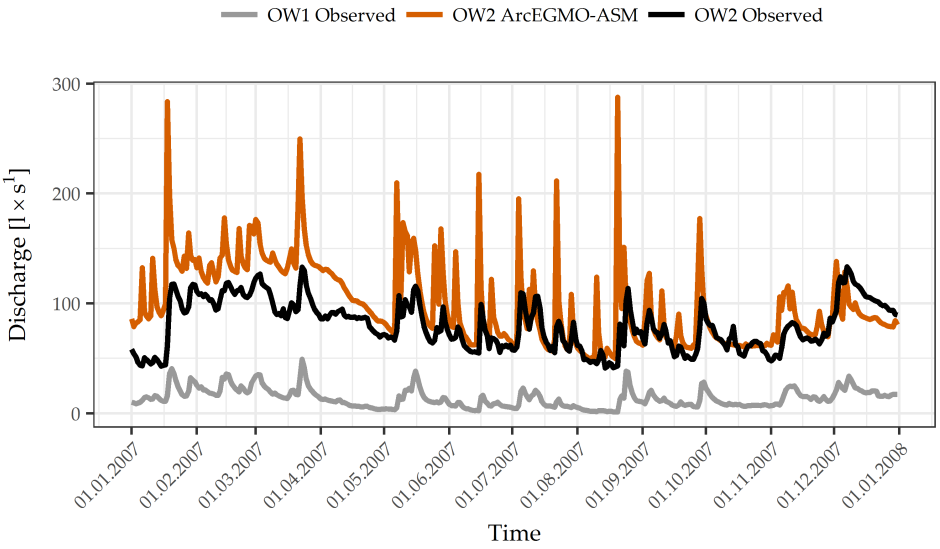

FIGURE 4.15: Comparison between observed discharge at gauges OW1 and OW2, and discharge simulated by ArcEGMO-ASM at OW2 during the calibration period 2007

important component in the evaluation of model results. The good reproduction of observed discharge dynamics by the models hence suggested a reasonable representation of involved mechanisms, although the integral response to precipitation events was not quantitatively simulated correctly.

A comparison of the model performances regarding discharge simulations at gauge OW6 yielded some differences to the comparison results at OW2. In the period from January to end of March the deviations between observed and simulated discharge were less than at OW2 for both models. The discharge was not under- or overestimated substantially, but the amplitude of observed discharge fluctuations was not reproduced well. ArcEGMO-ASM was slightly more accurate than HydroGeoSphere and managed to reproduce the discharge maximum of the discharge event on 23/03/2007. Similary to OW2, both models failed to reproduce the fast decrease of the discharge volume after this discharge event and hence overestimated the discharge until the beginning of May. During the vegetation period from May to October the comparison of the models yielded substantial differences. While HydroGeoSphere managed to simulate the discharge reasonably well, ArcEGMO-ASM failed to reproduce the observed discharge dynamics. The peak volumes of discharge events were clearly overestimated as well as the total amount of discharge during these events. However, the discharge events simulated by ArcEGMO-ASM at OW6 were smoother than at OW2 which reflected the presence of lakes, wetlands, and weirs upstream of OW6. The last months of the year were dominated by one major discharge event in November. This has been ascribed to a management measure upstream of OW6 at weir 11 (Pauli et al., 2008). This management measure, an opening of a weir, was not incoorporated in the models, and hence they failed to reproduce the discharge volumes during this period. Furthermore, discharge simulated by ArcEGMO-ASM showed a decline at the end of October, which could not be verified by the observed data. An explanation for this deviation could not be found. In December, ArcEGMO-ASM underestimated the discharge while HydroGeoSphere simulated discharge at OW6 reasonably well. The calculated Nash-Sutcliffe efficiency coefficients for

the simulated discharge at OW6 were 0.55 for HydroGeoSphere and 0.19 for ArcEGMO-ASM. These values were substantially higher than the NSE for OW2 for both models and suggested a satisfactory simulation of the catchment-wide integration of discharge processes at OW6. In general, HydroGeoSphere performed better than ArcEGMO-ASM. This may be due to the fact that HydroGeoSphere was calibrated on the basis of discharge and groundwater heads data from 2007, while ArcEGMO-ASM was calibrated using discharge data of the period from 1996 to 1999. This implies an advantage for HydroGeoSphere in comparison to ArcEGMO-ASM.

2008-2012 A comparison of the simulation results of ArcEGMO-ASM and HydroGeoSphere as well as the observed data during the period 2008 to 2012 is shown in Figure 4.10. In Table 4.1 the calculated Nash-Sutcliffe efficiencies are tabulated. At OW2 HydroGeoSphere overestimated the observed discharge and was not able to reproduce the observed amplitudes of the discharge dynamics. The simulation of discharge by the models at the beginning of the years 2009 and 2010 differed remarkably from each other. ArcEGMO-ASM reproduced the discharge more accurately but overestimated the amplitudes of the discharge dynamics. The comparison of the simulation results to the recorded snowdepths yielded an explanation for these differences. While HydroGeoSphere did not include the precipitation of snow, ArcEGMO-ASM interpreted precipitation in the beginning of 2009 and especially 2010 as snowfall due to temperatures below 0.1 °C. In 2010, this lead to a very good correspondence between observed discharge at OW2 and the discharge simulated by ArcEGMO-ASM, while HydroGeoSphere completely failed to reproduce the discharge dynamics.
During the vegetation period both models reproduced the discharge reasonably well. Similar to the results for the year 2007, ArcEGMO-ASM overestimated the maximum discharge volumes strongly. However, HydroGeoSphere failed to reproduce the amplitude of the fluctuations of discharge volumes and showed a very attenuated response to precipitation in comparison to the observed discharge. The values estimated for the roughness of the stream and land surfaces during calibration may be a reason for this attenuated response. The calculated Nash-Sutcliffe efficiency coefficients of 0.39 for HydroGeoSphere and 0.05 for ArcEGMO-ASM indicated a good performance only by HydroGeoSphere. However, the visual inspection of the simulation results of ArcEGMO-ASM yielded a good performance, especially during conditions with snowfall. The low NSE values were most likely caused by the strong overestimation of discharge peaks. The general discharge level and the fluctuations over the 5 year period were reproduced well by both models. At OW6, HydroGeoSphere and ArcEGMO-ASM performed very similar to OW2. The discharge peaks were, however, only slightly overestimated by ArcEGMO-ASM while the amplitudes were underestimated by HydroGeoSphere. The very high discharge levels after the snowmelt in the beginning of 2010 were not reproduced by both models. The Nash-Sutcliffe efficiency coefficient of 0.65 for both HydroGeoSphere and ArcEGMO-ASM suggested a good reproduction of the observed discharge dynamics. In general, both models were able to reproduce the discharge dynamics. The implementation of snowfall in ArcEGMO-ASM had a substantial impact on simulation quality.

Hydraulic heads

In this section the differences between the groundwater heads, calculated by ArcEGMO-ASM and HydroGeoSphere, are discussed. On the one hand time series of the simulated heads at groundwater observation wells are compared to observed heads. On the other hand the differences between the spatial patterns of groundwater heads calculated by the models are discussed to elaborate the differences between the models which are not visible if one only considers heads at observation wells. However, information about the (observed) spatial distribution of groundwater heads were not available. Therefore, this comparison only includes the model results. A comparison between the two models could not be carried out without any post-processing. ArcEGMO-ASM provided 2D results of the groundwater heads, at a grid of cells of 25 m × 25 m. HydroGeoSphere provided 3D results of the nodes at a mesh of finite elements of variable dimensions. Therefore, the surface of the saturated zone in HydroGeoSphere was extracted in Tecplot and the node values were rasterized on a grid with cells of 12.5 m × 12.5 m using the *raster* package in *GNU R* (Hijmans, 2016) and interpolated using an inverse distance weighting algorithm (Pebesma, 2004; Gräler et al., 2016). When differences had been calculated, the results have been smoothed by applying a moving window algorithm (Hijmans, 2016) which averaged the values in a window of 7 × 7 cells to ease the visual interpretation of the results.
The comparison of the calculated Pearson correlation coefficients, shown in Table 4.2, did not yield any substantial differences between the models. In general, during 2007 the higher values were distributed evenly among the models, while in the period 2008 to 2012 HydroGeoSphere seemed to have more accurate results. An inspection of time series (shown in Figures 4.9 and 4.11) yielded some differences, however.
The heads at the observation wells BU27 and BU30 were reproduced very well by HydroGeoSphere while ArcEGMO-ASM underestimated the heads by about 0.5 m to 0.8 m. However, ArcEGMO-ASM simulated the heads at the observation well BU01 better than HydroGeoSphere. The observation wells in the surrounding of the irrigation ponds are reproduced better by HydroGeoSphere, with the exception of BU01, better reproduced by ArcEGMO-ASM, and Senat7745, reproduced poorly by both models.
A major difference between the models are the groundwater head dynamics. HydroGeoSphere calculated dynamics with lower amplitudes than the observations and ArcEGMO-ASM. This was most likely mainly the result of the chosen parameter values for the porosity of the aquifer by the models and/or the low hydraulic conductivity in z-direction in HydroGeoSphere. With a porosity of 0.3, calibrated by PEST for HydroGeoSphere was three times as high as the porosity of 0.1, which was chosen for ArcEGMO-ASM by Mey (2011).
The comparison of the spatial distribution of averaged groundwater heads for the period 2008 to 2012 between the models is shown in Figure 4.16. The mean values were calculated with daily values from the end of each month, resulting in 60 values for each model. The comparison of the isolines of the heads between the models showed some differences. The streams are hydraulically more effective in ArcEGMO-ASM. In the lower and upper part of the catchment, the angle of isolines are steeper, meaning steeper gradients to the streams. In the center of the catchment, in the surrounding of the irrigation ponds the differences were not distinct. The area between the isolines 50 m and 51 m is much bigger in HydroGeoSphere and includes the Lake Bogenseekette while in ArcEGMO-ASM the

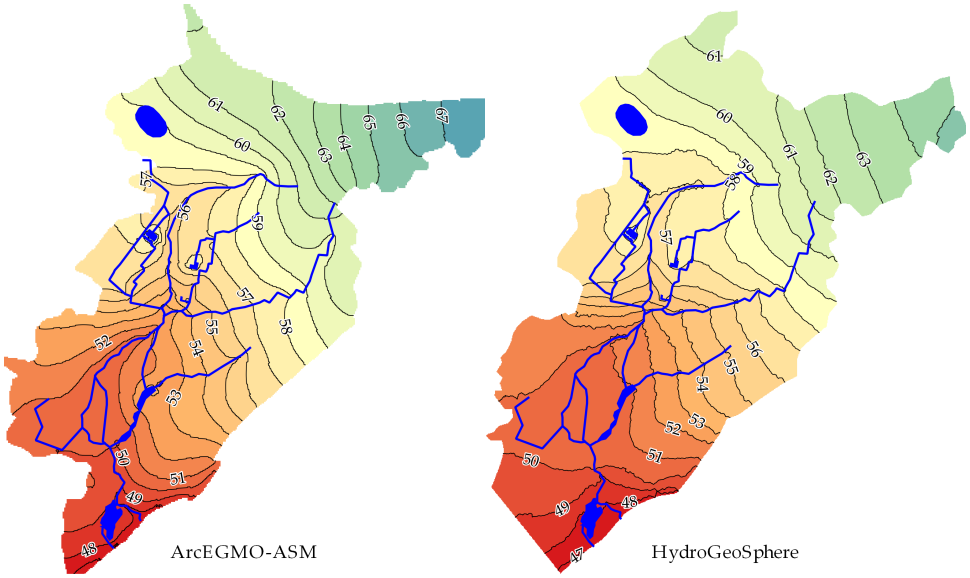

FIGURE 4.16: Mean hydraulic heads [m.a.s.l] calculated from simulation results of ArcEGMO-ASM (left) and HydroGeoSphere (right) for the period 2008 - 2012

Lake Bogenseekette is cut by isolines up to 53 m.
In Figure 4.17 the difference between the mean groundwater heads calculated by ArcEGMO-ASM and HydroGeoSphere as well as the differences between the distance from the land surface to the groundwater table are shown. For the left side, positive values indicate ArcEGMO-ASM heads being higher than HydroGeoSphere heads, negative values the opposite. In most parts of the catchment the heads calculated by ArcEGMO-ASM are higher than the heads by HydroGeoSphere. In the north-east corner of the catchment these differences are the highest with values up to 5 m. This should be an effect of the hydraulic conductivity and also boundary effects. However, in the central parts of the catchment HydroGeoSphere calculated heads higher than ArcEGMO-ASM. This suggests that in HydroGeoSphere more surface water is infiltrating into the subsurface than in ArcEGMO-ASM and/or that the evapotranspiration is higher in ArcEGMO-ASM in this zone. In the lower part of the catchment there is also a small area with distinct higher heads in HydroGeoSphere. This is a result of a weir in this area, which is located at a slightly different position in HydroGeoSphere in comparison to ArcEGMO-ASM.

The distance between the terrain surface and the saturated zone, the depth of the groundwater table, is an important factor for the vegetation. The availability of water to plants during periods with low or no precipitation is linked to the accessibility of water from the saturated zone. Hence, differences between the depths in HydroGeoSphere and ArcEGMO-ASM have been analysed. The differences between the mean depth of the groundwater table during the years 2008 to 2012 are shown in Figure 4.17 on the right. The spatial patterns of the differences do not coincide with the differences of the hydraulic heads shown on the left side of the figure. The deviation between ArcEGMO-ASM and HydroGeoSphere were very high in the north-eastern part of the catchment due to a lower groundwater table simulated by HydroGeoSphere. Since the absolute differences between groundwater table and terrain surface were several metres, this was not considered of substantial importance for the model performance. The highest relevant differences occured in the upper part of the Lietzengraben, north of the irrigation

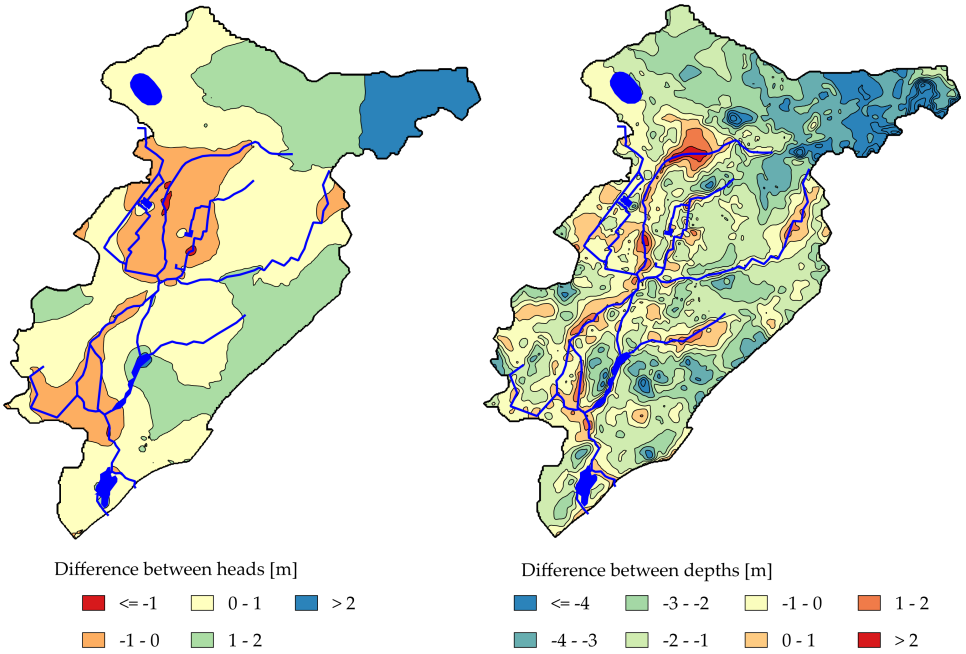

FIGURE 4.17: Difference between the mean groundwater heads calculated by ArcEGMO-ASM and HydroGeoSphere for the period 2008 - 2012 (left), negative values indicate higher heads simulated by HydroGeoSphere, and the difference between the mean depths from the surface to the groundwater table for the period 2008 - 2012 (right), negative values indicate a smaller disctance to the groundwater table simulated by ArcEGMO-ASM; streams, lakes, and ponds are shown in blue

ponds. The deviation between ArcEGMO-ASM and HydroGeoSphere ranged up to >2.0 m in this area. In general, along the streams of the catchment and in the area of the irrigation ponds there is a nearly constant offset between the two models. The explanation for these substantial differences lay in the elevation of the terrain surface, used for the calculation of the depth to the groundwater table. The digital elevation model (DEM) used for building the HydroGeoSphere model had a resolution of 10 m × 10 m and an accuracy of ±2.0 m. The DEM was edited prior to the transfer to the model mesh. Elevated streets, rail tracks, and a former dump with very steep slopes were deleted and the elevation was fit to the surrounding raster cells. The generated mesh nodes were equipped with the elevation values of the DEM. In a next step, the elevation of the nodes along streams, lakes, and the irrigation ponds were adjusted to the stream- and lakebed elevations as represented in ArcEGMO-ASM. The specifications of the DEM used in ArcEGMO-ASM were not known. However, the elevations of the stream- and lakebeds were not represented in the DEM since these informations were stored in a different module. This explained the deviations along the streams. In the area of the highest differences, the DEM of ArcEGMO-ASM yielded higher values than the HydroGeoSphere DEM. Additionally, the HydroGeoSphere model included some streams in this area, which were not represented in ArcEGMO-ASM and hydraulic heads calculated by HydroGeoSphere were up to 0.5 m higher than the heads by ArcEGMO-ASM. The deviations may have caused differences regarding the plant uptake of water and hence should also be considered in the analyses of the water balance in the next section.

TABLE 4.5: Precipitation and calculated actual evapotranspiration for ArcEGMO-ASM

	2007	**2008**	**2009**	**2010**	**2011**	**2012**
Precipitation [mm]	877	699	684	750	763	705
Evapotranspiration [mm]	727	547	551	580	663	633

Water balance

The quality of a numerical model is assessed by the fit of simulated to observed data, as shown in the previous sections. However, numerical models are subject to errors due to the numerical solution of equations describing the system behaviour. Numerical solutions are not exact solutions but are characterised by pre-defined convergence criteria, which prescribe the conditions under which the iterative solution of the equation matrix is accepted. This leads to errors in the mass balance of the models, which was accounted for in the analysis process. The absolute errors, the normalized errors, and the percentaged errors in relation to the water sinks of the models are shown in Table 4.6 for HydroGeoSphere and ArcEGMO-ASM for 2007 and the period 2008 to 2012.

The normalized errors made by HydroGeoSphere are smaller than the errors

TABLE 4.6: Water balance for HydroGeoSphere and ArcEGMO-ASM for 2007 and 2008-2012

	2007		**2008 - 2012**	
	HGS	**ArcEGMO–ASM**	**HGS**	**ArcEGMO–ASM**
Net water balance: Sources - sinks [mm]	–19	+47	–21	+172
Storage change [mm]	–7	–6	+48	+25
Error [mm]	–12	+53	–69	+147
Error [% of sinks]	1.5	5.9	1.9	3.8

made by ArcEGMO-ASM in general. However, the values of the calculated water balance are smaller in comparison to the calculated storage change in HydroGeoSphere while in ArcEGMO-ASM the value of the calculated water balance is higher than the storage change. While this normalized error accounts for the area of the model domain, the percentage error accounts for the absolute volume of the sum of the sinks for water in the models. The percentaged error of ArcEGMO-ASM was 2 to 4 times higher than the error of HydroGeoSphere, indicating that errors made due to numerical issues made by HydroGeoSphere are smaller than in ArcEGMO-ASM. However, one has to consider the different concepts which form the basis for the two compared models. HydroGeoSphere is a fully integrated model, the errors are based on the usage of two coupled domains, including all aspects of the water balance. On the contrary, ArcEGMO-ASM consists of several model layers forming the different domains of the model, as described in Section

TABLE 4.7: Difference between ArcEGMO-ASM and HydroGeoSphere regarding annual precipitation and actual evapotranspiration sums. Positive values indicate higher values for ArcEGMO-ASM

Year	**2007**	**2008**	**2009**	**2010**	**2011**	**2012**
Precipitation [mm]	91	42	34	72	74	51
Actual evapotranspiration [mm]	4	-4	-30	15	25	11

3.2.2. Each layer includes different inflows, outflows, and storage terms. The errors among these layers were not consistent. The percentaged errors of the module accounting for the soil water budget and discharge generation were 1.3 % and 0.2%, the error of the groundwater layer 7.3%, and the stream discharge module exhibited errors of 14.7% and 10.0% for the calibration period and the period 2008 - 2012, respectively.

The calculated net water balances of both models are shown in Table 4.6 as well as the storage change, including surface and subsurface storage, over the considered period of time. The components of the water balance, calculated by the models, were assessed to investigate the results accounting for the representation of the hydrologic regime by the models and to examine potential sources of deviations between the model results. The comparison of the storage changes calculated by HydroGeoSphere and ArcEGMO-ASM showed no substantial difference between the models in the calibration period. Both models exhibited a decrease of the storage content. In the course of the validation period 2008 to 2012, however, both models yielded a net increase of the storage content. The increase for HydroGeoSphere was twice as high as for ArcEGMO-ASM. The comparison of the net balances of the models, calculated on the basis of water sources and sinks, yielded results not consistent to the storage changes, which is reflected in the calculated errors in Table 4.6. For the calibration period, HydroGeoSphere exhibited a deficit of 19 mm, which corresponds qualitatively to the calculated storage change. ArcEGMO-ASM, however, showed a net gain of 47 mm, which differs not only quantitatively but qualitatively from the calculated storage change of –6 mm. The difference between the models regarding the net balance is linked to the differences in the precipitation input data. As illustrated in Table 4.5 for ArcEGMO-ASM and Table 4.3 for HydroGeoSphere, ArcEGMO-ASM received much more precipitation during 2007 than HydroGeoSphere while the calculated actual evapotranspiration was about the same. For the comparison of the models during the validation period, the applied precipitation and the calculated actual evapotranspiration were separated by years. An overview of the differences between the models regarding precipitation input and output via actual evapotranspiration is shown in Table 4.7. The precipitation input to ArcEGMO-ASM is always higher than the input of precipitation to HydroGeoSphere, with a mean value of 55 mm between 2008 and 2012. As described previously, in ArcEGMO-ASM the precipitation is not distributed spatially uniform. The precipitation values of various meteorological stations were interpolated and applied to the model domain. The precipitation input in HydroGeoSphere was distributed uniformly, based on the records of one meteorological station. The application of time series of spatially non uniformly distributed precipitation values was not available in HydroGeoSphere. Hence, the HydroGeoSphere model missed precipitation events in the upper catchment which contributed substantially to the annual precipitation sum. This is most likely the major source for the differences between ArcEGMO-ASM and HydroGeoSphere regarding water balance issues.
The calculated actual evapotranspiration, on the other hand, was very similar for both models. They used the same time series of potential evapotranspiration. As a result, the calculated net water balance for the period 2008 to 2012 for HydroGeoSphere was much lower than for ArcEGMO-ASM. HydroGeoSphere results yielded a net loss of 21 mm over the period, while ArcEGMO-ASM yielded a net gain of 172 mm. The spatial distribution of the differences regarding the actual evapotranspiration are shown in Figure 4.18. Negative values indicate a higher mean

actual evapotranspiration of HydroGeoSphere. While the total annual sums of actual evapotranspiration are very similar between the models, the spatial distribution of the differences between the mean actual evapotranspiration calculated by ArcEGMO-ASM and HydroGeoSphere differed. The mean evapotranspiration

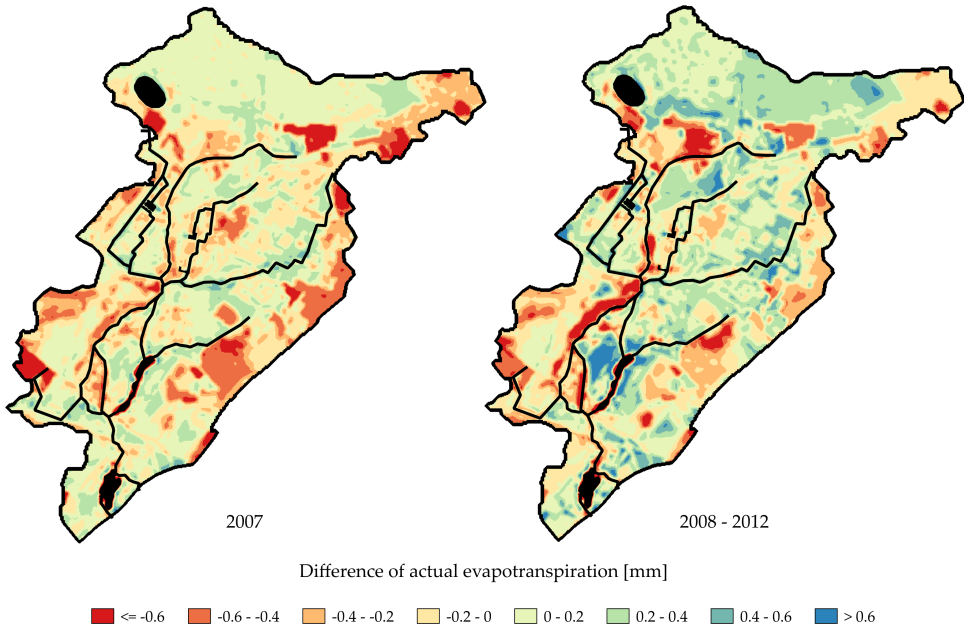

FIGURE 4.18: Differences between the mean actual evapotranspiration calculated by ArcEGMO-ASM and HydroGeoSphere for the year 2007 and the period 2008 - 2012, negative values indicate a higher mean actual evapotranspiration of HydroGeoSphere

of HydroGeoSphere was higher than the mean evapotranspiration simulated by ArcEGMO-ASM at some locations in the catchment and much lower in others. HydroGeoSphere exhibited higher evapotranspiration rates in a lowland connected to the Lietzengraben north of the irrigation pond “Teich 13”, west of the Lietzengraben between stream gauge OW2 and the furcation of the Lietzengraben downstream of the branch - off to Lake Bogenseekette, and in the south-east of the catchment near the urban areas. Between the Lake Bogenseekette and the Lietzengraben, ArcEGMO-ASM exhibited a much higher evapotranspiration than HydroGeoSphere. The most plausible driver for the deviation between the models was the availability of water for evapotranspiration, which is linked to the distance of the groundwater table to the surface.The spatial patterns of the differences in evapotranspiration coincide well with patterns apparent in the differences between the models regarding the depth of the groundwater table in Figure 4.17. The deviation of the actual evapotranspiration was most distinct in zones where the difference between the depths to the groundwater table differed substantially and the groundwater table was generally close to the terrain surface. These different depths simulated by the models were caused by the differences between the simulated hydraulic heads, but mostly by the differences between the elevation of the terrain surface represented in the models, due to the different digital elevation models which had been used during the model set-up. In the areas which were identified previously as zones of highly increased evapotranspiration by HydroGeoSphere in comparison to ArcEGMO-ASM, the terrain surface of HydroGeoSphere was much lower than the elevation used in ArcEGMO-ASM

and vice versa. The mean value of the deviation between the two DEMs, however, was only 0.03 m and hence the used elevation models only affected the model results on a local scale, resulting in generally similar evapotranspiration sums.
To summarize the results of the comparison of the water balances:

- HydroGeoSphere exhibited, based on the net water balance, a water shortage in 2007 which was not observed in the simulation results by ArcEGMO-ASM. The calculated storage changes, however, were very similar between the models.
- In the validation period 2008 - 2012 the differences in the calculated net water balance between the models was even more distinct.
- The comparison of the storage changes yielded similar results for both models in 2007. However, the deviation between calculated water balance and storage change was higher for ArcEGMO-ASM for both time periods, which is most likely a result of the error propagation caused by the use of several model layers in ArcEGMO-ASM.
- The drought in HydroGeoSphere was a result of an underestimation of the precipitation in the catchment due to the limitation of the model when it comes to time series of spatially non uniformly distributed precipitation.
- The differences between the models regarding the sums of calculated actual evapotranspiration were minor. The spatial differences of the actual evapotranspiration, however, suggested an influence by the used digital elevation models.
- The results suggested that both models showed reasonable results. However, it is likely that the results provided by ArcEGMO-ASM are favourable since the model was calibrated over a longer period of time and hence took different years with changing meteorological conditions into account. Furthermore, the results regarding the water balance were comparable to values found in literature (Gerstengarbe et al., 2003; Lahmer and Pfützner, 2003).

Groundwater discharge: Modelled vs. measured results

The exfiltration rates simulated by ArcEGMO-ASM are provided on the spatial resolution of the pre-defined stream reaches. The reach of “Graben 1”, which was subject to the field measurements described in Section 4.1, was represented in ArcEGMO-ASM by two stream features. The stream reach, however, covered the stream features only partially. Thus, a detailed spatial comparison was not possible. In order to compare the general interaction intensity, however, the exfiltration rate calculated by ArcEGMO-ASM was derived through Equation (3.33) to (3.35) with the properties of the stream features as given in Table 4.8. Since the stream features were longer than the cells of the model layer accounting for groundwater, every feature was tied to 5 groundwater cells. The elevation of the groundwater table was assumed to be equal to the hydraulic head. The elevation was derived by averaging the simulated heads on 08/08/2012 for the cells of the aquifer, which were tied to the stream features. For stream feature 19, the exfiltration of groundwater was determined as $q = 411\,\mathrm{mm\,d^{-1}}$. The corresponding value for stream reach 92, downstream of feature 19 was $q = 154\,\mathrm{mm\,d^{-1}}$.

TABLE 4.8: Geometries of the stream features and mean groundwater heads linked to the features

Feature	l_{reach} [m]	$width_{sb}$ [m]	s_{bank} [-]	$h_{streambed}$ [m]	$h_{groundwater}$ [m]
19	100.4	1.7	0.5	52.61	52.78
92	101.5	1.5	0.5	52.28	52.61

The exchange fluxes simulated by HydroGeoSphere on 08/08/2012 were derived by the extraction of nodal exchange flux values from a post-processed result file. The spatial discretisation of the stream reach at "Graben 1" in HydroGeoSphere lead to 4 distinct exchange flux values along the stream reach. A comparison of the estimated exfiltration fluxes based on field measurements with the fluxes calculated by ArcEGMO-ASM and HydroGeoSphere is shown in Figure 4.19. The mean value of the exfiltration rates from field measurements is 101 mm d^{-1}. The values obtained through HydroGeoSphere are shown below the red dots, which indicate the position of the corresponding node along the stream reach. The coloured blocks indicate the stream features as represented in ArcEGMO-ASM along the stream reach. The comparison of the results showed clearly that it was

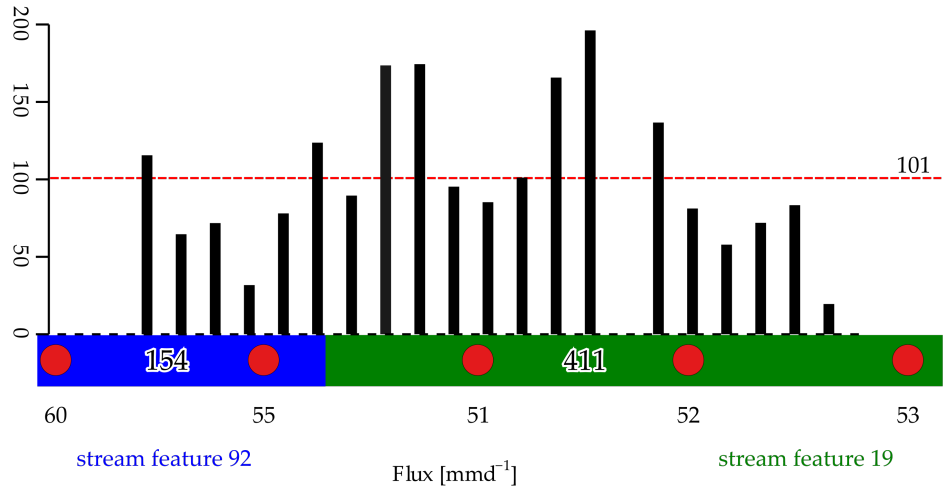

FIGURE 4.19: Comparison of groundwater exfiltration rates derived from masurements (black bars), HydroGeoSphere (red dots), and ArcEGMO-ASM (coloured blocks). The mean value of measured exfiltration rates is indicated by the dashed line in red. All values shown in mm d^{-1}

not possible to reproduce spatial variations of the exfiltration rates by the simulations. This is a result of the spatial discretisation of the stream reach and the adjacent aquifer. Furthermore, both models assumed homogeneous conditions of the aquifer and the streambed. Natural heterogeneity was not represented in either model. The assumption of the existing groundwater exfiltration to "Graben 1" due to the stream morphology and the adjacent discharge of treated wastewater at irrigation pond "Teich 11" was confirmed by both models and the measurements. Although the measured exfiltration rates were likely overestimated, as pointed out in Section 4.1.4, a comparison between the mean rate of the estimated groundwater exfiltration and model results showed some differences.
HydroGeoSphere underestimated the exfiltration of groundwater with values about half as high as the mean value of measurements. The simulated values

ranged from 51 to 60 mm d^{-1}. Besides the discretisation, a potential reason for the underestimation of exfiltration fluxes is the strong anisotropy of the (simulated) aquifer with hydraulic conductivities in z-direction being several orders of magnitude lower than the conductivity in xy-direction. ArcEGMO-ASM overestimated the exfiltration rates by a factor of 4 at the stream feature 19 and by a factor of 1.5 at stream feature 92. Due to the concept of the spatial discretisation of subsurface and surface features, both stream features used for this comparison obtained groundwater from several cells of the aquifer. This approach represents an advantage regarding efficiency and applicability of the model, but limits the possibilities to analyse surface - subsurface interactions in more detail. However, this limitation is acceptable as these interactions are not part of the intended application of the model.

Handling & capabilities

HydroGeoSphere and ArcEGMO-ASM are two very different models regarding the basic principle of simulations, the required input data, and the tools which are provided to represent catchment features. The goal of this section is to compare the limitations and advantages of ArcEGMO-ASM and HydroGeoSphere, focussing on the aspects in which ArcEGMO-ASM and HydroGeoSphere differed most to each other.

Management features The Lietzengraben catchment includes weirs, bifurcated streams, and the discharge of treated wastewater to irrigation ponds. ArcEGMO-ASM provides tools to account for such features. Weirs can be defined by their type and width and height. An active steering of the height of the weir is possible in principle and was realised in the Lietzengraben model as fixed cycle. Streams can be bifurcated and the proportion of water discharging into the two branches can be defined in advance. Due to its modular character, the definition of new features or the withdrawal of existing features is easily accomplished. The stream network in ArcEGMO-ASM consists of distinct stream reaches. In the early stages of the discharge of treated wastewater to the Lietzengraben catchment, the route of the water through the catchment was varied. This was also possible using ArcEGMO-ASM with limitations since it is not possible to change the routing during the simulation runs.
The version of HydroGeoSphere used in this study did not provide these possibilities. Since the stream network is not predefined, the best way to represent streams and weirs was to alter the digital elevation model. It was relatively easy to adjust the surface to streambed elevations in order to achieve a good representation of the stream network. In order to represent weirs, the streambed elevation was increased at the locations of weirs. The material properties of the adjacent elements were changed to an impermeable surface to mimic the impermeable properties of a weir. The time varying alteration of the height of the weir was not possible. Since the weirs in the catchment were mostly only actively controlled to avoid damage during stormflow events, this simplification was acceptable.
The discharge of treated wastewater was represented in ArcEGMO-ASM by discharging water to selected stream reaches. In HydroGeoSphere, the discharge of treated wastewater was represented by using a specific flux boundary condition. The flux was given as a length and the volume was calculated by multiplying the specified flux with the area of the applied zone. Due to the high volumes of treated

wastewater, this approach led to numerical instabilities in HydroGeoSphere. The discharge of treated wastewater was slowly increased from zero to the mean value of the water discharge. The time series of the discharge is not continuously, hence the sudden decline or increase of the discharge led to very small time steps during these changes and therefore increased the computational time. This implies that a simulation of a period without discharge followed by periods with discharge is not possible with this model setup.

The simulation of catchments including management features and dynamic management strategies is difficult using HydroGeoSphere. By adding functionalities like for example weirs and the bifurcation of streams this limitation could be eliminated. On the contrary, ArcEGMO-ASM provides user-friendly and efficient tools to include management features and dynamic management measures. Due to its modular concept, the coupling to additional programs needed to solve problems is possible. For example by the coupling of ArcEGMO to a three dimensional groundwater model.

Technical requirements In this study, ArcEGMO-ASM was executed on a dual-core PC, while HydroGeoSphere was executed on a high performance multi-core server blade. The simulation of time periods of up to 17 years was possible within hours using ArcEGMO-ASM and the time steps were constant. The simulation of a period of one year using HydroGeoSphere could take up to days. Since the HydroGeoSphere model included highly non-linear unsaturated flow and a multitude of spatial elements in comparison to ArcEGMO-ASM, the computational effort to solve the underlying mathematical descriptions was much higher than in ArcEGMO-ASM. The time steps used by HydroGeoSphere were variable and were adjusted in order to satisfy the convergence criteria. This lead to unpredictable computational times. In the beginning of this study, numerical instabilities often led to a termination of the simulation. This was critical, especially during the calibration process, which was carried out using a calibration algorithm. With the given resources, it was not possible to calibrate over a period longer than one year. Nevertheless, the duration of the final calibration process was several weeks. Most likely, the numerical instabilities were caused by the coarse grid in some locations and failed attempts to achieve convergence during drying and re-wetting processes. However, with the given computational resources, it was not possible to realize a finer discretisation and hence substantial compromises had to be accepted.
In terms of user friendliness, HydroGeoSphere has potential for further improvements. The manual, which was provided with the software, was not satisfactory. Some functionalities had not been described, others were contained in the manual while actually being out-dated. This made it difficult to identify problems or locate errors during the model set-up.

4.2.3 Flow paths and residence times

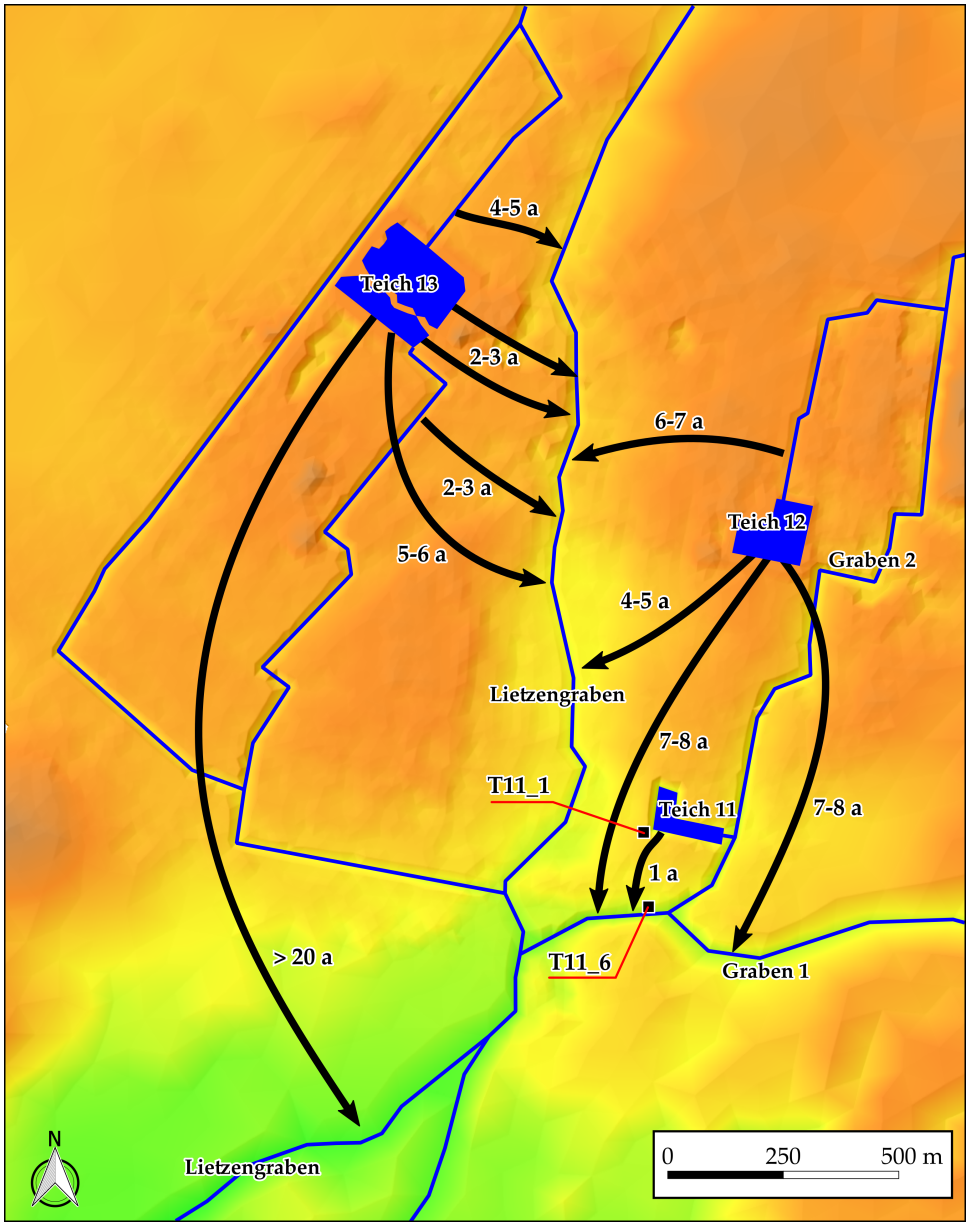

FIGURE 4.20: Stream traces derived on basis of the mean flow velocities from 2008 to 2012 and the corrosponding time from infiltration into the subsurface until exfiltration into a stream in years. The locations of the groundwater observation wells T11_1 and T_6 south of "Teich 11" are indicated as black squares.

The post-processing analysis of flow paths and residence times was conducted using the stream traces functionality of Tecplot. Basis for the estimation of these were the mean subsurface flow velocities during the period from 2008 to 2012 (monthly values, n=60). Starting point for the routing of flow paths were located within the irrigation ponds and at the adjacent reach of the corresponding outlet. The results are shown in Figure 4.20. The majority of the streamtraces indicated a passage of infiltrated water to the Lietzengraben ("Teich 12" and "Teich 13") within two to seven years. Flow paths starting at "Teich 11" ended at the adjacent stream to the south, "Graben 1" after approximately one year.
However, some flow paths were unexpected. A part of the water infiltrating at

"Teich 13" seemingly passed underneath the adjacent streams and exfiltrated to the Lietzengraben in the west of Lake Bogenseekette. The residence time for this passage was over 20 years. Furthermore, streamtraces originating in "Teich 12" passed between the Lietzengraben and "Teich 11" and exfiltrated into "Graben 1" after 7-8 years. Additionally, a streamtrace was identified, which passed underneath "Graben 2" in the south-east of "Teich 12" and exfiltrated into "Graben 1" upstream of the confluence of "Graben 2" and "Graben 1".
The estimated flow paths suggest that most of the water, which infiltrates into the subsurface at the irrigation ponds, discharges to the adjacent surface streams. Only a small proportion of infiltrated treated wastewater remains in the subsurface over longer distances. The calculated residence times, however, were relatively short. To check the results for plausibility, the horizontal hydraulic gradient between two groundwater observation wells was used to calculate a rough estimate of the effective subsurface flow velocity. The location of the observation wells is shown in Figure 4.20. The effective flow velocity of subsurface water between the wells was calculated as:

$$v_{\text{eff}} = \frac{-k_{\text{f}} \times i}{n} \tag{4.1}$$

where:

v_{eff} = Effective flow velocity $[LT^{-1}]$
k_{f} = Hydraulic conductivity in x, y-direction $[LT^{-1}]$
i = Hydraulic gradient
n = Porosity [-]

The mean hydraulic gradient between the wells during the year 2012 was –0.008,7 m m^{-1}. The distance between the wells was 185 m. An interpolated value of the hydraulic conductivities reported by Wachholz (2005) was used as an estimate of the hydraulic conductivity between the wells. The porosity of the aquifer was taken from Mey (2011). With an estimated hydraulic conductivity of 3.0 m d^{-1} and a porosity of 0.1, the effective flow velocity was calculated after Equation (4.1) as 0.29 m d^{-1}. Based on this flow velocity, the distance between the wells is covered within 1.7 years. This value is within the range of the value derived from analysis of HydroGeoSphere results. However, the value of the porosity was 0.3 in HydroGeoSphere and hence three times as high as in ArcEGMO-ASM and as it is considered to be realistic. The effective flow velocity of the HydroGeoSphere model would be substantially higher if HydroGeoSphere would use a more realistic, lower porosity. This would lead to even shorter residence times. Another source of error for the estimation of residence times based on HydroGeoSphere is the inability of the model to reproduce the groundwater heads at the observation well Senat7745, which is located in between "Teich 11" and "Graben 1" (see Figure 4.7). The heads were substantially underestimated. Since the water level at "Teich 11" was plausible, the resulting horizontal gradient between the pond and the stream was substantially overestimated, leading to higher effective flow velocities. The calculation of the residence time based purely on observed hydraulic heads and estimates of hydraulic conductivity and porosity is, however, also prone to error. It does not take the three dimensionality of flow into account and hence is most likely underestimating the residence time.
Therefore, it is concluded that the estimation of residence times based on the HydroGeoSphere simulations underestimated the actual values substantially. However, they may allow to compare the residence times of different flow paths to

each other. The determination of the flow paths is less prone to error and should be more accurate, since the discussion of the simulation results in Section 4.2.1 showed the model's ability to reproduce the general groundwater dynamics.

5 Summary & conclusions

The goal of this work was to test the applicability of a fully integrated, physically based numerical model to a problem originating in management measures on a field site and to compare advantages, opportunities and possible pitfalls of the model to a hydrological iterative model, which has been commonly been used to tackle questions concerning management measures and the water budget on a catchment scale.
Additionally to this comparison, the calculated exfiltration rates of groundwater to surface streams were compared to values based on field measurements in the streams to evaluate the performance of the spatial models ArcEGMO-ASM and HydroGeoSphere regarding groundwater - surface water interaction.

Although the application of the fully integrated model HydroGeoSphere on a catchment scale, including the influence of the discharge of wastewater, faced serious challenges and despite the necessity of substantial simplifications the model was capable to reproduce the catchment dynamics, as shown by the comparison between simulated and observed groundwater heads and discharge data.

Flow paths of water which infiltrated into the subsurface in the area of irrigation ponds and exfiltrated to surface streams were successfully calculated. Furthermore, residence times of water in the subsurface following these flow paths were approximated. However, due to implausible parameter values derived during the automated calibration of the model, the reliability of these results is uncertain.

The simulation of groundwater - surface water interaction yielded exfiltration rates alongside a stream reach, which were compared to values obtained on the basis of field measurements.

Applying HydroGeoSphere, the calibration and validation procedures showed reasonably good agreement between measured and simulated discharge volumes at the two gauged stations. Although a perfect fit to the observed values was not accomplished, the general dynamics and the response to precipitation events in the catchment were reproduced well. This was also supported by the calculated Nash-Sutcliffe efficiencies of 0.55 and 0.65 at OW6 at the catchment outlet for the calibration and validation periods, respectively. However, it was not possible to account for single management measures which were executed in late 2007 to advert damage from weir 11, upstream of OW6. The opening of the weir could not be simulated, which lead to significant deviation between simulated and observed discharge volumes in the calibration period. The model fit to the observed discharge at gauge OW2 in the upper part of the catchment showed a weaker performance and yielded a Nash-Sutcliffe efficiency of -0.45 and 0.39 for the calibration and validation periods, respectively.

Groundwater heads were represented satisfactorily by HydroGeoSphere. However, the quality of the calibration results was quite heterogeneous spatially. The seasonal dynamics were reproduced well in general. At some observation wells,

heads were however systematically underestimated, while they were overestimated at other observation wells. The deviations between observed and simulated heads were substantial and reached up to 50 cm. Only at the well BU27, the offset was very small and the seasonal dynamics were represented very well. With regard to the calculation of flow paths and residence times, especially the results at Senat7745 can be considered as critical, since this observation well is situated downstream of irrigation pond "Teich 11", between the pond and the stream "Graben 1", where the estimation of groundwater-surface-water interactions had been undertaken. The inaccuracy of simulated groundwater heads impacted the calculation of groundwater - surface water exchange. A good agreement between observed and simulated hydraulic heads in the surrounding of the exchange interface would hence be beneficial, since it reduces the number of sources of errors and leads to improved comparability.

These deviations could have resulted from the spatial distributions of the hydraulic conductivity and porosity, which were not altered during the calibration process in their relation to each other. Furthermore, the spatial discretisation of the subsurface domain can have a substantial impact on the quality of simulation results (Sciuto and Diekkrüger, 2010; Vogel and Ippisch, 2008). In general, the accuracy of simulation results tend to increase with finer discretisation (Wildemeersch et al., 2014). Since the distance between pond "Teich 11" and "Graben 1" ist about 190 metres and the horizontal extend of the grid elements in this area is about 25 metres, the deviation is most likely a result of the low number of elements between pond and stream. The parameters values derived during the calibration procedure were predominantly reasonable. Some aspects, however, should be underlined.

The Manning's roughness coefficient describing the surficial roughness was much higher than values found in the literature (Arcement and Schneider, 1989; Hornberger, 1998; Li et al., 2008; Partington et al., 2013; Alaghmand et al., 2014; Wildemeersch et al., 2014). However, the discharge dynamics were not represented well using these values and hence the parameter was included in the calibration process. The calibrated values for the Manning's roughness of the implemented surface zones were consistent with streams having a lower Manning's n than the land surface. The value estimated for surface water bodies like ponds and lakes were between land and streams, which is plausible. Goderniaux et al. (2009) also estimated Manning's n higher than expected. Goderniaux et al. (2009) explained these deviations between literature and calibrated values as a result of a coarse spatial and temporal discretisation, which did most likely apply to the model set up in this study, too.

Another parameter which was altered during calibration was the saturated hydraulic conductivity of the aquifer. The hydraulic conductivities used in ArcEGMO-ASM (Mey, 2011) were based on the work of Wachholz (2005). For the HydroGeoSphere model, hydraulic conductivities from borehole data, provided by Wachholz (2005), were interpolated. During the calibration process, the distribution of hydraulic conductivities was preserved and a global multiplier value was adjusted. Additionally, we had to include the vertical conductivity as well. We restricted the calibration algorithm to a anisotropy ratio of the vertical to the horizontal saturated hydraulic conductivity not smaller than 1/180 and not greater than 1. The hydraulic conductivity in x- and y-directions was assumed to be equal.

The calibration resulted in a ratio of 1/180, corresponding to the limit defined

in advance. Differences between horizontal and vertical hydraulic conductivity of aquifers over the order of several magnitudes have been reported (Freeze and Cherry, 1979; Paradis and Lefebvre, 2013). However, in our opinion this is not likely in our case due to the glacial formation history of the sandy aquifer (Benda, 1995), which should show less anisotropy (Cherkauer and Zager, 1989; Kidmose et al., 2011; Juckem et al., 2017).

Parameters for the estimation of unsaturated hydraulic conductivities were obtained by application of the model Rosetta, described by Schaap et al. (2001). These parameters determined the calculation of unsaturated hydraulic conductivities and pressure-saturation dependencies. Input parameters for the model were the proportion of sand, silt, and clay in the sub-surface layers. The soil description used by Mey (2011) for the ArcEGMO-ASM model was adopted for this purpose and clustered to obtain spatially larger units of material properties. This approach lead to higher uncertainties and therefore to possible errors (Sciuto and Diekkrüger, 2010). Since the calculation of van Genuchten-Mualem parameters based on soil texture is subject to uncertainty (Ghanbarian-Alavijeh et al., 2010), we preferred this simplified approach over an approach were a highly heterogeneous distribution of parameters would have suggested an exact parametrisation of material properties, which was not realistic.

Overall, for some parameters, we had to make use of values, which are not plausible. This was however necessary to create a response of the model to input data which matched the observed system dynamics. This was identified as one of the core problems using models with such a large of number of (physically based) parameters (Beven, 1989; Brunner and Simmons, 2012). Furthermore, the reproduction of the (same) system dynamics may be possible using different sets of parameter values which reduces the explanatory power of these models. Over-parametrisation and equifinality seemed to be an issue in our case.
This does not necessarily mean that the results derived from the model are wrong. Yet, one has to be careful applying this model to assess processes and scenarios which differ from the ones considered in this work. The simulation of the system dynamics without proper implementation of system processes due to an incorrect set of parameters is likely and limits the applicability of the model.

The simulation of the catchment using the model system ArcEGMO-ASM yielded reasonable results as well. The model was completed by including the irrigation pond "Teich 11", several observation wells, and by updating input time series (Pfützner, 2013). The model was not calibrated and the set of parameters previously determined by Mey (2011) was used, since the changes were minor and Mey (2011) showed the principal capability of the model to reproduce discharge and groundwater heads in the Lietzengraben catchment sufficiently. Since the calibration of ArcEGMO-ASM is not automated, the effort of another calibration seemed disproportional to the expected improvement of the model fit. Although the model was not calibrated after integration of the additional irrigation pond, the model performed well. The deviation between simulated and observed groundwater heads ranged up to one metre while the general dynamics were reproduced quite well. In general, the discharge dynamics were reproduced well. However, ArcEGMO-ASM overestimated discharge peaks substantially in some cases.

The comparison between the simulation results obtained by HydroGeoSphere and ArcEGMO-ASM and observed data showed that both models were able to reproduce the observed groundwater heads and discharge behaviour. The performance of HydroGeoSphere was slightly better than ArcEGMO-ASM. The discharge

behaviour could be reproduced more accurate and groundwater heads were simulated more accurately, too. However, both models deviated from observed values.

The point measurements of sediment temperature profiles in the streambed along the stream reach of "Graben 1" yielded exfiltration rates between 30 and 200l d^{-1} m^{-2} in August 2012. The measurements of temperatures along the stream reach using FO-DTS in February 2012 and August 2012 yielded a similar distribution of groundwater exfiltration zones. Overall, the results based on the different methods were consistent with each other. The results confirmed the expected exfiltration of groundwater to the stream during the whole year, as suggested by the stream morphology and the hydraulic conditions due to the discharge of treated wastewater.

However, the comparison to the exchange flows as suggested by the numerical models HydroGeoSphere and ArcEGMO-ASM showed the difficulty of combining measurements with simulation results at different spatial scales. Due to the coarse horizontal discretisation of the stream, only few nodes of the model lay within the investigated stream reach. The values provided by HydroGeoSphere were within the range of values estimated on the basis of field measurements, but did not reproduce any heterogeneities, which were estimated by the measurements. The same applied to the results of ArcEGMO-ASM, with the difference, that ArcEGMO-ASM only provided two values for the investigated stream reach due to the modelling concept of the interaction between streams and subsurface. Hence, the stream reach was only represented by two predefined stream elements which only provided one value each describing the exchange flux between surface and subsurface.

On the basis of the flow fields calculated by HydroGeoSphere, we were able to estimate flow paths originating in the irrigation ponds. The results showed that most flow paths reached adjacent surface streams within 2 to 7 years. The results showed that infiltrated solutes at the irrigation ponds did not necessarily exfiltrate into the directly adjacent streams. This would increase the residence times significantly. In some cases, the particles crossed underneath the adjacent surface streams and exfiltrated into streams more distant. This increased the residence time of these particles in the subsurface up to more than 20 years. On the other hand, the results of the flow path estimation were linked to the calibration results of HydroGeoSphere. Especially the ratio of 1/180 between vertical and horizontal saturated hydraulic conductivities had most likely a significant impact on the flow field governing the flow paths. Therefore, the results of the flow path analysis were a qualitative assessment of possible spreading of infiltrated treated wastewater and the linked residence times, and were not necessarily accurate.

Since the focus of this work was not only the quality of results, but also the successful handling of the fully integrated model, the challenges while building and running the model were assessed. The process of setting up a catchment model using HydroGeoSphere was quite challenging and many compromises had to be made until numerical stability was sufficient and computational times were acceptable.
The spatial discretisation of a catchment characterised by small artificial streams, which cut deep into the terrain in order to drain the area, was a challenge. The spatial grid had to be fine enough to account for a large number of streams and the simulation of subsurface flow between irrigation ponds and streams while reducing the total number of grid elements to achieve managable computation

times. Large differences between the size of the spatial elements of streams and adjacent elements were furthermore a source of numerical issues and had to be handled carefully.

The retrieval of spatially distributed physical parameters such as the rooting depth of plants, van Genuchten-Mualem parameters to account for the unsaturated hydraulic conductivity and other parameters was quite challenging during the process of building the model. It is not possible to perform sufficient measurements of these parameters in the field or in the lab, because this would be very time consuming and expensive. Furthermore, spatial heterogeneity was very high, rendering a meaningful parametrisation extremely difficult. Hence, many parameters had to be estimated using literature data and significant simplifications had to be made. The van Genuchten-Mualem parameters were computed using a model based on the proportions of sand, silt, and clay in the soil.

In general, computational times of HydroGeoSphere were long, which resulted in a long duration of the calibration procedure. Additionally, different types of numerical issues caused the model to crash often. After each crash, the specific source of the problem had to be identified and solved. Often this resulted in trial and error and was very time consuming.
First of all, the irrigation of treated wastewater to the irrigation ponds was quite difficult to handle. The discharge volume of water to the ponds varied in large steps due to the seasonally dependent management strategy. This resulted in extremely small time steps in order to achieve convergence of the numerical solution. Although the lower limit of time steps was set to a very small value of 0.086 seconds, this limit was often reached. However, the time step often was not small enough for the solution to satisfy the convergence criteria. As a consequence, the simulation was aborted.
The second major source of problem was the drying and re-wetting of surficial elements due to dry periods and following precipitation events. In some cases this lead to a non-convergence of the solution and hence the simulation was terminated.
We identified the spatial discretisation as the source of this behaviour, the problem was partially fixed by altering the material properties of the affected elements regarding the van Genuchten-Mualem parameters, the residual saturation, and the rooting depth. A finer discretisation of the whole catchment was not possible since previous test runs showed that unmanageable computational times would have been the result. Therefore these numerical problems lead to ongoing simplifications of parameter sets and a coarsening of the spatial distribution of soil properties in areas where we observed these problems. As a consequence of these simplifications, the uncertainty of the model results increased. This is a general trade-off in the application of numerical models. In order to investigate catchments and set up a working model, certain simplifications may be necessary. At the same time the validity of the model must be ensured, in order to achieve reliable results.

In contrast, the iterative coupled model ArcEGMO-ASM is closely linked to geoinformation systems like ArcGIS. This makes the data handling and processing relatively easy for users with some GIS experience. The computational effort to run the model was relatively small. The model could run several years on a regular PC within a few hours. The numerical stability of the ArcEGMO-ASM code was not assessed within this work since we had access to the working model used by Mey (2011).

In conclusion of the summarised results of this work, the application of the fully integrated, physically based model HydroGeoSphere was successful, but not superior to the hydrological iterative model ArcEGMO-ASM. The process of catchment discretisation was more difficult than expected and numerical instabilities were severe in the beginning of this thesis. Discretisation issues and numerical problems lead to a higher degree of simplification of spatially distributed parameters with HydroGeoSphere than originally planned.

The achieved fit of simulated to observed data for HydroGeoSphere was better than the calibration result of the hydrological iterative model ArcEGMO-ASM, but some of the derived parameters were not plausible, which contradicts the idea of physically based parameters. The determination of flow paths and residence times of solutes in the subsurface were error-prone due to unrealistic parameter sets. Therefore, the potential expansion of solutes in the subsurface was estimated rather qualitatively than quantitatively. This is sufficient for basic questions regarding the dispersal of solutes, but could be achieved using less sophisticated models.

The effort to build such a sophisticated model was in the end not justified by the additional information one got from the simulations in comparison to an iterative model. The version of HydroGeoSphere which was used in this work is clearly a research tool, and users apart from science will not benefit substantially. If the application of the code gets more convenient and tools to simulate structures like weirs and their functionality are provided by the publisher, HydroGeoSphere could become a tool to work on engineering problems like this. Especially, the possibility to simulate the transport of solutes and/or heat within an integrated modelling system is promising.

Bibliography

Abwasserverband Braunschweig (2017). *Das Braunschweiger Modell: Ein Wasser-Nährstoff-Energiekreislauf*. URL: http://www.abwasserverband-bs.de/de/was-wir-machen/braunschweiger-modell/.

Alaghmand, S., S. Beecham, I.D Jolly, K.L Holland, J.A Woods, and A. Hassanli (2014). "Modelling the impacts of river stage manipulation on a complex river-floodplain system in a semi-arid region". In: *Environmental Modelling & Software* 59, pp. 109–126. DOI: 10.1016/j.envsoft.2014.05.013.

Anderson, J. (2003). "The environmental benefits of water recycling and reuse". In: *Water Science & Technology Water Supply* 3.4, pp. 1–10.

Anderson, R.B, D.L Naftz, F.D Day-Lewis, R.D Henderson, Donald O. Rosenberry, B.J Stolp, and P. Jewell (2014). "Quantity and quality of groundwater discharge in a hypersaline lake environment". In: *Journal of Hydrology* 512, pp. 177–194. DOI: 10.1016/j.jhydrol.2014.02.040.

Angermann, Lisa, Jörg Lewandowski, Jan H. Fleckenstein, and Gunnar Nützmann (2012). "A 3D analysis algorithm to improve interpretation of heat pulse sensor results for the determination of small-scale flow directions and velocities in the hyporheic zone". In: *Journal of Hydrology* 475, pp. 1–11. DOI: 10.1016/j.jhydrol.2012.06.050.

Anibas, Christian, Jan H. Fleckenstein, Nina Volze, Kerst Buis, Ronny Verhoeven, Patrick Meire, and Okke Batelaan (2009). "Transient or steady-state? Using vertical temperature profiles to quantify groundwater-surface water exchange". In: *Hydrological Processes* 23.15, pp. 2165–2177. DOI: 10.1002/hyp.7289.

Anibas, Christian, Kerst Buis, Ronny Verhoeven, Patrick Meire, and Okke Batelaan (2011). "A simple thermal mapping method for seasonal spatial patterns of groundwater–surface water interaction". In: *Journal of Hydrology* 397.1-2, pp. 93–104. DOI: 10.1016/j.jhydrol.2010.11.036.

Anibas, Christian, Uwe Schneidewind, Gerd Vandersteen, Ingeborg Joris, Piet Seuntjens, and Okke Batelaan (2016). "From streambed temperature measurements to spatial-temporal flux quantification: using the LPML method to study groundwater-surface water interaction". In: *Hydrological Processes* 30.2, pp. 203–216. DOI: 10.1002/hyp.10588.

AP Sensing GmbH (2009). *Agilent N4385A/N4386A Distributed Temperature System: User's Guide*. Ed. by AP Sensing GmbH. Böblingen.

Arcement, George J. and Verne R. Schneider (1989). *Guide for selecting Manning's roughness coefficients for natural channels and flood plains: Water Supply Paper 2339*. Ed. by U.S. Geological Survey.

Asano, T. and A. Lavine (1996). "Wastewater reclamation, recycling and reuse: past, present, and future". In: *Water Science and Technology* 33.10-11, pp. 1–14. DOI: 10.1016/0273-1223(96)00401-5.

BAH (2011). *Dokumentation ArcEGMO: Teil 1*. URL: http://www.doku.arcegmo.de/.

Baron, Jill S., N. LeRoy Poff, Paul L. Angermeier, Clifford N. Dahm, Peter H. Gleick, Nelson G. Hairston, Robert B. Jackson, Carol A. Johnston, Brian D. Richter, and Alan D. Steinman (2002). "Meeting ecological and societal needs for

freshwater". In: *Ecological Applications* 12.5, pp. 1247–1260. DOI: 10.2307/3099968.

Bear, Jacob (1988). *Dynamics of fluids in porous media*. New York: Dover.

Becker, A., B. Klöcking, W. Lahmer, and Bernd Pfützner (2002). "The hydrological modelling system ARC/EGMO". In: *Mathematical models of large watershed hydrology*. Ed. by V. P. Singh and Donald K. Frevert. Highlands Ranch and Colo: Water Resources Publications, pp. 321–338.

Becker, Bernhard (2010). "Zur gekoppelten numerischen Modellierung von unterirdischem Hochwasser". Dissertation. Aachen: RWTH.

Benda, Leopold [Hrsg.] (1995). *Das Quartär Deutschlands: i. A. der Deutschen Quartärvereinigung hrsg. von Leopold Benda gemeinsam mit den Geologischen Diensten der Bundesrepublik Deutschland zum 14. Kongreß der Internationalen Quartärvereinigung (INQua) in Berlin 1995*. Stuttgart: Borntraeger.

Beven, Keith (1989). "Changing ideas in hydrology — The case of physically-based models". In: *Journal of Hydrology* 105.1-2, pp. 157–172. DOI: 10.1016/0022-1694(89)90101-7.

— (2002). "Towards an alternative blueprint for a physically based digitally simulated hydrologic response modelling system". In: *Hydrological Processes* 16.2, pp. 189–206. DOI: 10.1002/hyp.343.

Blume, Theresa, Stefan Krause, Karin Meinikmann, and Jörg Lewandowski (2013). "Upscaling lacustrine groundwater discharge rates by fiber-optic distributed temperature sensing". In: *Water Resources Research* 49.12, pp. 7929–7944. DOI: 10.1002/2012WR013215.

Bollrich, Gerhard (2000). *Grundlagen*. 5th ed. Vol. 1. Technische Hydromechanik. Berlin: Verl. für Bauwesen.

Bredehoeft, J. D. and I. S. Papaopulos (1965). "Rates of vertical groundwater movement estimated from the Earth's thermal profile". In: *Water Resources Research* 1.2, pp. 325–328. DOI: 10.1029/WR001i002p00325.

Brookfield, Andrea E., Edward A. Sudicky, Y.-J Park, and Brewster Conant (2009). "Thermal transport modelling in a fully integrated surface/subsurface framework". In: *Hydrological Processes* 23.15, pp. 2150–2164. DOI: 10.1002/hyp.7282.

Brooks, R.H and A.T Corey (1964). *Hydraulic properties of porous media*. Fort Collins and Colorado.

Brunke, Matthias (1999). "Colmation and Depth Filtration within Streambeds: Retention of Particles in Hyporheic Interstices". In: *International Review of Hydrobiology* 84.2, pp. 99–117. DOI: 10.1002/iroh.199900014.

Brunke, Matthias and T. O.M. Gonser (1997). "The ecological significance of exchange processes between rivers and groundwater". In: *Freshwater Biology* 37.1, pp. 1–33. DOI: 10.1046/j.1365-2427.1997.00143.x.

Brunner, Philip and Craig T. Simmons (2012). "HydroGeoSphere: A Fully Integrated, Physically Based Hydrological Model". In: *Ground Water* 50.2, pp. 170–176. DOI: 10.1111/j.1745-6584.2011.00882.x.

Brunner, Philip, Craig T. Simmons, Peter G. Cook, and René Therrien (2010). "Modeling Surface Water-Groundwater Interaction with MODFLOW: Some Considerations". In: *Ground Water* 48.2, pp. 174–180. DOI: 10.1111/j.1745-6584.2009.00644.x.

Bundesrepublik Deutschland. *Verordnung zum Schutz des Grundwassers: GrwV*.

Cable, Jaye E., Jonathan B. Martin, and John Jaeger (2006). "Exonerating Bernoulli? On evaluating the physical and biological processes affecting marine seepage

meter measurements". In: *Limnology and Oceanography: Methods* 4, pp. 172–183.

Canadell, J., Robert B. Jackson, J. B. Ehleringer, H. A. Mooney, O. E. Sala, and E.-D Schulze (1996). "Maximum rooting depth of vegetation types at the global scale". In: *Oecologia* 108.4, pp. 583–595. DOI: 10.1007/BF00329030.

Cherkauer, Douglas S. and John P. Zager (1989). "Groundwater interaction with a kettle-hole lake: Relation of observations to digital simulations". In: *Journal of Hydrology* 109.1-2, pp. 167–184. DOI: 10.1016/0022-1694(89)90013-9.

Cooley, Richard L. (1971). "A Finite Difference Method for Unsteady Flow in Variably Saturated Porous Media: Application to a Single Pumping Well". In: *Water Resources Research* 7.6, pp. 1607–1625. DOI: 10.1029/WR007i006p01607.

Cornelissen, Thomas, Bernd Diekkrüger, and Heye R. Bogena (2013). "Using HydroGeoSphere in a Forested Catchment: How does Spatial Resolution Influence the Simulation of Spatio-temporal Soil Moisture Variability?" In: *Procedia Environmental Sciences* 19, pp. 198–207. DOI: 10.1016/j.proenv.2013.06.022.

— (2014). "Significance of scale and lower boundary condition in the 3D simulation of hydrological processes and soil moisture variability in a forested headwater catchment". In: *Journal of Hydrology* 516, pp. 140–153. DOI: 10.1016/j.jhydrol.2014.01.060.

Doherty, John (2010). *PEST: Model-Independent Parameter Estimation: User Manual: 5th Edition*.

DVWK (1996). *Ermittlung der Verdunstung von Land- und Wasserflächen*. Vol. 238. DVWK-Merkblätter zur Wasserwirtschaft. Bonn: Wirtschafts- u. Verl.-Ges. Gas u. Wasser.

DWD Climate Data Center (2018). *Historical daily precipitation observations for Germany: version v006*.

Freeze, R.Allan and John A. Cherry (1979). *Groundwater*. Englewood Cliffs and NJ: Prentice Hall.

Freeze, R.Allan and R.L Harlan (1969). "Blueprint for a physically-based, digitally-simulated hydrologic response model". In: *Journal of Hydrology* 9.3, pp. 237–258. DOI: 10.1016/0022-1694(69)90020-1.

Frei, Sven and Jan H. Fleckenstein (2014). "Representing effects of micro-topography on runoff generation and sub-surface flow patterns by using superficial rill/depression storage height variations". In: *Environmental Modelling & Software* 52, pp. 5–18. DOI: 10.1016/j.envsoft.2013.10.007.

Frei, Sven, K. H. Knorr, Stefan Peiffer, and Jan H. Fleckenstein (2012). "Surface micro-topography causes hot spots of biogeochemical activity in wetland systems: A virtual modeling experiment". In: *Journal of Geophysical Research: Biogeosciences* 117.G4, n/a. DOI: 10.1029/2012JG002012.

Fritz, Birgit, Stephanie Rinck-Pfeiffer, Gunnar Nützmann, and Bernd Heinzmann (2004). "Conservation of water resources in Berlin, Germany, through different re-use of water". In: *Wastewater re-use and groundwater quality*. Ed. by J. H. A. M. Steenvoorden and Theodore A. Endreny. Vol. 285. Wallingford and Oxfordshire [England]: IAHS, pp. 48–52.

Gerstengarbe, F.-W., F. Badeck, F. Hattermann, V. Krysanova, W. Lahmer, P. Lasch, M. Stock, F. Suckow, and F. Wechsung (2003). *PIK Report No. 83: Studie zur klimatischen Entwicklung im Land Brandenburg bis 2055 und deren Auswirkungen auf den Wasserhaushalt, die Forst- und Landwirtschaft sowie die Ableitung erster Perspektiven*. Ed. by F.-W. Gerstengarbe. Potsdam.

Ghanbarian-Alavijeh, B., A. Liaghat, Guan-Hua Huang, and Martinus Th. van Genuchten (2010). "Estimation of the van Genuchten Soil Water Retention Properties from Soil Textural Data". In: *Pedosphere* 20.4, pp. 456–465. DOI: 10.1016/S1002-0160(10)60035-5.

Ginzel, Gerhard (1999). "Methoden zur ökologischen Sanierung der ehemaligen Rieselfelder in Berlin-Buch". In: *Boden- und Grundwasserpassage*. Ed. by Joachim Wolff. Vol. Jg. 1999, H. 1/2. Zentralblatt für Geologie und Paläontologie Allgemeine, angewandte, regionale und historische Geologie. Stuttgart: Schweizerbart, pp. 93–109.

Ginzel, Gerhard and Gunnar Nützmann (1998). "Veränderungen ökohydrologischer und hydrochemischer Verhältnisse in einem ehemaligen Rieselfeldareal im Nordosten Berlins". In: *Bodenökologie & Bodengenese* 26, pp. 73–85.

Glugla, G. (1969). "Berechnungsverfahren zur Ermittlung des aktuellen Wassergehaltes und Gravitationswasserabflusses im Boden". In: *Albrecht-Thaer-Archiv* 13, pp. 371–376.

Glugla, G. and B. König (1989). *VERMO - Ein Modell für die Berechnung des Jahresganges der EVaporation, Versickerung und Grundwasserneubildung*. Berlin.

Goderniaux, Pascal (2010). "Impact of climate change on groundwater reserves". Dissertation. Liège and Belgium: University of Liège.

Goderniaux, Pascal, Serge Brouyère, Hayley J. Fowler, Stephen Blenkinsop, René Therrien, Philippe Orban, and Alain Dassargues (2009). "Large scale surface–subsurface hydrological model to assess climate change impacts on groundwater reserves". In: *Journal of Hydrology* 373.1-2, pp. 122–138. DOI: 10.1016/j.jhydrol.2009.04.017.

Goderniaux, Pascal, Serge Brouyère, Philippe Orban, Samuel Wildemeersch, and Alain Dassargues (2011). "Uncertainty of climate change impact on groundwater resources considering various uncertainty sources." In: *Conceptual an Modelling Studies of Integrated Groundwater, Surface Water, and Ecological Systems*. Ed. by International Association of Hydrological Sciences. Oxfordshire and UK: IAHS Press, pp. 139–144.

Gomez-Velez, Jesus D., Stefan Krause, and John L. Wilson (2014). "Effect of low-permeability layers on spatial patterns of hyporheic exchange and groundwater upwelling". In: *Water Resources Research* 50.6, pp. 5196–5215. DOI: 10.1002/2013WR015054.

Gräler, Benedikt, Edzer Pebesma, and Gerard Heuvelink (2016). "Spatio-Temporal Interpolation using gstat". In: *The R Journal* 8.1, pp. 204–218.

Gupta, Vulli L. and Peter J. Sinclair (1976). "Time of concentration of overland flow". In: *ASCE J. Hydraul. Divison* 4, pp. 547–553.

Hare, Danielle K., Martin A. Briggs, Donald O. Rosenberry, David F. Boutt, and John W. Lane (2015). "A comparison of thermal infrared to fiber-optic distributed temperature sensing for evaluation of groundwater discharge to surface water". In: *Journal of Hydrology* 530, pp. 153–166. DOI: 10.1016/j.jhydrol.2015.09.059.

Hayashi, Masaki and Donald O. Rosenberry (2002). "Effects of Ground Water Exchange on the Hydrology and Ecology of Surface Water". In: *Ground Water* 40.3, pp. 309–316. DOI: 10.1111/j.1745-6584.2002.tb02659.x.

Heath, Ralph C. (1983). *Basic ground-water hydrology: Water supply paper 2220*. Reston and VA.

Hijmans, Robert J. (2016). *raster: Geographic Data Analysis and Modeling*. URL: https://CRAN.R-project.org/package=raster.

Hill, Mary C. and Claire R. Tiedeman (2007). *Effective groundwater model calibration: With analysis of data, sensitivities, predictions, and uncertainty*. Hoboken and N.J: Wiley-Interscience.

Hoffmann, Anja and Günter Gunkel (2011). "Bank filtration in the sandy littoral zone of Lake Tegel (Berlin): Structure and dynamics of the biological active filter zone and clogging processes". In: *Limnologica - Ecology and Management of Inland Waters* 41.1, pp. 10–19. DOI: 10.1016/j.limno.2009.12.003.

Hölting, Bernward and Wilhelm Georg Coldewey (2005). *Hydrogeologie: Einführung in die allgemeine und angewandte Hydrogeologie ; 69 Tabellen*. 6th ed. München: Elsevier, Spektrum Akad. Verl.

Hornberger, George M. (1998). *Elements of physical hydrology*. Baltimore: The Johns Hopkins University Press.

Hupfer, Peter and Frank-Michael Chmielewski (1990). *Das Klima von Berlin: Mit 74 Tabellen*. Berlin: Akad.-Verl.

Huyakorn, Peter S. and George F. Pinder (1988). *Computational methods in subsurface flow*. 4th ed. New York [u.a.]: Acad. Press.

Jacob, Daniela, Holger Göttel, Sven Kotlarski, Philip Lorenz, and K. Sieck (2008). *Klimaauswirkungen und Anpassung in Deutschland: Phase 1: Erstellung regionaler Klimaszenarien für Deutschland. – Abschlussbericht zum UFOPLAN-Vorhaben 204 41 13*. Ed. by Umweltbundesamt. Dessau.

Jones, Jon P., Edward A. Sudicky, and R. G. McLaren (2008). "Application of a fully-integrated surface-subsurface flow model at the watershed-scale: A case study". In: *Water Resources Research* 44.

Juckem, Paul F., Brian R. Clark, and Daniel T. Feinstein (2017). *Simulation of groundwater flow in the glacial aquifer system of northeastern Wisconsin with variable model complexity: U.S. Geological Survey Scientific Investigations Report 2017–5010*. DOI: 10.3133/sir20175010.

Kempe, K. (1991). *Floristisch-vegetationskundliches Gutachten der Karower Teiche, innerhalb der ehemaligen Rieselfelder Blankenfelde und Buch: Gutachten im Auftrag der Senatsverwaltung für Stadtentwicklung und Umweltschutz Berlin*.

Kidmose, Jacob, Peter Engesgaard, Bertel Nilsson, Troels Laier, and Majken C. Looms (2011). "Spatial Distribution of Seepage at a Flow-Through Lake: Lake Hampen, Western Denmark". In: *Vadose Zone Journal* 10, pp. 110–124. DOI: 10.2136/vzj2010.0017.

Kinzelbach, Wolfgang and Randolf Rausch (1995). *Grundwassermodellierung: Eine Einführung mit Übungen*. Stuttgart [u.a.]: Borntraeger.

Klemm, G. and W. Lindner (1995). "Berliner Naturschutzgebiete". In: *Naturschutz und Landschaftspflege in Berlin*. Ed. by H. Sukopp. Berlin, pp. 3–116.

Klöcking, B., F. Suckow, and Bernd Pfützner (2012). *Das ökohydrologische PSCN-Modul innerhalb des Flussgebietsmodells ArcEGMO: Theoretische Modellbeschreibung*. URL: http://www.arcegmo.de/PSCN.pdf.

Koch, Julian, Thomas Cornelissen, Zhufeng Fang, Heye R. Bogena, B. Diekkrüger, Stefan J. Kollet, and Simon Stisen (2016). "Inter-comparison of three distributed hydrological models with respect to seasonal variability of soil moisture patterns at a small forested catchment". In: *Journal of Hydrology* 533, pp. 234–249. DOI: 10.1016/j.jhydrol.2015.12.002.

Koitsch, R. (1977). "Schätzung der Bodenfeuchte aus meteorologischen Daten, Boden- und Pflanzenparametern mit einem Mehrschichtenmodell". In: *Zeitschrift für Meteorologie* 27, pp. 302–306.

Krause, Stefan and Theresa Blume (2013). "Impact of seasonal variability and monitoring mode on the adequacy of fiber-optic distributed temperature sensing at aquifer-river interfaces". In: *Water Resources Research* 49.5, pp. 2408–2423. DOI: 10.1002/wrcr.20232.

Krause, Stefan, David M. Hannah, Jon P. Sadler, Paul J. Wood, Jan H. Fleckenstein, C. M. Heppell, D. Kaeser, R. Pickup, G. Pinay, and A. L. Robertson (2011). "Inter-disciplinary perspectives on processes in the hyporheic zone". In: *Ecohydrology* 4.4, pp. 481–499. DOI: 10.1002/eco.176.

Krause, Stefan, Theresa Blume, and Nigel J. Cassidy (2012). "Investigating patterns and controls of groundwater up-welling in a lowland river by combining Fibre-optic Distributed Temperature Sensing with observations of vertical hydraulic gradients". In: *Hydrology and Earth System Sciences* 16.6, pp. 1775–1792. DOI: 10.5194/hess-16-1775-2012.

Kristensen, K.J and S.E Jensen (1975). "A model for estimating actual evapotranspiration from potential evapotranspiration". In: *Nordic Hydrol.* 6, pp. 170–188.

Kurth, A.-M, N. Dawes, John S. Selker, and Mario Schirmer (2013). "Autonomous distributed temperature sensing for long-term heated applications in remote areas". In: *Geoscientific Instrumentation, Methods and Data Systems* 2.1, pp. 71–77. DOI: 10.5194/gi-2-71-2013.

Lahmer, W. and Bernd Pfützner (2003). *PIK Report No. 85: Orts- und zeitdiskrete Ermittlung der Sickerwassermenge im Land Brandenburg auf der Basis flächendeckender Wasserhaushaltsberechnungen.* Ed. by F.-W. Gerstengarbe. Potsdam.

Lahmer, W., Bernd Pfützner, and A. Becker (2001). "Assessment of land use and climate change impacts on the mesoscale". In: *Physics and Chemistry of the Earth, Part B: Hydrology, Oceans and Atmosphere* 26.7-8, pp. 565–575. DOI: 10.1016/S1464-1909(01)00051-X.

LBGR Brandenburg. *Grundkarte der BÜK 300 im Onlinekatalog.* URL: www.lbgr.brandenburg.de.

Lewandowski, Jörg, Lisa Angermann, Gunnar Nützmann, and Jan H. Fleckenstein (2011). "A heat pulse technique for the determination of small-scale flow directions and flow velocities in the streambed of sand-bed streams". In: *Hydrological Processes* 25.20, pp. 3244–3255. DOI: 10.1002/hyp.8062.

Li, Q., A. Unger, Edward A. Sudicky, D. Kassenaar, E. Wexler, and S. Shikaze (2008). "Simulating the multi-seasonal response of a large-scale watershed with a 3D physically-based hydrologic model". In: *Journal of Hydrology* 357.3-4, pp. 317–336. DOI: 10.1016/j.jhydrol.2008.05.024.

Liggett, Jessica E., Daniel Partington, Sven Frei, Adrian D. Werner, Craig T. Simmons, and Jan H. Fleckenstein (2015). "An exploration of coupled surface–subsurface solute transport in a fully integrated catchment model". In: *Journal of Hydrology* 529, pp. 969–979. DOI: 10.1016/j.jhydrol.2015.09.006.

Lischeid, G. and M. Nathkin (2011). "The Potential of Land-Use Change to Mitigate Water Scarcity in Northeast Germany – a Review". In: *Die Erde* 142.1-2, pp. 97–113.

Lowry, Christopher S., John F. Walker, Randall J. Hunt, and Mary P. Anderson (2007). "Identifying spatial variability of groundwater discharge in a wetland

stream using a distributed temperature sensor". In: *Water Resources Research* 43. DOI: 10.1029/2007WR006145.

McLaren, R. G. (2011). *Grid Builder: A pre-processor for 2-D, triangular element, finite element programs.*

Meinikmann, Karin, Jörg Lewandowski, and Gunnar Nützmann (2013). "Lacustrine groundwater discharge: Combined determination of volumes and spatial patterns". In: *Journal of Hydrology* 502, pp. 202–211. DOI: 10.1016/j.jhydrol.2013.08.021.

Mey, Silke (2011). "Simulation von Wassermangelsituationen im Nordostdeutschen Tiefland mittels gekoppelter Oberflächen- und Grundwassermodelle". Dissertation. Berlin: Humboldt-Universität. URL: https://edoc.hu-berlin.de/handle/18452/16976.

Morita, Masaru and Ben Chie Yen (2002). "Modeling of conjunctive two-dimensional surface-three-dimensional subsurface flows". In: *Journal of Hydraulic Engineering* 128.2, pp. 184–200. DOI: 10.1061/(ASCE)0733-9429(2002)128:2(184).

Mualem, Yechezkel (1976). "A new model for predicting the hydraulic conductivity of unsaturated porous media". In: *Water Resources Research* 12.3, pp. 513–522. DOI: 10.1029/WR012i003p00513.

Munz, Matthias, Sascha E. Oswald, and Christian Schmidt (2016). "Analysis of riverbed temperatures to determine the geometry of subsurface water flow around in-stream geomorphological structures". In: *Journal of Hydrology* 539, pp. 74–87. DOI: 10.1016/j.jhydrol.2016.05.012.

Mwashote, B.M, William C. Burnett, J. Chanton, I.R Santos, Natasha T. Dimova, and P.W Swarzenski (2010). "Calibration and use of continuous heat-type automated seepage meters for submarine groundwater discharge measurements". In: *Estuarine, Coastal and Shelf Science* 87.1, pp. 1–10. DOI: 10.1016/j.ecss.2009.12.001.

Nakayama, Tadanobu and Masataka Watanabe (2008). "Missing role of groundwater in water and nutrient cycles in the shallow eutrophic lake Kasumigaura, Japan". In: *Hydrological Processes* 22.8, pp. 1150–1172. DOI: 10.1002/hyp.6684.

Nash, J.E and J.V Sutcliffe (1970). "River flow forecasting through conceptual models part I — A discussion of principles". In: *Journal of Hydrology* 10.3, pp. 282–290. DOI: 10.1016/0022-1694(70)90255-6.

Neumann, Shlomo P. (1973). "Saturated-unsaturated seepage by finite elements". In: *ASCE J. Hydraul. Divison* 12, pp. 2233–2251.

Nützmann, Gunnar and Silke Mey (2007). "Model-based estimation of runoff changes in a small lowland watershed of north-eastern Germany". In: *Journal of Hydrology* 334.3-4, pp. 467–476. DOI: 10.1016/j.jhydrol.2006.10.026.

Nützmann, Gunnar, Gerhard Ginzel, H. Handke, Hubertus Scholz, G. Siegert, and D. Schwamm (1992). *Abschlußbericht über die hydrologisch-hydrogeologischen Untersuchungen der ehemaligen Rieselfelder Berlin-Buch.* Berlin.

Nychka, Douglas, Reinhard Furrer, John Paige, and Stephan Sain (2015). *fields: Tools for spatial data.* Boulder and Colorado. DOI: 10.5065/D6W957CT. URL: www.image.ucar.edu/fields.

Paradis, Daniel and René Lefebvre (2013). "Single-well interference slug tests to assess the vertical hydraulic conductivity of unconsolidated aquifers". In: *Journal of Hydrology* 478, pp. 102–118. DOI: 10.1016/j.jhydrol.2012.11.047.

Partington, Daniel, Philip Brunner, Craig T. Simmons, René Therrien, Adrian D. Werner, G. C. Dandy, and H. R. Maier (2011). "A hydraulic mixing-cell method to quantify the groundwater component of streamflow within spatially distributed fully integrated surface water–groundwater flow models". In: *Environmental Modelling & Software* 26.7, pp. 886–898. DOI: 10.1016/j.envsoft.2011.02.007.

Partington, Daniel, Philip Brunner, Sven Frei, Craig T. Simmons, Adrian D. Werner, René Therrien, H. R. Maier, G. C. Dandy, and Jan H. Fleckenstein (2013). "Interpreting streamflow generation mechanisms from integrated surface-subsurface flow models of a riparian wetland and catchment". In: *Water Resources Research* 49.9, pp. 5501–5519. DOI: 10.1002/wrcr.20405.

Pauli, Astrid, Nils Kade, and Klaus Möller (2008). *Wiederbewässerung der Rieselfelder um Hobrechtsfelde und Lietzengrabengebiet: Grund- und Oberflächenwassermonitoring 2007 - Bericht: Steuerungsempfehlung zur Bewirtschaftung Lietzengraben*. Berlin.

Pebesma, E.J (2004). "Multivariable geostatistics in S: the gstat package". In: *Computers & Geosciences* 30, pp. 683–691.

Pfützner, Bernd (2003). *Modelldokumentation ArcEGMO*. Ed. by Bernd Pfützner. URL: http://www.arcegmo.de.

— (2004). *Wasserhaushaltsuntersuchungen im Einzugsgebiet des Lietzengrabens: Im Auftrag der Senatsverwaltung für Stadtentwicklung, Referat IE*. Berlin.

— (2005). *Wasserhaushaltsuntersuchungen im Einzugsgebiet des Lietzengrabens: II. Bearbeitungsetappe: Im Auftrag der Senatsverwaltung für Stadtentwicklung, Referat IE*. Berlin.

— (2007). *Wasserhaushaltsuntersuchungen im Einzugsgebiet des Lietzengrabens: III. Bearbeitungsetappe - Abschlussbericht: Im Auftrag der Senatsverwaltung für Stadtentwicklung, Referat IE*. Berlin.

— (2013). *Aktualisierung des gekoppelten Wasserhaushaltsmodells für das Einzugsgebiet des Lietzengrabens im Rahmen von ELAN*. Ed. by BAH Büro für Angewandte Hydrologie.

Pfützner, Bernd, Silke Mey, Gunnar Nützmann, and Eckhart Scheffler (2006). "A model-based analysis of the basin water balance in a catchment in the northeast of Berlin". In: *Hydrology and Water Resources Management - Germany* 50.1, pp. 12–19.

R Core Team (2016). *R: A Language and Environment for Statistical Computing*. Vienna and Austria. URL: https://www.R-project.org/.

Rose, Liliana, Stefan Krause, and Nigel J. Cassidy (2013). "Capabilities and limitations of tracing spatial temperature patterns by fiber-optic distributed temperature sensing". In: *Water Resources Research* 49.3, pp. 1741–1745. DOI: 10.1002/wrcr.20144.

Rosenberry, Donald O. (2005). "Integrating seepage heterogeneity with the use of ganged seepage meters". In: *Limnology and Oceanography: Methods* 3.2, pp. 131–142. DOI: 10.4319/lom.2005.3.131.

— (2008). "A seepage meter designed for use in flowing water". In: *Journal of Hydrology* 359.1-2, pp. 118–130. DOI: 10.1016/j.jhydrol.2008.06.029.

Rosenberry, Donald O. and James W. LaBaugh (2008). *Field techniques for estimating water fluxes between surface water and groundwater: U.S. Geological Survey Techniques and Methods 4-D2*.

Rosenberry, Donald O. and Roger H. Morin (2004). "Use of an Electromagnetic Seepage Meter to Investigate Temporal Variability in Lake Seepage". In: *Ground*

Water 42.1, pp. 68–77. DOI: 10.1111/j.1745-6584.2004.tb02451.x.

Rosenberry, Donald O., Laura Toran, and Jonathan E. Nyquist (2010). "Effect of surficial disturbance on exchange between groundwater and surface water in nearshore margins". In: *Water Resources Research* 46.6. DOI: 10.1029/2009WR008755.

Rudnick, Sebastian, Jörg Lewandowski, and Gunnar Nützmann (2014). "Estimation of lacustrine groundwater discharge using heat as a tracer and vertical hydraulic gradients – a comparison". In: *Complex Interfaces Under Change: Sea – River – Groundwater – Lake*. Ed. by C. Cudennec, M. Kravchishina, Jörg Lewandowski, D. Rosbjerg, and P. Woodworth. Vol. 365, pp. 79–84.

Rühmland, S., A. Wick, T.A Ternes, and M. Barjenbruch (2015). "Fate of pharmaceuticals in a subsurface flow constructed wetland and two ponds". In: *Ecological Engineering* 80, pp. 125–139. DOI: 10.1016/j.ecoleng.2015.01.036.

Scanlon, Bridget R., Richard W. Healy, and Peter G. Cook (2002). "Choosing appropriate techniques for quantifying groundwater recharge". In: *Hydrogeology Journal* 10.1, pp. 18–39. DOI: 10.1007/s10040-001-0176-2.

Schaap, Marcel G., Feike J. Leij, and Martinus Th. van Genuchten (2001). "rosetta: A computer program for estimating soil hydraulic parameters with hierarchical pedotransfer functions". In: *Journal of Hydrology* 251.3-4, pp. 163–176. DOI: 10.1016/S0022-1694(01)00466-8.

Schälchli, Ueli (1992). "The clogging of coarse gravel river beds by fine sediment". In: *Hydrobiologia* 235-236.1, pp. 189–197. DOI: 10.1007/BF00026211.

Scheffler, Eckhart and Moritz Werkethin (2012). *Wiederbewässerung der Rieselfelder um Hobrechtsfelde und Lietzengrabengebiet: Grund- und Oberflächenwassermonitoring 2011 - Ergebnisbericht zur Diskussion am 21.02.2012: Im Auftrag der Berliner Forsten, Referat B, Senatsverwaltung für Stadtentwicklung, I E 21*. Berlin.

Schmidt, Christian, Martí Bayer-Raich, and Mario Schirmer (2006). "Characterization of spatial heterogeneity of groundwater-stream water interactions using multiple depth streambed temperature measurements at the reach scale". In: *Hydrology and Earth System Sciences* 10, pp. 849–859. DOI: 10.5194/hess-10-849-2006.

Schmidt, Christian, Brewster Conant, Martí Bayer-Raich, and Mario Schirmer (2007). "Evaluation and field-scale application of an analytical method to quantify groundwater discharge using mapped streambed temperatures". In: *Journal of Hydrology* 347.3-4, pp. 292–307. DOI: 10.1016/j.jhydrol.2007.08.022.

Schornberg, Christina, Christian Schmidt, Edda Kalbus, and Jan H. Fleckenstein (2010). "Simulating the effects of geologic heterogeneity and transient boundary conditions on streambed temperatures — Implications for temperature-based water flux calculations". In: *Advances in Water Resources* 33.11, pp. 1309–1319. DOI: 10.1016/j.advwatres.2010.04.007.

Schwoerbel, Jürgen (1999). *Einführung in die Limnologie*. 8th ed. Stuttgart [u.a.]: Fischer.

Sciuto, G. and Bernd Diekkrüger (2010). "Influence of Soil Heterogeneity and Spatial Discretization on Catchment Water Balance Modeling". In: *Vadose Zone Journal* 9.4, p. 955. DOI: 10.2136/vzj2009.0166.

Selker, John S., Luc Thévenaz, Hendrik Huwald, Alfred Mallet, Wim Luxemburg, Nick van de Giesen, Martin Stejskal, Josef Zeman, M.C Westhoff, and Marc B.

Parlange (2006a). “Distributed fiber-optic temperature sensing for hydrologic systems”. In: *Water Resources Research* 42.

Selker, John S., Nick van de Giesen, M.C Westhoff, Wim Luxemburg, and Marc B. Parlange (2006b). “Fiber optics opens window on stream dynamics”. In: *Geophysical Research Letters* 33.24. DOI: 10.1029/2006GL027979.

Sophocleous, Marios (2002). “Interactions between groundwater and surface water: the state of the science”. In: *Hydrogeology Journal* 10.1, pp. 52–67. DOI: 10.1007/s10040-001-0170-8.

Spekat, Arne, Wolfgang Enke, and Frank Kreienkamp (2007). *Neuentwicklung von regional hoch aufgelösten Wetterlagen für Deutschland und Bereitstellung regionaler Klimaszenarios auf der Basis von globalen Klimasimulationen mit dem Regionalisierungsmodell WETTREG auf der Basis von globalen Klimasimulationen mit ECHAM5/MPI-OM T63L31 2010 bis 2100 für die SRES-Szenarios B1, A1B und A2*. Ed. by Umweltbundesamt. Dessau.

Stonestrom, David A. and Kyle W. Blasch (2003). “Determining temperature and thermal properties for heat-based studies of surface-water ground-water interactions: Appendix A”. In: *Heat as a tool for studying the movement of ground water near streams (Cir1260)*. Reston and VA, pp. 73–80.

Suárez, Francisco, J. E. Aravena, M. B. Hausner, A. E. Childress, and S. W. Tyler (2011a). “Assessment of a vertical high-resolution distributed-temperature-sensing system in a shallow thermohaline environment”. In: *Hydrology and Earth System Sciences* 15.3, pp. 1081–1093. DOI: 10.5194/hess-15-1081-2011.

Suárez, Francisco, Mark B., Jeff Dozier, John S., and Scott W. (2011b). “Heat Transfer in the Environment: Development and Use of Fiber-Optic Distributed Temperature Sensing”. In: *Developments in Heat Transfer*. Ed. by Marco Aurelio Dos Santos Bernardes. InTech. DOI: 10.5772/19474. URL: https://www.intechopen.com/books/developments-in-heat-transfer/heat-transfer-in-the-environment-development-and-use-of-fiber-optic-distributed-temperature-sensing.

Suck, Maria (2008). *Grundwasserexfiltration in einem Spreealtarm*. Berlin.

Sudicky, Edward A., Jon P. Jones, Y.-J Park, Andrea E. Brookfield, and Dennis Colautti (2008). “Simulating complex flow and transport dynamics in an integrated surface-subsurface modeling framework”. In: *Geosciences Journal* 12.2, pp. 107–122. DOI: 10.1007/s12303-008-0013-x.

Therrien, René (1992). “Three-dimensional analysis of variably-saturated flow and solute transport in discretly-fractured porous media”. Dissertation. Waterloo and Ontario: University of Waterloo.

Therrien, René, R. G. McLaren, Edward A. Sudicky, and Y.-J Park (2012). *HydroGeoSphere: A three-dimensional numerical model describing fully-integrated subsurface and surface flow and solute transport.*

van Genuchten, Martinus Th. (1980). “A Closed-form Equation for Predicting the Hydraulic Conductivity of Unsaturated Soils1”. In: *Soil Science Society of America Journal* 44.5, p. 892. DOI: 10.2136/sssaj1980.03615995004400050002x.

Vereecken, H., M. Weynants, M. Javaux, Y. Pachepsky, Marcel G. Schaap, and Martinus Th. van Genuchten (2010). “Using Pedotransfer Functions to Estimate the van Genuchten–Mualem Soil Hydraulic Properties: A Review”. In: *Vadose Zone Journal* 9.4, p. 795. DOI: 10.2136/vzj2010.0045.

Vogel, H.-J and O. Ippisch (2008). "Estimation of a Critical Spatial Discretization Limit for Solving Richards' Equation at Large Scales". In: *Vadose Zone Journal* 7.1, p. 112. DOI: 10.2136/vzj2006.0182.

Vogt, Tobias, Philipp Schneider, Lisa Hahn-Woernle, and Olaf A. Cirpka (2010). "Estimation of seepage rates in a losing stream by means of fiber-optic high-resolution vertical temperature profiling". In: *Journal of Hydrology* 380.1-2, pp. 154–164. DOI: 10.1016/j.jhydrol.2009.10.033.

Vogt, Tobias, Mario Schirmer, and Olaf A. Cirpka (2012). "Investigating riparian groundwater flow close to a losing river using diurnal temperature oscillations at high vertical resolution". In: *Hydrology and Earth System Sciences* 16.2, pp. 473–487. DOI: 10.5194/hess-16-473-2012.

Wachholz, Matthias (2005). *Einzugsgebietsmodellierung des Lietzengrabens*. Berlin.

Wharton, Geraldene, Seyed Hossein Mohajeri, and Maurizio Righetti (2017). "The pernicious problem of streambed colmation: a multi-disciplinary reflection on the mechanisms, causes, impacts, and management challenges". In: *Wiley Interdisciplinary Reviews: Water* 4.5, e1231. DOI: 10.1002/wat2.1231.

Wickham, Hadley (2016). *Ggplot2: Elegant graphics for data analysis*. Second edition. Use R! [Cham]: Springer.

Wiese, B. and Gunnar Nützmann (2009). "Transient Leakance and Infiltration Characteristics during Lake Bank Filtration". In: *Ground Water* 47.1, pp. 57–68. DOI: 10.1111/j.1745-6584.2008.00510.x.

Wildemeersch, Samuel, Pascal Goderniaux, Philippe Orban, Serge Brouyère, and Alain Dassargues (2014). "Assessing the effects of spatial discretization on large-scale flow model performance and prediction uncertainty". In: *Journal of Hydrology* 510, pp. 10–25. DOI: 10.1016/j.jhydrol.2013.12.020.

Willgoose, Garry, Rafael L. Bras, and Ignacio Rodriguez-Iturbe (1991). "A coupled channel network growth and hillslope evolution model: 1. Theory". In: *Water Resources Research* 27.7, pp. 1671–1684. DOI: 10.1029/91WR00935.

Winter, Thomas C., Judson W. Harvey, Lehn O. Franke, and William M. Alley (1998). *Ground Water and Surface Water: A Single Ressource // Ground water and surface water: A single resource: U.S. Geological survey Circular 1139*. Vol. 1139. Denver and Colorado: U.S. Geological Survey.

Wintgens, T., F. Salehi, R. Hochstrat, and T. Melin (2008). "Emerging contaminants and treatment options in water recycling for indirect potable use". In: *Water Science & Technology* 57.1, p. 99. DOI: 10.2166/wst.2008.799.

Wittenberg, Hartmut, Jan H. Fleckenstein, Junfeng Luo, Konrad Miegel, Gunnar Nützmann, Matthias Schöniger, Heinz Theis, Joachim Wald, Thomas Salzmann, Silke Mey, Bernd Pfützner, and Dirk Barion (2013). *Wechselwirkungen zwischen Grund- und Oberflächenwasser: DWA-Themen T 2/2013*. Vol. T 2013,2. DWA-Themen. Hennef (Sieg): Deutsche Vereinigung für Wasserwirtschaft, Abwasser und Abfall.

Young, Hillary S., Douglas J. McCauley, Mauro Galetti, and Rodolfo Dirzo (2016). "Patterns, Causes, and Consequences of Anthropocene Defaunation". In: *Annual Review of Ecology, Evolution, and Systematics* 47.1, pp. 333–358. DOI: 10.1146/annurev-ecolsys-112414-054142.

Zomlot, Z., B. Verbeiren, M. Huysmans, and Okke Batelaan (2015). "Spatial distribution of groundwater recharge and base flow: Assessment of controlling factors". In: *Journal of Hydrology: Regional Studies* 4, pp. 349–368. DOI: 10.1016/j.ejrh.2015.07.005.

Appendices

A Declaration of independent work

I hereby declare that this thesis and the work presented in it is entirely my own except where otherwise indicated. I have only used the documented utilities and references.

Hiermit erkläre ich, dass ich die vorliegende Dissertation selbständig verfasst habe und keine anderen als die angegebenen Quellen und Hilfsmittel verwendet habe.

Karlsruhe, 12/05/2018: _____

Sebastian RUDNICK

B Talks and publications

Talks

- Rudnick, S.; Lewandowski, J.; Nützmann, G.: Talk at the IAHS - IAPSO - IASPEI Joint Assembly, Gothenburg 2013: *Investigation of groundwater-surface water interactions in shallow lakes using hydraulic head data and a groundwater net balance.*

- Rudnick, S.; Nützmann, G.; Fleckenstein, J.H.; Lewandowski, J.: Talk at the 26th annual assembly of the German Limnological Society, Bayreuth 2010: *Charakterisierung der Grundwasser-Oberflächenwasser- Wechselwirkung zweier eutropher Flachseen in Brandenburg*

Articles

- Nuber, T.; Rudnick, S.; Lensing, H.-J.; Siebenborn, G.; Roeloffzen, F.; Otte, K.: *Bau von Grundwasser- und Porenwasserdruckmessstellen zur Grundwasserbeweissicherung an der Unterems*, Conference proceedings, 68. Deutsche Brunnenbauertage und BAW-Baugrundkolloquium, Rostrup/Bad Zwischenhahn 2017

- Rudnick, S.; Lewandowski. J.; Nützmann, G.: *Investigating groundwater-lake interaction by hydraulic heads and a water balance*, Article, Groundwater, Vol. 53 (2), 2015, DOI: 10.1111/gwat.12208

- Rudnick, S.; Lewandowski, J.; Nützmann, G.: *Estimation of lacustrine groundwater discharge using heat as a tracer and vertical hydraulic gradients - A comparison.*, Conference proceedings, IAHS - IAPSO - IASPEI Joint Assembly, Göteborg 2013

- Zak, D.; Cabezas, A.; Rudnick, S., Hallermann, J.; Gelbrecht, J.: *Einfluss einer potenziellen Flachabtorfung auf den Nitratrückhalt und die Phosphorfreisetzung in wiedervernässten Niedermooren – dargestellt am Beispiel des Kleinen Landgrabentals (Mecklenburg-Vorpommern)*, Article, TELMA(42), 2012

- Schnauder, I.; Rudnick, S.; Garcia, X.-F.; Aberle, J.: *Incipient Motion and Drift of Benthic Invertebrates in Boundary Shear Layers*, Conference proceedings, RiverFlow 2010, Braunschweig